Title
Droplet-Based Microfluidic Systems: Finger-Powered Pumps, Reactors and Magnetic Capsules

Author
Iwai, Kosuke

Publication Date
2014

Peer reviewed|Thesis/dissertation

Droplet-Based Microfluidic Systems:

Finger-Powered Pumps, Reactors and Magnetic Capsules

By

Kosuke Iwai

A thesis submitted in partial satisfaction of the

requirements for the degree of

Doctor of Philosophy

in

Engineering - Mechanical Engineering

in the

Graduate Division

of the

University of California, Berkeley

Committee in charge:

Professor Liwei Lin, Chair

Professor Albert P. Pisano

Professor Luke P. Lee

Spring 2014

Abstract

Droplet-Based Microfluidic Systems:

Finger-Powered Pumps, Reactors, and Magnetic Capsules

by

Kosuke Iwai

Doctor of Philosophy in Mechanical Engineering

University of California, Berkeley

Professor Liwei Lin, Chair

The combination of microfabrication and microfluidics has enabled a variety of opportunities in making new tools for biological and diagnostic applications. For example, microdroplets-based systems have attracted lots of attentions in recent years due to potential advantages in controlled environments with fast reaction time, high-throughput and low noises. This work presents a number of advanced microfluidic systems in process, control and manipulation of microdroplets, including finger-powered pumps to generate microdroplets, continuous-flow rupture reactors for the rupture and content retrieval of microdroplets, and magnetic microcapsules for drug delivery applications.

Prototype 'finger-powered' pumping systems have been designed and constructed and integrated with passive fluidic diodes to pump microfluidics, including the formation of microdroplets. No electrical power is needed for pumping by using a human finger as the actuation force to generate pressure heads. Both multilayer soft lithography and injection molding processes have been successfully utilized to make the pumping systems. Experimental results revealed that the pressure head generated from a human finger could be tuned based on the geometric characteristics of the system, with a maximum observed pressure of 7.6±0.1 kPa. In addition to the delivery of multiple, distinct fluids into microfluidic channels, the finger-powered pumping system is also employed to achieve rapid formation of both water-in-oil droplets (106.9±4.3 μm in diameter) and oil-in-water droplets (75.3±12.6 μm in diameter), as well as the encapsulation of endothelial cells in microdroplets without using any external or electrical controllers.

To advance the technology of microdroplets in microfluidic systems, the technique to rupture microdroplets *via* the continuous-flow micropost array railing systems has been developed. The key step is to transport water-in-oil microdroplets with surfactant into the pure oil microchannel to wash away the surfactant and allow the washed microdroplets to transport to the next water

microchannel and rupture at the oil-water interface boundary. Microdroplets-based nanoparticle synthesis systems have been fabricated to demonstrate synthesis and retrieval of iron oxide nanoparticles without the need of an external centrifuge machine. In a second demonstration, a rapid solution alteration system for the bead-in-droplet microreactors has been demonstrated *via* the continuous flow micropost array railing technique. The prototype system has accomplished: (*i*) the retrieval of microbeads in water-in-oil droplets by the 'rupture' of the droplets, (*ii*) transfer of the released microbeads into a second solution, and (*iii*) the formation of new water-in-oil droplets containing the original microbeads and a different, second droplet solution. In these experiments, a total of four different microdroplets generation systems have been fabricated and different designs and operation conditions result in different sizes of microdroplets, including 41.1 μm for the basic microdroplets rupture demonstration, 67.5 μm for nanoparticle synthesis experiments, 61.1 μm in the original solution, and 38.6 μm for the new solution in the bead-in-droplets alternation experiments.

In the last example, a new class of magnetic microcapsules with aqueous core and polymer shell containing magnetic nanoparticles has been demonstrated for possible drug delivery applications. The combination of multi-layer flow-focusing methodology and an optofluidic polymerization process is employed to form double emulsions of water-in-photocurable polymer microdroplets. A subsequently polymerization process cure the magnetic polymer shells and encapsulates drug materials in the core. Experimentally, remote manipulations of the magnetic microcapsules by applying an external magnetic field have been achieved. As such, the proposed microcapsules have the potential to overcome a number of hurdles associated with current state-of-art technologies: (1) magnetic shells can be guided by DC magnetic field for location control; (2) magnetic particles can be heated by AC magnetic field to break or change the porosity of the shells for active drug release control; and (3) encapsulated microdroplets can prevent the possible degradation and contamination of the drug materials during the transportation processes.

Dedication

This work is dedicated to my parents,
Tomoyo and Masaki Iwai,
for their substantial support and encouragement.

Table of Contents

List of Figures

Chapter 1

Chapter 2

Chapter 3

Chapter 4

Chapter 5

List of Tables

Chapter 2

Chapter 4

Acknowledgements

My experience at UC Berkeley is certainly beyond any describable words in my language. It was a huge change to come to Berkeley from Japan without expecting how wonderful life would be awaiting. I have cultivated tremendous growth not only intellectually, but also in all the aspects of my life. I have no doubt that all the accomplishment would never exist without the interactions with many valuable people who provided unlimited thoughtful contributions, whom I would like to acknowledge here.

First of all, I am truly grateful to my advisor, Prof. Liwei Lin, for all the incredible guidance and enormous support during my PhD career. For those in the same field, it is widely know how tremendous opportunity it is to get involved with his research and experiences. He has been exceptionally helpful not only in the essential aspects of the research, but also provided generous support how to survive and spend the pleasant graduate life.

Prof. Albert P. Pisano and Prof. Luke Lee have been kind enough to serve as the dissertation committee members, and provided supportive comments and discussions in my projects. Without their contributions of deep knowledge in material science and bioengineering, the projects never reached at current level. I also would like to thank the qualifying exam committee members, Prof. Dorian Liepmann, Prof. Song Li, Prof. Lydia Sohn, and Prof. Alice M. Agogino, for supportive remarks.

No explanation would be enough to describe how Dr. Ryan D. Sochol has been vital for me to survive in the graduate school. His brilliance and insight made him an ideal research partner, but his understanding, thoughtfulness, and selflessness elevate her from just a partner to one of my very best friends.

I cannot imagine that graduate school would have been so enjoyable without such a wonderful environment for research. My mentors, Dr. Nazly Fatimah Pirmoradi, Dr. Adrienne Higa, Dr. Chen Yang, and Dr. Brian Sosnowchik, were critical in helping me develop my skills as a researcher. They certainly elevated my knowledge, and were always willing to provide much-needed advice. I would like to thank Alina Kozinda, Casey Glick, Jiyoung Chang, Kevin Limkrailassiri, Ken Shih, Michael Dommer, and all of the members of the Liwei Lin Lab for their awesome help and assistance. Much of my work would not exist without the support and contributions of researchers who I have advised during my graduate career. I especially want to thank Vishnu Jayaprakash, Thomas Brubaker, Kye Lee, Ki Tae, Mohit Jethi, April Jung, Aritro Mukherjee, Jessica Sun, and all the members of the Micro Mechanical Methods for Biology (M3B) Laboratory. Working in outside laboratories can be difficult, but the laboratories of Prof. Albert P. Pisano and Prof. Luke Lee as well as Berkeley Nanotechnology Center (BNC) have been incredibly welcoming and supportive. In particular, I greatly appreciate the help of Dr. Yegan Erdem and Paul Lum.

Being a part of the Berkeley Sensor and Actuator Center (BSAC) has been fantastic, and a large part of that is due to my interactions with Helen Kim, John Huggins, Richard Lossing, Kim Ly, Yulia Golubovskaya, and Alain Kesseru. I also want to thank the mechanical engineering department's staff, including Donna Craig, Patricia Giddings, and Yawo Akpawu.

Outside of school, having family and friends that I can rely on has meant a lot to me. Not only as a sibling but also as one of the best friend, my brother, Shinsuke, has always been incredibly supportive and provided reviving conversations to release the tension when I am in trouble. I am exceptionally thankful to Dr. Yuka Yajima, for being there for me, in addition to her intellectual support and generous dedications for making the life truly enjoyable. I realized that all the roommates in past few years, Dr. Sadao Ota and Aya Ota, Dr. Hiroki Satooka, and Dr. Daisuke Kiriya, have helped me a lot to relieve the stress as well as valuable discussions. I guess the graduate school is not supposed to be so much fun, but spending time with my friends has made these past few years some of the best of my life. Taiki Hatakeyama, Ryo Mori, Kunitoshi Chiba, Yoshitaka Oritatsu, Jesús Javier Téllez, Eduardo Manilla, Andrew Utada, Remi Asada, Takeshi Ohishi, Michael Caringal, Ayako Takaku, Sascha Kuzins, Sean Robitaille, Shimon Tanaka, Marie Nishiyama, Sujan Chakradher, Takuya Suzuki, Frederick and Jennifer Matsuda, Masato Kato, Kosuke Nakao, Atsushi Nakanishi, and Ayaka Sago, as well as all the people from ABC, JGRB, CJC, Tlab, and Wish – it's been a pleasure.

Lastly, I want to thank Dietrich Mateschitz for his incredible invention of Redbull, which have given me energy wings with wonderful inspiration during multiple all-nighters in lab.

Chapter 1: Introduction

1.1 Dissertation Introduction

Microfluidic systems have been explored exponentially in recent years as promising tools to regulate the fluids at the microscale for biological and chemical applications.[1]-[5] Compared with conventional bulk scale systems, the technologies of microfluidic systems have the advantages in performing liquid-based assays with significantly less volume of reagents or samples and shorter reaction time due to much smaller reaction volumes. Combined with a variety of fundamental sciences in physics, biology, and chemistry to technics in electrical and mechanical engineering, microfluidic technologies have great potential in various applications, such as tissue engineering,[6]-[8] genomics,[9]-[13] quantitative cell biology,[1], [14], [15] nanomaterial synthesis,[6], [8], [16] and biomedical diagnostics.[9], [11], [17] However, one of the indispensable key components in the microfluidic systems is the mechanical pump, which move and control the fluidic movements for various functionalities such as mixing, assaying, washing and transporting fluidic flows in the microchannels and micro reactors. The state-of-art microfluidic systems have been using syringe pumps which are bulky, expensive and consume large amount of electrical power. As such, the first task of this dissertation work is to investigate the feasibility of making "finger-power" pumping systems to pump microfluidic systems without the need of any electricity. We believe full development and characterizations of such pumping systems could be directly applicable for point-of-care systems without the needs of bulky and expensive pumps are needed.

In terms of state-of-art microfluidic systems, two technologies are especially attractive in recent years; (*i*) continuous-flow microfluidic systems[14], [15], [18], [19] and (*ii*) microdroplets-based microfluidic systems.[16] Specifically, fluid flows in the microscale are mainly in the low-Reynolds number regime with laminar characteristics where the viscosity term dominates the inertia effects. Continuous-flow microfluidic systems can utilize the laminar flow behavior to achieve good control of the micro fluidic environments in terms of temperature and concentration. While continuous-flow microfluidic systems generally deploy a large number of microreactors to pass through different fluid flows of the same kinds for fast and continuous multiple reactions, microdroplets-based microfluidic systems manipulate the flows of different fluids to produce many compartmentalized microreactors. Microdroplets-based systems offer several advantages; (*i*) fast reaction time due to short heat and mass transfer, (*ii*) potentially high-throughputs without increasing the size or complexity of the systems, and (*iii*) low background noises as the microreactors are separated from each other.[17] For example, researchers have demonstrated the feasibility to produce highly mono-dispersed microdroplets at rates of up to twenty thousand droplets per second [18], [19] for multiplexed experiments and large sets of data acquisitions. Furthermore, it is possible to use microdroplets-based microfluidics systems to make multi-layered particles, including double emulsions [2]-[5], [20], microcapsules [7], [21], and gas plugs [10], [12], [13], [22], [23] for a wide range of biomedical and chemical applications such as point-of-care diagnostics, synthesis of biomolecules, and therapeutic drug delivery. Therefore, we investigate the combination and integration of continuous-flow

microdroplets systems in this dissertation to demonstrate new capabilities and schemes in microfluidic systems.

The concepts of three key microfluidics systems demonstrated in this dissertation are shown in **Figure 1.1**. **Figure 1.1a** illustrates the concept of a 'finger-powered' integrated pumping system as a modular element to provide pressure head for microfluidic systems. By utilizing a human finger for the actuation force, electrical power for pumping are completely avoided. Passive fluidic diodes have been designed and implemented to pump distinct fluids from multiple inlet ports using a single actuation source. Both multilayer soft lithography and injection molding processes have been successfully utilized to make prototype pumping systems. Experimental results reveal that the pressure head generated from a human finger could be tuned based on the geometric characteristics of the pumping system, with a maximum observed pressure of 7.6±0.1 kPa. In addition to the demonstration of pumping multiple, distinct fluids into microfluidic channels, we also employ the finger-powered pumping system to achieve rapid formations of both water-in-oil microdroplets (106.9±4.3 μm in diameter) and oil-in-water microdroplets (75.3±12.6 μm in diameter), as well as the encapsulation of endothelial cells in microdroplets without using any external or electrical controllers.

To advance the technology of microdroplets in microfluidic systems, the technique of rupture of microdroplets via the continuous-flow micropost array railing is presented in **Fig. 1.1b**. Water-in-oil microdroplets with surfactant are sequentially transferred to the pure oil flow to wash away the surfactant. Rupture of microdroplets occurs as the microdroplets are entering the third microfluidic microchannel of water flow. As such, the contents inside microdroplets can be retrieved Micropost arrays for the guidance of microdroplets between multiple continuous flows have been designed, fabricated, and experimentally tested to accomplish continuous wash and rupture of microdroplets reactors. The presented rupture system is further integrated with a microreactors-based nanoparticle synthesis system for high-throughput and uniform synthesis and separation of iron oxide nanoparticles. In another demonstration of the microdroplets rupture system, a T-junction and a different water assay solution are incorporated to the end of the basic microdroplets rupture system to realize rapid alteration of the fluidic solution inside the microdroplets for various applications based on the bead-in-microdroplets architecture.

In the other demonstration of the microdroplets systems, a new class of microcapsules with aqueous core and polymer shell containing magnetic nanoparticles is presented as depicted in **Fig. 1.1c**. In this work, the combination of the multi-layer microfluidic flow-focusing methodology and optofluidic polymerization of photocurable polymer enables continuous encapsulations of drug materials. Flow-focusing structures have been designed, fabricated and experimentally demonstrated to accomplish the formation of double emulsions of water and photocurable polymer solution containing magnetic nanoparticles. These double emulsions can be subsequently polymerized *via* UV light exposure with proper time, wavelength and intensity. Experimental demonstrations have been performed for remote manipulations of the magnetic microcapsules by applying an external magnetic field. These magnetic microcapsules could provide the ability to transport encapsulated drugs to target sites (without the degradation of encapsulated drug). A possible on-demand drug release strategy by rupturing the microcapsules with an alternating external magnetic field could be applied to remotely release the aqueous drug for drug delivery applications.

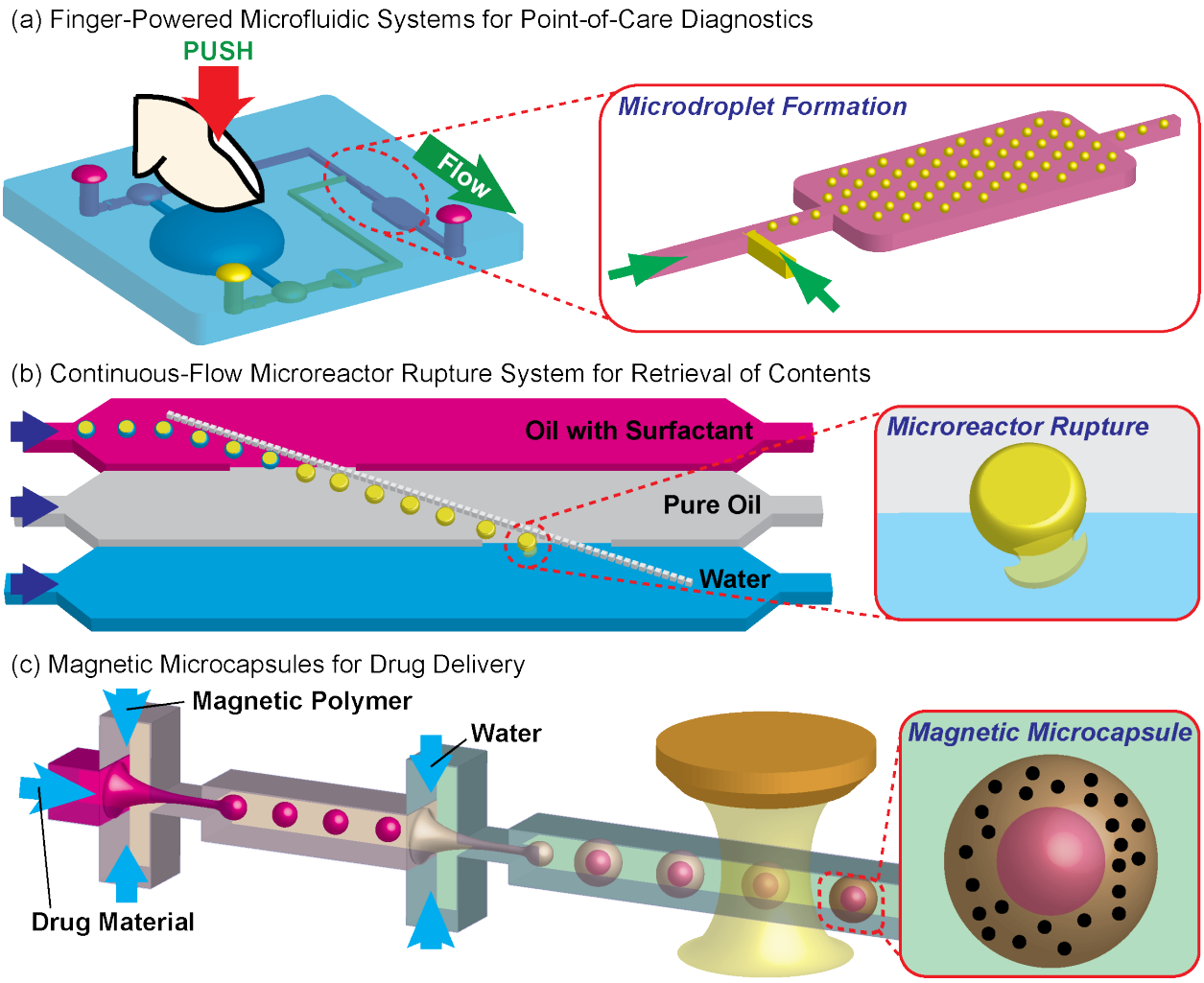

Figure 1.1 *Microdroplets-based microfluidic systems:* ***(a)*** *finger-powered pumps for the formation of microdroplets,* ***(b)*** *continuous-flow microdroplets rupture system, and* ***(c)*** *magnetic microcapsules for drug delivery.*

1.2 Dissertation Overview

In **Chapter 2**, the methodology of 'finger-powered' integrated pump system as a modular element to provide low-power, low-cost and portable pressure head for microfluidic systems applications is presented. An overview of prior efforts for minimizing the microfluidic pump system is described, as well as prior demonstrations of human finger power systems for biomedical applications. The design and fabrication of the finger-powered pump system using both multi-layer soft lithography process and the injection molding process are discussed. Examples of three finger-powered microfluidic systems are presented: (*i*) a microdroplets generator, (*ii*) a cell encapsulation microfluidic system, and (*iii*) a bead-in-droplet microreactor. Experimental methods, procedures and data acquisition details are described. Results for the characteristics of finger-powered pump systems are presented and discussed, with a primary focus on control of pressure head and droplet generation experiments.

In **Chapter 3**, the technique incorporating arrayed microposts into microfluidic systems to rupture and retrieve the contents of microreactors is presented. An overview of prior efforts for continuous handling of microdroplets in microfluidic systems is briefed, including prior uses of micropost arrays. The design and fabrication of three different classes of continuous-flow microdroplets rupture platforms are presented, including: (i) basic microdroplets rupture system *via* a continuous-flow micropost array railing design, (*ii*) synthesis and centrifuge-free retrieval of nanoparticles from the microdroplets systems, and (*iii*) solution alternations for the bead-in-microdroplets systems. The methods associated with experimental procedures, data acquisitions on each platform are detailed with full discussions on the results for the performance of these microdroplets rupture systems.

In **Chapter 4**, the technique employing microfluidic flow to generate microdroplets and encapsulate drug materials in magnetic polymer shell is presented. Prior efforts in utilizing micro/nano particles for drug delivery applications are first discussed, including the formation of capsules and magnetic particles in microfluidic systems. The design and fabrication of the microdroplets for the optofluidic formation of microcapsules are discussed. Results for the formation and the characteristics of the magnetic microcapsules are presented and discussed, with a primary focus on size control of the microcapsules and polymerization process.

Conclusions for the dissertation are discussed in **Chapter 5**. The performance of the presented droplet-based microfluidic systems is summarized. Future directions and applications for the presented technologies are discussed.

References of Chapter 1

[1] D. Di Carlo and L. P. Lee, "Dynamic single-cell analysis for quantitative biology," *Anal Chem*, vol. 78, no. 23, pp. 7918–7925, 2006.

[2] P. Dittrich and A. Manz, "Lab-on-a-chip: microfluidics in drug discovery," *Nature Reviews Drug Discovery*, vol. 5, no. 3, pp. 210–218, 2006.

[3] G. Whitesides, "The origins and the future of microfluidics," *Nature*, vol. 442, no. 7101, pp. 368–373, 2006.

[4] K. Gupta, D.-H. Kim, D. Ellison, C. Smith, A. Kundu, J. Tuan, K.-Y. Suh, and A. Levchenko, "Lab-on-a-chip devices as an emerging platform for stem cell biology," *Lab on a Chip*, vol. 10, no. 16, pp. 2019–2031, 2010.

[5] L. Gervais, N. De Rooij, and E. Delamarche, "Microfluidic Chips for Point-of-Care Immunodiagnostics," *Advanced Materials*, vol. 23, no. 24, pp. H151–H176, 2011.

[6] E. M. Chan, R. A. Mathies, and A. P. Alivisatos, "Size-controlled growth of CdSe nanocrystals in microfluidic reactors," *Nano Lett*, vol. 3, no. 2, pp. 199–201, 2003.

[7] B. G. Chung, K.-H. Lee, A. Khademhosseini, and S.-H. Lee, "Microfluidic fabrication of microengineered hydrogels and their application in tissue engineering," *Lab on a Chip*, vol. 12, no. 1, pp. 45–59, 2012.

[8] E. M. Chan, A. P. Alivisatos, and R. A. Mathies, "High-Temperature Microfluidic Synthesis of CdSe Nanocrystals in Nanoliter Droplets," *J. Am. Chem. Soc.*, vol. 127, no. 40, pp. 13854–13861, Oct. 2005.

[9] R. Gorkin, J. Park, J. Siegrist, M. Amasia, B. S. Lee, J.-M. Park, J. Kim, H. Kim, M. Madou, and Y.-K. Cho, "Centrifugal microfluidics for biomedical applications," *Lab on a Chip*, vol. 10, no. 14, pp. 1758–1773, 2010.

[10] K. A. Heyries, C. Tropini, M. Vaninsberghe, C. Doolin, O. I. Petriv, A. Singhal, K. Leung, C. B. Hughesman, and C. L. Hansen, "Megapixel digital PCR," *Nat Methods*, vol. 8, no. 8, pp. 649–U64, 2011.

[11] L. Malic, D. Brassard, T. Veres, and M. Tabrizian, "Integration and detection of biochemical assays in digital microfluidic LOC devices," *Lab on a Chip*, vol. 10, no. 4, pp. 418–431, 2010.

[12] P. Kumaresan, C. J. Yang, S. A. Cronier, R. G. Blazej, and R. A. Mathies, "High-throughput single copy DNA amplification and cell analysis in engineered nanoliter droplets," *Anal Chem*, vol. 80, no. 10, pp. 3522–3529, 2008.

[13] R. G. Blazej, P. Kumaresan, and R. A. Mathies, "Microfabricated bioprocessor for integrated nanoliter-scale Sanger DNA sequencing," *P Natl Acad Sci Usa*, vol. 103, no. 19, pp. 7240–7245, 2006.

[14] T. M. Squires and S. R. Quake, "Microfluidics: Fluid physics at the nanoliter scale," *Rev Mod Phys*, vol. 77, no. 3, p. 977, 2005.

[15] E. M. Lucchetta, M. S. Munson, and R. F. Ismagilov, "Characterization of the local temperature in space and time around a developing Drosophila embryo in a microfluidic device," *Lab on a Chip*, vol. 6, no. 2, pp. 185–190, 2006.

[16] M. T. Guo, A. Rotem, J. A. Heyman, and D. A. Weitz, "Droplet microfluidics for high-throughput biological assays," *Lab on a Chip*, vol. 12, no. 12, p. 2146, 2012.

[17] S.-Y. Teh, R. Lin, L.-H. Hung, and A. P. Lee, "Droplet microfluidics," *Lab on a Chip*, vol. 8, no. 2, pp. 198–220, 2008.

[18] I. Kobayashi, K. Uemura, and M. Nakajima, "Formulation of monodisperse emulsions

using submicron-channel arrays," *Colloids and Surfaces A: Physicochemical and Engineering Aspects*, vol. 296, no. 1, pp. 285–289, 2007.
[19] P. Garstecki, M. Fuerstman, H. Stone, and G. Whitesides, "Formation of droplets and bubbles in a microfluidic T-junction - scaling and mechanism of break-up," *Lab on a Chip*, vol. 6, no. 3, pp. 437–446, 2006.
[20] A. S. Utada, E. Lorenceau, D. R. Link, P. D. Kaplan, H. A. Stone, and D. A. Weitz, "Monodisperse double emulsions generated from a microcapillary device," *Science*, vol. 308, no. 5721, pp. 537–541, 2005.
[21] S.-H. Kim, J. W. Kim, J.-C. Cho, and D. A. Weitz, "Double-emulsion drops with ultra-thin shells for capsule templates," *Lab on a Chip*, vol. 11, no. 18, pp. 3162–3166, 2011.
[22] E. Talu, K. Hettiarachchi, R. L. Powell, A. P. Lee, P. A. Dayton, and M. L. Longo, "Maintaining monodispersity in a microbubble population formed by flow-focusing," *Langmuir*, vol. 24, no. 5, pp. 1745–1749, 2008.
[23] W. Duncanson, A. Abbaspourrad, H. Shum, S.-H. Kim, L. Adams, and D. Weitz, "Monodisperse Gas-Filled Microparticles from Reactions in Double Emulsions," *Langmuir*, vol. 28, no. 17, p. 6742, 2012.

Chapter 2: Finger-Powered Microfluidic Systems Using Multilayer Soft Lithography and Injection Molding Processes

2.1 Introduction

At present, the majority of diagnostics processes are performed in centralized laboratories using bulky, complex, and time-consuming medical instruments. Blood tests, for example, typically require: (*i*) the collection of raw blood samples from patients, (*ii*) transportation of the blood sample to centralized clinical laboratories, (*iii*), sample preparations and separations such as centrifugations, and (*iv*) chemical analyses and tests by trained clinicians. In each of these aforementioned steps, the controlled conveyance of fluids is needed and pumps are often the chosen apparatuses. The pricy and bulky equipment often prevents people in need of urgent diagnostics the opportunities of being treated promptly such as those in the battlefields or technologically disadvantaged regions.[1] As a result, chip-scale microfluidic technologies have been widely investigated in recent years to provide quick and low-cost POC diagnostics[1], [2] as well as possible tools for basic scientific studies, such as quantitative cellular characterizations.[3]-[5]

In the state-of-the-art microfluidic devices, significant cost reduction has been achieved by shifting the fabrication process from the labor-intensive conventional soft lithography process to rapid and mass-producible manufacturing such as injection molding[6]-[12], hot embossing[13] and laser ablation.[14] Despite the successful cost-reductions in microfluidic components, one or more big and power-hungry syringe pumps are often used in microfluidic systems, which have been the critical bottlenecks in applying chip-scale microfluidics system to practical market places (*e.g.*, POC applications). Researchers in both academic and industrial laboratories have developed low-cost, low-power, and portable micropumps using simple methodologies to pump microfluidic systems, such as the application of capillary driving forces based on microfluidic systems made of polydimethylsiloxane (PDMS)[15]-[17] or paper;[18], [19] osmotic forces based on water-powered actuators and pumps;[20], [21] negative pressure based on pre-vacuumed PDMS chambers;[22] and finger-actuation sponges[23] and pouches.[24] However, a number of limitations have constrained the broad implementation of these techniques - the magnitudes of capillary forces are small; the osmotic actuation responses are slow; the negative pressure chambers have short shelf-life due to leakages; and both negative pressure chambers and finger-actuation pumps are single usage devices. The desirable micro pumps should have good characteristics of: (*i*) low/no electrical power consumption, (*ii*) fluidic deliveries with fast, suitable and controllable pressure heads, and (*iii*) feasibilities of multiple usages; and (*iv*) applications in complex and multiple microfluidic systems. On the other hand, recent developments in microdroplet-based technologies have shown significant benefits for biochemical processes, including: (*i*) quick mixing of samples *via* fast diffusion rates,[25] (*ii*) low background noise, (*iii*) precise volume control of samples and reagents, and (*iv*) well-established knowledge in handling droplets.[26], [27] Although microdroplet-based technologies have been widely investigated[25], [28]-[30] and utilized for various chemical and biological fluidic processes, such as digital polymerase chain reaction (PCR) for DNA sequencing[31]-[33] and microcapsule synthesis for drug delivery applications,[34] these aforementioned demonstration are all limited to laboratory operations.

Recently, hand-powered pumps have been utilized in microfluidic devices,[35] glucose sensors,[36] and integrated syringe systems.[37] These pumps were used to transport singular fluids with simple functions without characterizations on generated pressure heads and without the possibility of complex fluidic controls. Furthermore, there have been no demonstrations on high volume productions. In this work, we propose and advance the state-of-art of hand-powered pumps to integrated, multi-port infusion systems *via* a single-finger actuation and operation. The highly complex controllability of the system is illustrated by the integration, construction and demonstrations of microdroplet generators using finger-powered microfluidic systems. Furthermore, both a multilayer soft lithography process and an injection molding process have been utilised to construct the finger-powered microfluidic systems. **Figure 2.1a** illustrates the basic concept of the pump. It has a deformable chamber that can be pressurized (*i.e*., pushed) by a human finger to infuse fluids into the microfluidic systems. During the infusion process, passive fluidic diodes direct multiple/different fluids from distinct inlet ports to the outlet port *via* the sample storage chambers connected to the pressure chamber. Here, we measure the pressures generated inside the pressure chamber to determine the efficacy of the finger-powered pumps and investigate the effects of the pressure chamber geometry on the magnitudes of the generated pumping pressure. Two prototype systems are designed and fabricated: (1) PDMS prototypes based on a multi-layer soft lithography process; and (2) silicon rubber prototypes based on an injection molding process. With fabricated prototypes, we demonstrate pumping of various types of fluids *via* pressure heads generated exclusively from the application of a human finger without electricity. We further demonstrate the formation of microdroplets *via* a droplet generator composed of an integrated finger-powered pump and a T-junction. These low-cost, portable, and easy-to-operate finger-powered microfluidic systems could generate pressure-sources without consuming electricity in practical applications of microfluidic technologies, such as POC diagnostics.

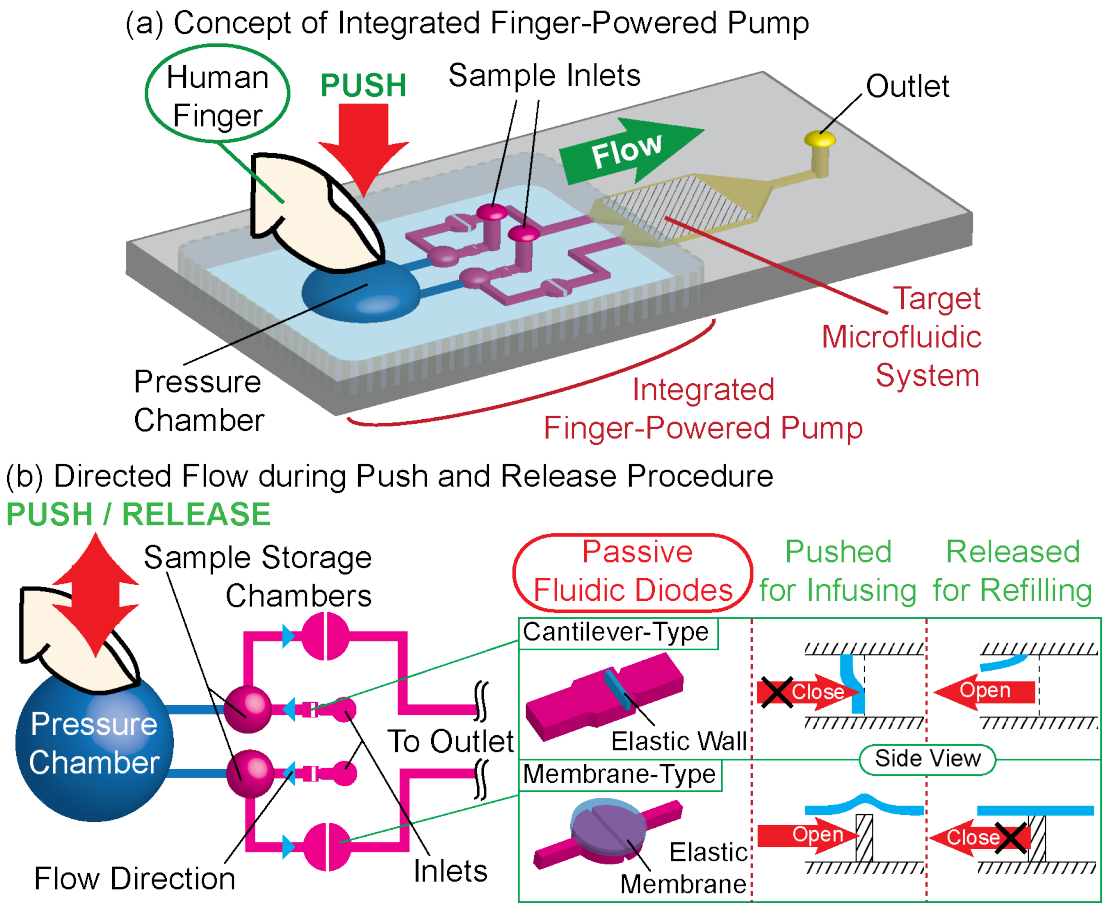

Figure 2.1 ***(a)*** *Concept of the integrated human-powered pumping system. By pushing the deformable chamber, mechanical pressure infuses the solution from the inlets to the outlets (guided by passive fluidic diodes).* ***(b)*** *Pumping procedure of the finger-powered pump with the push-and-release actions. When the pressure chamber is pushed, embedded cantilever-type fluidic diodes are closed while membrane-type fluidic diodes are opened in order to infuse the fluids from the sample storage chambers to the outlet. When the finger is released, the membrane-type fluidic diodes are closed while the cantilever-type fluidic diodes are opened in order to refill the sample storage chambers with fluids from the inlets.*

2.2 Methods

2.2.1 Pumping Principle

Figure 2.1b shows the pumping principle of the proposed system based on the design of a multi-layer soft lithography process, which consists of four major components: (*i*) a deformable pressure chamber, (*ii*) a microchannel network with inlet and outlet ports, (*iii*) sample storage chambers, (*iv*) cantilever-type fluidic diodes[38], and (*v*) membrane-type fluidic diodes.[39] These passive fluidic diodes are utilized to control the fluidic flows. The cantilever-type fluidic diode has a thin vertical plate fixed on the top surface. A forward fluidic pressure pushes and

deforms the cantilever to open the diode, while a backward pressure closes the diode as the cantilever plate is stopped against the narrower region of the microchannel.[38] The circular-shape, membrane-type fluidic diode consists of two chambers separated by a vertical rigid plate while a thin elastic membrane is positioned on top and fixed at the boundary of the two chambers. When a positive pressure is applied (in either directions), the elastic membrane deforms upwards and the two chambers are connected, thereby permitting fluid to flow.[39] Under a negative pressure (*e.g.*, vacuum), the thin membrane deforms downwards and blocks the fluidic path between the two chambers. When a human finger presses the pressure chamber, the resulting positive pressure facilitates the transport of fluids from the sample storage chambers to the outlets while the fluidic path from the inlet ports to the sample storage chambers are blocked by the cantilever-type diodes. When the finger is released, the deformable chamber reverts back to its original shape, generating a negative pressure to allow fluids to move from the inlet ports to the sample storage chambers while the fluid path from the sample storages to the outlet ports are blocked by the membrane-type diodes. By repeating the push-and-release operations, fluids are pumped from the inlet to outlet ports sequentially.

For the majority of microfluidic systems, control of flow rates is a critical parameter for system operation. The flow rate for rectangular-shape channel can be calculated from the Hagen-Poiseuille equation:[40]

$$Q \approx \frac{(wh)^3}{8\mu L(w+h)^2}\Delta P = \frac{\Delta P}{R} \quad \textbf{(2.1)}$$

where ΔP, Q, R, μ, w, h, and L denote the input pressure difference, flow rate, fluidic resistance, dynamic viscosity, width, height, and length of the channel, respectively. In our prototype designs, the inlet ports are connected to the single pressure chamber such that the input pressure remains the same for each channel. Therefore, one way to tune the flow rate of different microchannels is to design the fluidic resistance, which is proportional to the length of the microchannels.

2.2.2 Pressure Measurement and Control

The deformation of the pressure chamber by a human finger will result in pressure increment for pumping. However, it is difficult to regulate the pressure increments in practice as each person or even the same person at each occurrence may produce different magnitudes of force. One alternative is to design the pressure chamber to assure full deformation (the top cap of the chamber is deformed and in contact with the bottom substrate) under a normal force. In the ideal case, when the pressure chamber deforms and reaches the bottom substrate, the pressure will not increase further even if the applied force is increased. This is analysed further under the assumption that the gas leakage in the short push-and-release process is negligible and temperature remains constant. The ideal gas law is described as:

$$P_{MAX} = \frac{V_0}{V_{min}}P_0 \quad \textbf{(2.2)}$$

where P_{MAX} is the pressure when the pressure chamber is fully deformed; P_0 is atmospheric pressure; V_0 is the volume of the pressure chamber with its original shape; and V_{min} is the

remaining volume of the pressure chamber when it is fully deformed. Both V_0 and V_{min} depend on the shape and size of the pressure chamber. In general, V_{min} will be a small number pending on the specific chamber design/size such that the maximum pressure is strongly related to V_0 and can be designed by setting the right dimensions of the pressure chamber.

To further illustrate this concept, we fabricated 6 samples containing pressure chambers of various diameters. The diameter/overall height of the pressure chambers were 2.5/1, 5/1.5, 7.5/2, 10/2, 12.5/2, and 15/2 mm, respectively. The inlet port was connected to a pressure transducer (Model 68075 Pressure Transducer, Cole-Parmer Instrument, IL, USA). The force to the pressure chambers was applied *via* a force probe mounted on a manual force stage (Model-2256 Manual Stage, Aikoh Engineering Co., Ltd., Japan) and recorded using a force instrument (RX Series, Aikoh Engineering Co., Ltd., Japan) while the resulting pressure was measured and recorded (**Fig. 2.2**) with a data logger (Model 34970A Data Logger Switch Unit, Agilent, CA, USA).

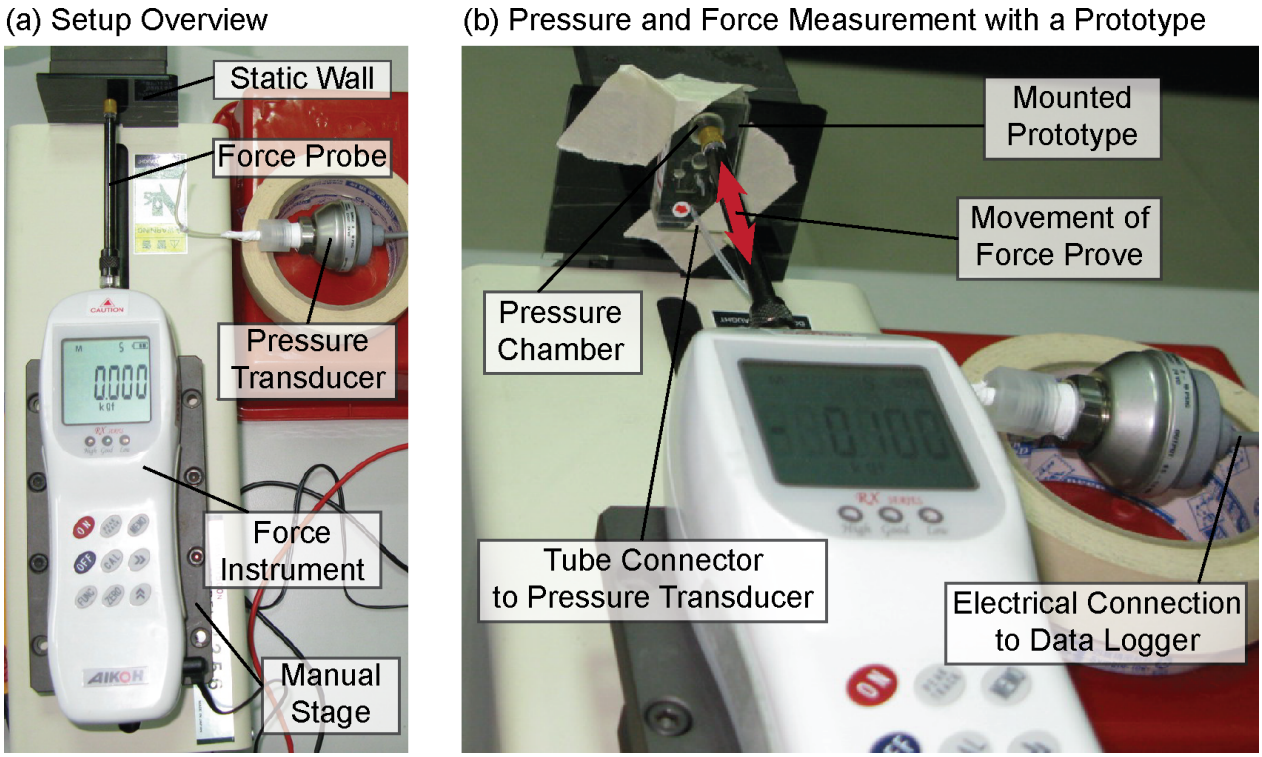

Figure 2.2 *Setup for measurements of pressure and required force.* ***(a)*** *Applied force from a force probe and a force instrument mounted on a manual stage.* ***(b)*** *The prototype microfluidic system is mounted on a static wall during the measurements with a pressure transducer and a data logger.*

2.2.3 Fabrication Process *via* Soft Lithography

A three-layer soft lithography process using PDMS as the main material was used to fabricate the prototype pumps. **Figure 2.3** shows the fabrication process. A standard soft lithography process[41] with two layers of SU-8 was used to fabricate the mold inserts with thicknesses of 10 μm (SU-8/2010) and 90 μm (SU-8/2050), respectively (**Fig. 2.3a**). The overall thickness of 100 μm was the target height of the microchannels and the 10 μm SU-8/2010 was used to define the gap between the elastic plate and the microchannel for the cantilever-type diode. On the other hand, the nominal width of the microfluidic channels was 500 μm in width. Afterwards, SU-8 droplets with height of 2 mm and 1 mm were deposited and cured to form the mold inserts for the deformable pressure and sample storage chambers, respectively (**Fig. 2.3b**). The microfluidic devices were molded using PDMS, which was cut to create the top and bottom PDMS layers after curing and the inlet/outlet ports are punched open (**Fig. 2.3c**). Afterwards, a thin elastic membrane for the membrane-type fluidic diodes was fabricated on another silicon substrate by spin-coating (1000 rpm) an 80 μm-thick layer of PDMS on top of a the SU-8/2010 for reduced adhesion force (**Fig. 2.3d**). The top PDMS layer was first bonded with the PDMS membrane **(Fig. 2.3e)** and the assembly was peeled off from the silicon substrate and bonded with the bottom PDMS layer (**Fig. 2.3f**). Oxygen plasma and thermal treatment conducted at 75 °C for 1 hour were utilized in the bonding process to enhance the bonding force. It was also important to separate the divider and the elastic membrane before the heating process for the membrane-type diode by applying a negative pressure on top of the diodes *via* the opening hole as drawn. Otherwise, the bonding process could seal off the membrane-type diode. To prevent misalignment of the PDMS layers, the top and bottom PDMS layers were designed to be fabricated together on a single silicon wafer to have approximately the same rate of shrinkage during the curing process. **Figure 2.3g** shows the result of a fabricated PDMS prototype system.

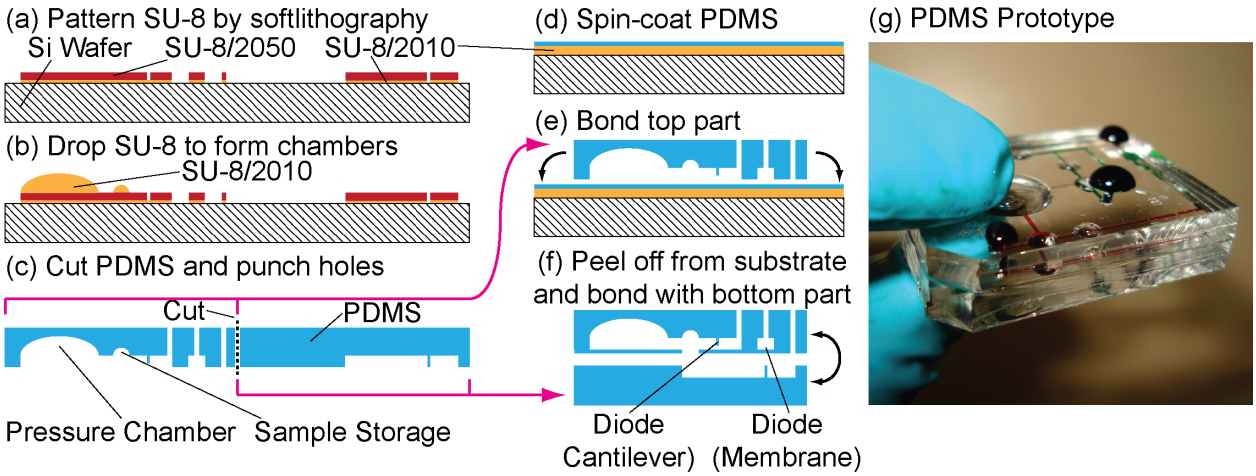

Figure 2.3 *Fabrication via the multilayer soft lithography process.* ***(a-f)*** *The device consists of three layers of PDMS and is fabricated by the soft lithography process using SU-8 photoresist as the primary mold insert material.* ***(g)*** *A fabricated PDMS pumping system.*

2.2.4 Fabrication Process *via* Injection Molding

In addition to the multilayer soft lithography process, we also developed the injection molding process for low-cost, mass production based on our previous works.[7], [8] Several changes were made. First, we changed the height of the microchannels from 100 μm to 300 μm due to the limitations of precision mechanical machining in making the steel mold inserts in the injection molding process. We also increased the size of the pressure chamber to 10 mm in diameter and 2.5 mm in thickness, and sample storage chamber to 5 mm in diameter and 1.25 mm in thickness. Second, a new passive diode design (**Fig. 2.4a**) was chosen to replace both the cantilever-type and memberne-type diodes as they required fine manufacturing dimensions. Third, the polymeric material was changed to transparent elastic silicon rubber (XE15-645, Momentive Performance Materials, Japan) – a widely-used material for the injection molding process. Inverted structures of the three layers similar to the multilayer soft lithography process were machined by precision mechanical machining processes on medium carbon steel to make the mold inserts (**Fig. 2.4b**). In our prototype design, the thickness of the top, middle and bottom layers was 5 mm, 300 μm and 2.5 mm, respectively. Most of the features were constructed by using computer numerical control (CNC) milling machines, while structures with high aspect ratio such as inlet/outlet ports were processed with the electrical discharge machine. The internal surfaces of the mold inserts were polished to get glossy surface and a 2 μm-thick chrome layer was electroplated to prevent corrosion. Next, elastic silicon rubber was used in the injection molding process. We set pressure at 15±2 MPa, clamping force at 360 tons, temperature at 130±5 °C, and curing time at 120 sec. Lastly, the three layers were assembled using the oxygen plasma and thermal treatment conducted at 75 °C for 1 hour for the bonding process. **Figure 2.4c** shows a prototype system by the injection molding process.

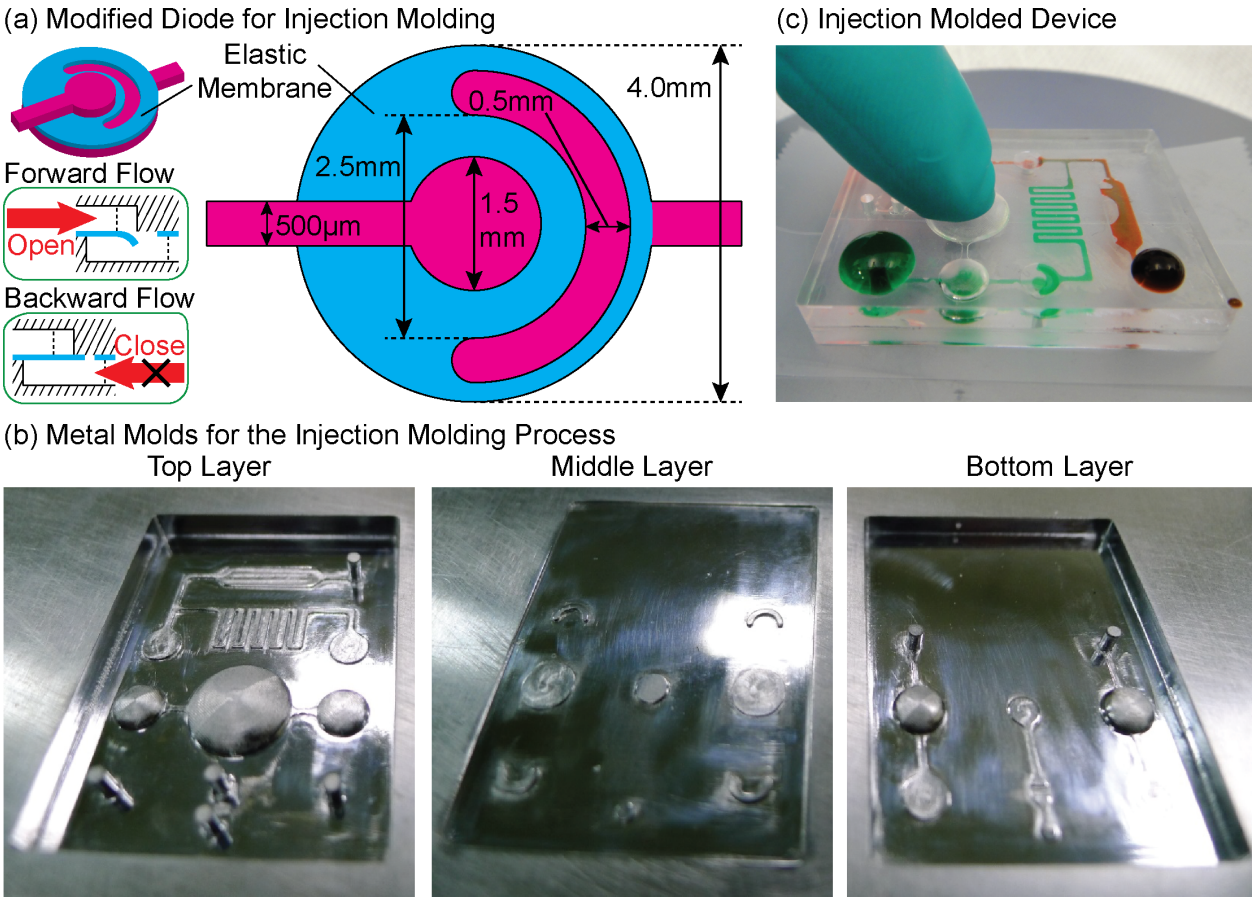

Figure 2.4 *Fabrication via the injection molding process.* ***(a)*** *Design and top view of a modified diode used in the injection molding process.* ***(b)*** *Metal molds for the injection molding process. The structures are constructed and machined on medium carbon steel with a CNC milling machine and electrical discharge machine. Bottom surface of the molds is polished to get glossy surface and chrome is electroplated to prevent corrosion.* ***(c)*** *A fabricated prototype via the injection molding process.*

2.2.5 Design of Passive Fluidic Diodes

The passive fluidic diodes used in the finger-powered pumping systems are key components as they regulate the flow patterns. Among the three passive diodes, the cantilever-type diode was placed in a specially designed microchannel region of 200 μm in width and was used to connect microchannels of 150 μm in width as shown in **Fig. 2.5a**. It had a vertical elastic plate of 160 μm in width and 20 μm in thickness. The gaps between the elastic plate and microchannel were 20 μm from the side walls of the microchannels, 20 μm away from the left blocking wall, and 10 μm above the bottom substrate. The blocking wall on the left side had a smaller opening of 100 μm to physically block the elastic plate under the leftward fluidic flows. On the other hand, for the rightward fluidic flows, the elastic plate could bend rightwards to allow flow passages. The membrane-type diode had a circular shape of 2 mm in diameter. A rigid vertical divider of 200

μm in width was used to divide the chamber into two smaller ones as shown in **Fig. 2.5b**. The elastic membrane on top of the chamber was 80 μm in thickness with a circular shape of 1.5 mm in diameter. We modified the diode design for the injection molding process based on a previously published design concept (**Fig. 2.4a**).[42] Specifically, the top and bottom channels of 500 μm in width and 300 μm in height were separated with an elastic membrane of 300 μm in thickness with a semi-circular shape with detailed dimensions illustrated in **Fig. 2.4a**. Under forward flows, the membrane was deformed downward to allow the passage of fluidic flow. Under the backward flow, the membrane was blocked by the channel to stop the fluidic flow. In addition to the design of these three types of passive diodes, the other key design dimensions of the systems, including PDMS prototypes, microdroplet generators, and injection molded prototypes were illustrated in **Fig. 2.6**.

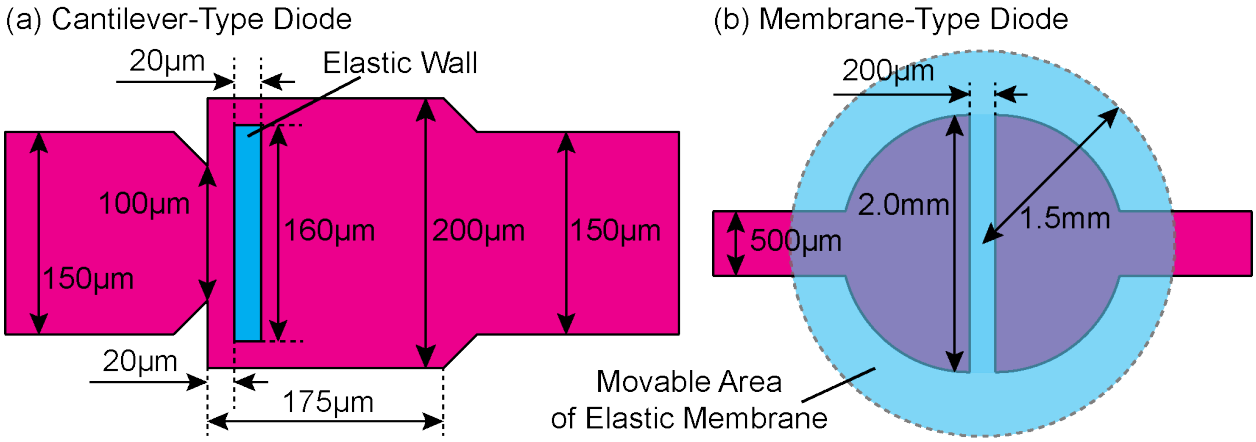

Figure 2.5 *Detailed design dimensions of the fabricated passive diodes.* ***(a)*** *Top view of a cantilever-type diode.* ***(b)*** *Top view of a membrane-type diode.*

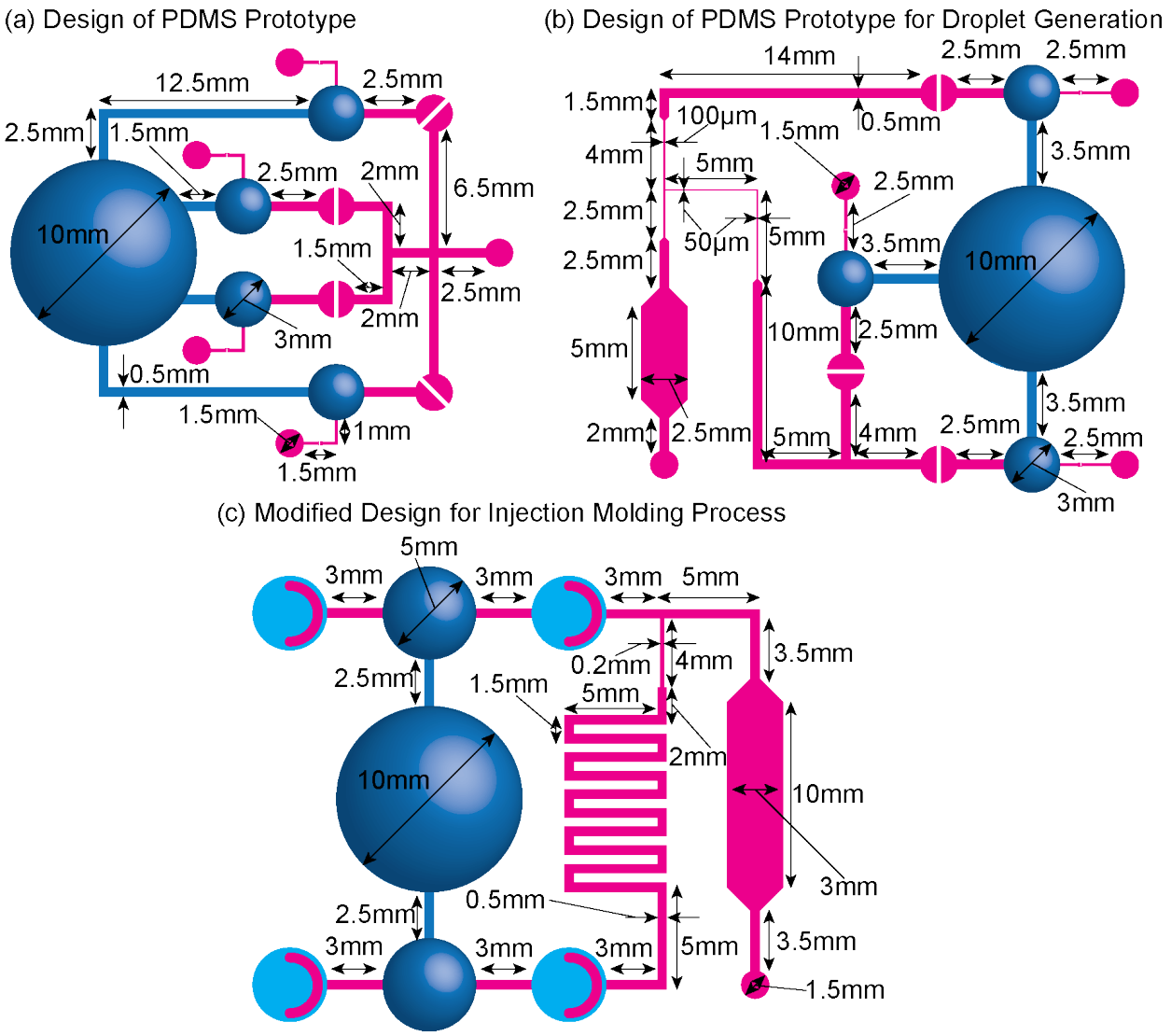

Figure 2.6 *Detailed design dimensions of the fabricated prototype microfluidic systems.* ***(a)*** *A basic PDMS prototype system with four inlet ports (microfluidic components are 100 μm in thickness).* ***(b)*** *A PDMS droplet generator (microfluidic components are 100 μm in thickness).* ***(c)*** *The basic dimensions of the injection molded prototype microfluidic system (microfluidic components are 300 μm in thickness).*

2.3 Results and Discussion

2.3.1 Experimental Pressure Characterizations

To quantify the relationship between the size of the pressure chamber and the working pressure head, prototype PDMS pressure chambers were tested with results shown in **Figure 2.7a**. It is observed that as the diameter of the pressure chamber increases from 2.5 mm to 15.0 mm, the

generated pressure heads increase from 0.2±0.1 to 7.6±0.1 kPa (average from 15 repeated tests on each pressure chamber) under the condition of "fully deformed chamber." This implies that the pumping pressure head can be designed and customized by the diameter and geometry of the pressure chamber.

In order to further validate the concept, **Figure 2.7b** shows experimental results for pressure head *versus* applied force on a prototype pressure chamber of 10 mm in diameter using a load cell mounted on a manual stage (to mimic a human finger). Pressure head was measured using a pressure transducer connected to the inlet port and the other ports were closed with plugs. It is found that the pressure head increases linearly with respect to the applied force as expected until it reaches the magnitude of maximum pressure. After that, larger force could only generate about the same maximum pressure. An approximate force of 12 N was required to generate the maximum pressure head of 4.2 kPa. **Figure 2.7c** shows the results on an injection molded pressure chamber of 10 mm in diameter. The same trend was recorded while a higher maximum pressure head of 7.3 kPa under a higher force of 27 N were logged. The higher force requirement is due to stiffer elastic modulus and thickness of silicon rubber than those of PDMS while the higher resulting pressure is from the larger pressure chamber size (2.5 vs. 2 mm in height differences). Since the typical pinch force of a human finger has previously been characterized as 84 N,[43] these results suggest that the average human finger can produce more than enough force to reach the maximum pressure for these prototype devices. We also investigated the variations of maximum pressure heads for both prototype devices as shown in **Figure 2.7d**. The experimental results reveal that the variation is 4.7% with maximum pressure of 4.2±0.2 kPa for the PDMS prototypes (10 mm in diameter and 2 mm in height) and with 1.8% variation with maximum pressure of 7.3±0.1 kPa for the injection molded prototypes (10 mm in diameter and 2.5 mm in height). In addition to the enhanced reproducibility, the new design of the passive fluidic diode in the injection molding process also helped improving the performance. **Figure 2.7e** shows the measured flow rate of deionized (DI) water on the new diode in both directions under a controlled pressure pump (Fluigent, MFCS series with flow-rate platform). It is found that under the negative pressure, the backward flow is negligible and the diode has a diodicity of 2316. These results imply that prototype pumps fabricated by the injection molding process with the modified passive fluidic diode offer superior performances than those made by the multi-layer soft lithography process.

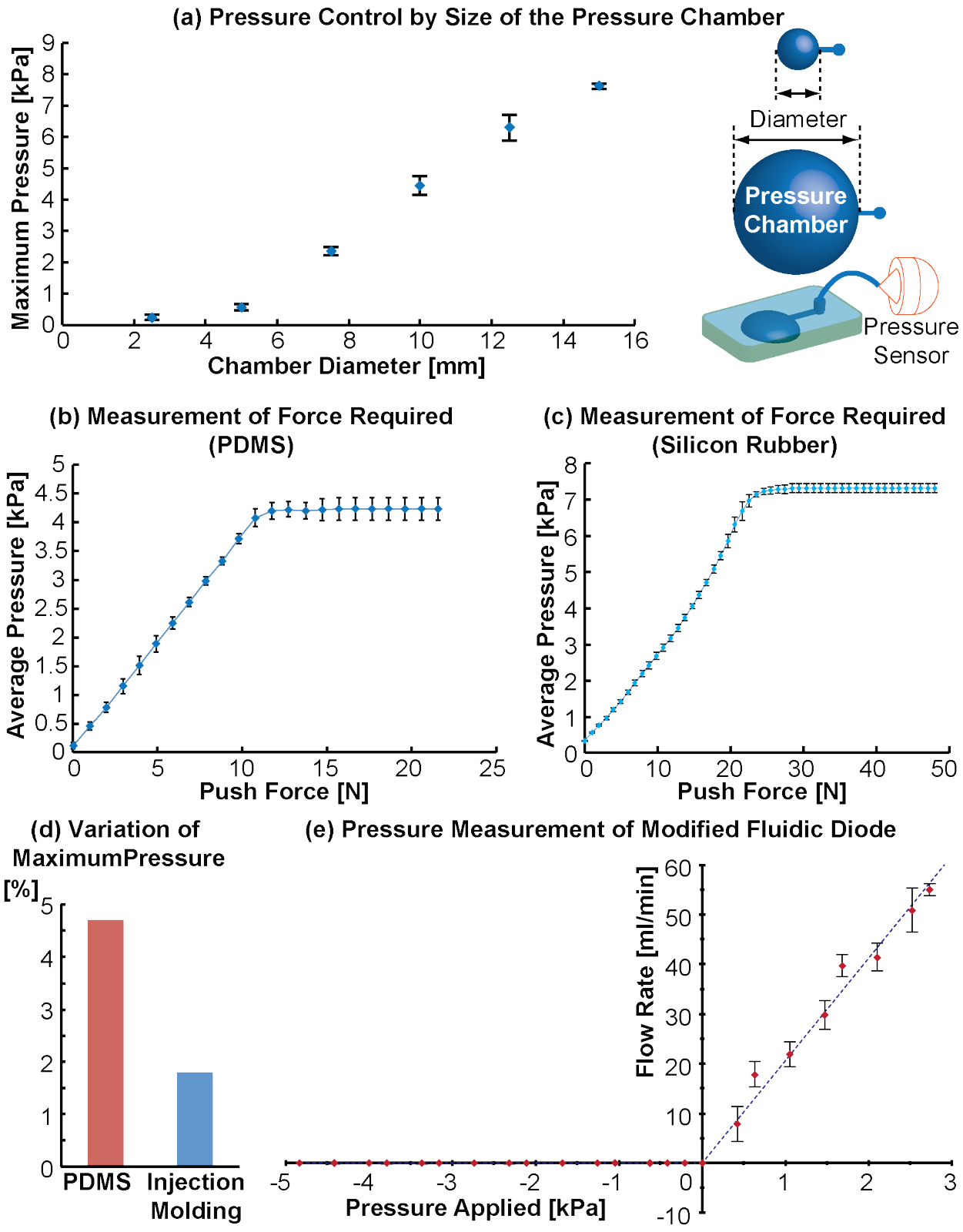

Figure 2.7 *Pressure testing results on prototype pressure chambers.* ***(a)*** *Generated pressure head versus pressure chamber diameter for a PDMS prototype of 10 mm in diameter and 2 mm*

in height. ***(b)*** *Generated pressure head versus applied force on the same pressure chamber.* ***(c)*** *Generated pressure head versus applied force for an injection molded chamber of 10 mm in diameter and 2.5 mm in height.* ***(d)*** *Variations of generated maximum pressure head versus fabricated prototype pumps.* ***(e)*** *Flow rate versus applied pressure on the modified diode by the injection molding process with high diodicity of 2316. Error bars denote standard deviations.*

2.3.2 Basic Finger-Pumping Demonstrations

Experimentally, multiple fluids from up to four distinct inlet ports have been pumped in the prototype microfluidic system simultaneously. For example, **Figure 2.8** shows a fabricated PDMS prototype device (total dimension of 32.5 × 22.5 × 0.8 mm^3 without counting the height of the 10 mm in diameter pressure chamber) with four inlet ports and one outlet port. The sample solutions were added to each inlet port by a pipette, and were pumped through the microchannels to the outlet *via* the push-and-release procedure using a human finger. The green dyed water was simultaneously pumped from the four inlet ports to the outlet port (**Fig. 2.8**). For the system shown in **Fig. 2.8**, approximately 10 μL of sample solution was pumped by a single push-and-release operation (a total of 100 μL after 10 operations). We also conducted the pumping demonstration on the injection molded prototypes with green dyed water as shown in **Fig. 2.9**.

The finger-pumping demonstrations were extended to other fluidic systems. For example, the ability to pump solutions with suspended particulates (*e.g.*, microbeads and cells) is a key demonstration for many chemical and biological applications.[44]-[48] Thus, we performed experiments with suspensions of both polystyrene microbeads (ø = 15 μm) and endothelial cells. Experimental results revealed that the pressure head generated from the finger-powered pumping cycles enabled the fluidic handling capable of both microbeads and endothelial cells inside microchannels (**Fig. 2.10**). We observed the transport of the introduced microbeads and endothelial cells along the flow direction during the pushed state, while the particles remained relatively immobile during the release state. During experimentation, select numbers of microbeads and endothelial cells were observed to 'stick' to the surface of the PDMS walls during device operation – a phenomenon that can be mitigated by utilizing surfactants as described previously.[49] Nonetheless, these results revealed that the passive fluidic diodes did not prevent the pumping of suspended microparticles, thereby demonstrating that the presented finger-powered pumping system can be applied to pump solutions with suspensions of microparticulates.

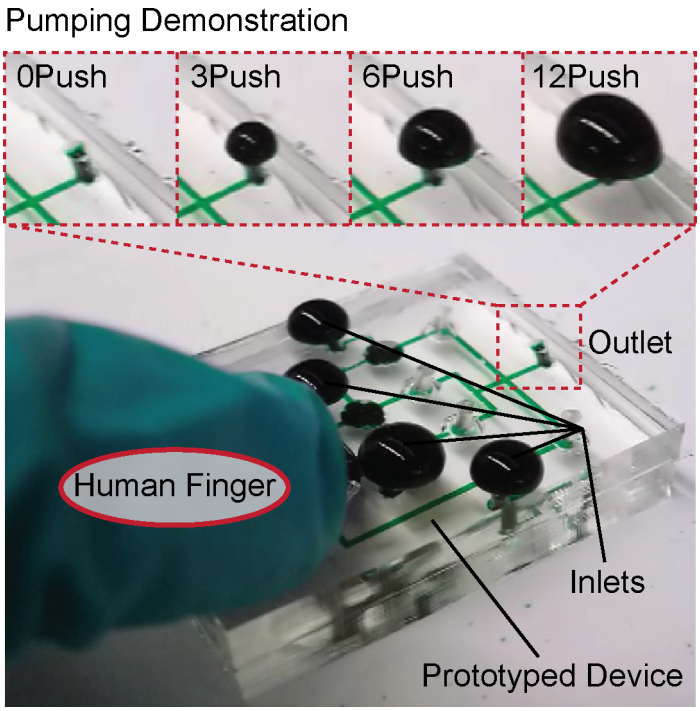

Figure 2.8 *Experimental results for the operation of a PDMS-based finger-powered microfluidic system. A finger-powered pumping system with four inlets and one outlet. Green dyed water can be pumped through the device and to the outlet port (inset) via repeated push-and-release cycles. ESI Movie 1 includes real-time video of this process.*

(a) Pumping in the Injection Molded Device with One Inlet Port

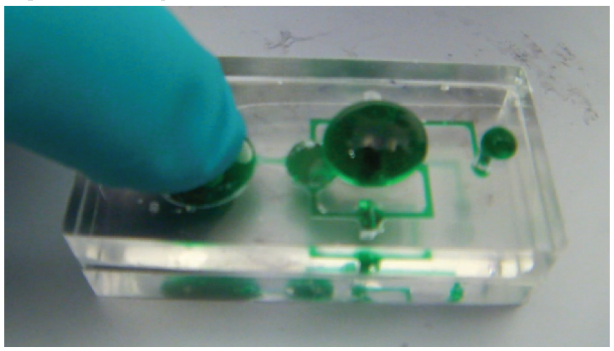

(b) Pumping in the Injection Molded Device with Two Inlet Ports

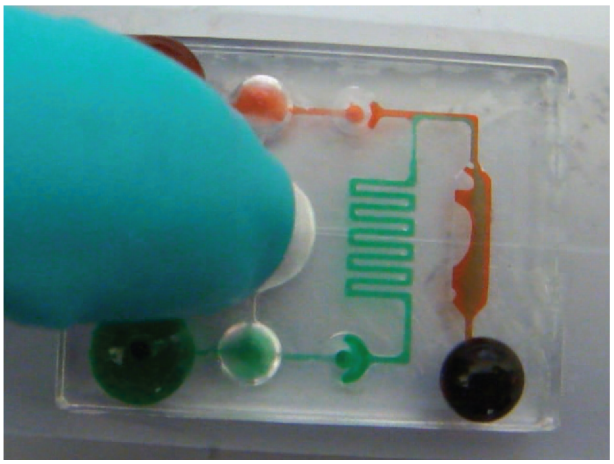

Figure 2.9 *Demonstration of pumping fluids in silicon rubber-based microfluidic systems fabricated via an injection molding process. The entire pumping operation was conducted by a single human finger on the fabricated prototypes with* ***(a)*** *one inlet port and* ***(b)*** *two inlet ports.*

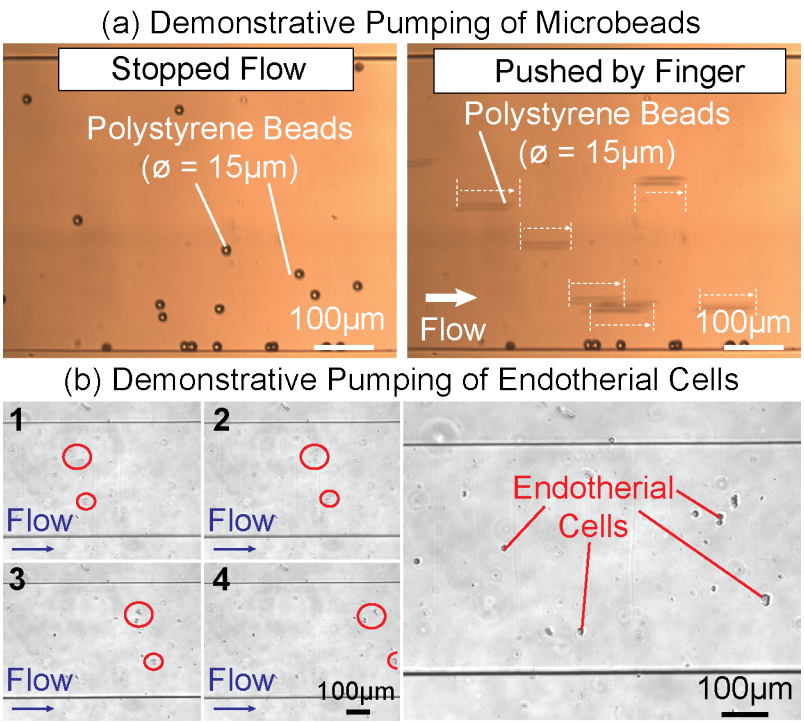

Figure 2.10 *Pumping of fluidic solution containing particles with finger-powered microfluidic systems, including* ***(a)*** *microbeads and* ***(b)*** *endotherial cells. This demonstration shows that our diode structure does not block small particles in the fluidic solution.*

2.3.3 Consistency and Reliability

In addition to the pressure head measurements associated with a single push operation (**Fig. 2.7**), we quantified the consistency of repeated push-and-release procedures executed by a human finger with duty cycles of 0.5, 5, and 10 seconds in **Figs. 2.11a-c,** respectively, using a pressure chamber of 10 mm in diameter. Specifically, under a short duty cycle of 0.5 second, the pressure head was measured as 3.4±0.3 (**Fig. 2.11a**), which is lower than other tests with a much large standard deviation. We believe that during the short and fast push-and-release operations, the finger have trouble deforming the chamber consistently and fully such that the output pressure head is reduced and non-uniform. The consistency improves for the duty cycles of 5 seconds and the output magnitude also increases to 3.7±0.2 (**Fig. 2.11b**). Results from the duty cycles of 10 seconds show the pressure head further increases a bit (**Fig. 2.11c**). It also reveals that under a longer operation period, the compressed gas in the system is leaking as the resulting pressure head is decreasing over time. These results suggest that the peak pressure during the push operation can generally be achieved and sustained without a significant pressure drop. The slightly pressure drop, on the other hand, could be attributed to the leakage and absorption of air by the porous PDMS structure.[50] For applications in which reducing this pressure drop is a critical parameter, prior reports have found that this absorption effect can be limited by conducting an additional surface coating process.[51]

To examine the reliability of the PDMS-based finger-powered pumping system, we also performed reliability testing with a repeated 5 seconds duty cycle over the course of 1 hour (360 cycles) on a different prototype pump as shown in **Figure 2.11d**. Each data point represents the pressure difference between the maximum and minimum pressure inside the chamber during each push-and-release procedure. The pressure was found to remain relatively constant during the 1-hour operation, which suggests that the system has sufficient durability for many common microfluidic applications. The average pressure increase during each push-and-release procedure was 4.11±0.3 kPa (**Fig. 2.11d** – *red dashed line*). The variation of the generated pressure was found to increase slightly to 6.58% compared with the variation of the pressure measurements using a load cell (**Fig. 2.7d**).

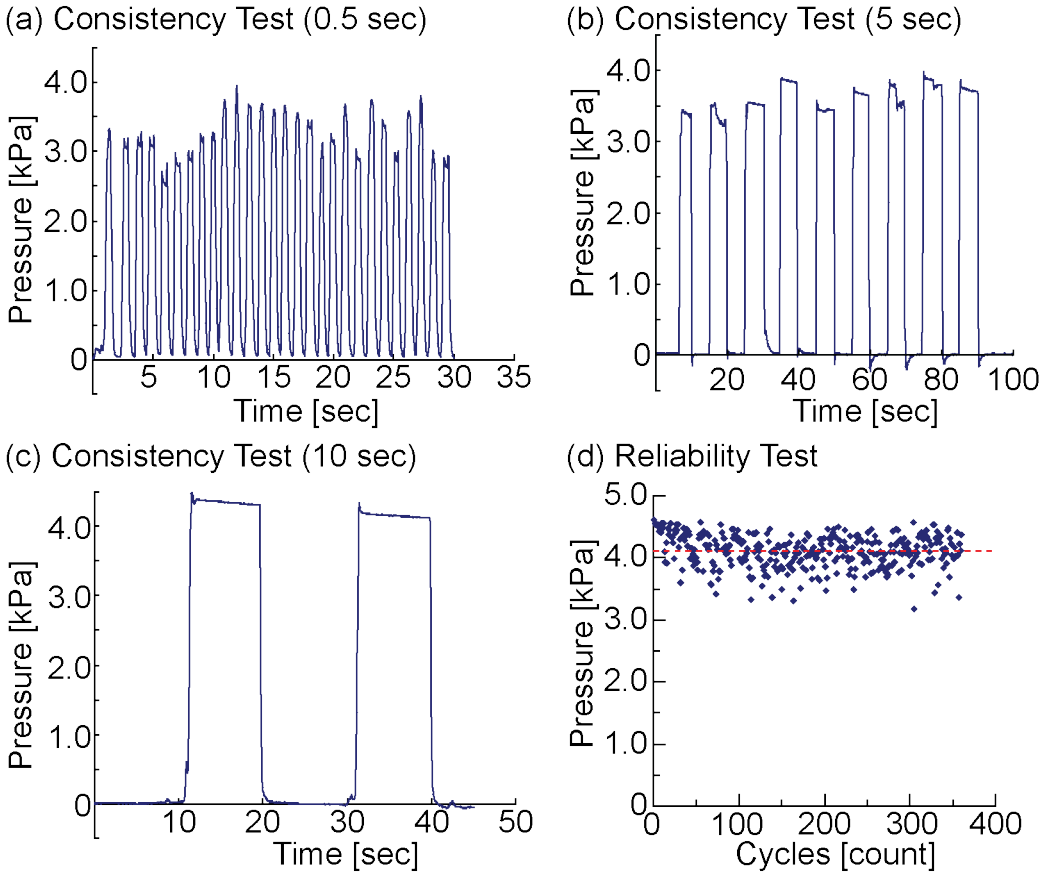

Figure 2.11 *Real-time measurement of pressure increment of the pressure chamber during repeated push-and-release by a human finger with duty cycle of* ***(a)*** *0.5 seconds,* ***(b)*** *5 seconds, and* ***(c)*** *10 seconds.* ***(d)*** *Pressure increment from continuous operations of 10 seconds in duty cycle for 1 hour.*

2.3.4 Finger-Powered Microdroplet Generation

The implementation of finger-powered pumps to microdroplet generation systems has two fundamental challenges: (*i*) two different fluids, oil and water, must be loaded simultaneously,

and (*ii*) their flow rates must be controlled adequately to ensure successful generations of droplets.[28] We fabricate a system with multiple inlets for different fluids and the finger-powered pump with the design of a T-junction to form microdroplets (**Fig. 2.6 and Fig. 2.12a**). The T-junction consists of a narrow channel for droplet fluids and a main channel for outer fluids. We designed the narrow channel with 50 μm in width and 10 mm in length, and the main channel with 100 μm in width and 4 mm in length (**Fig. 2.6b**). With these dimensions, the fluidic resistance for the droplet fluids is approximately eleven times larger than the main channel from the Hagen-Poiseuille equation (**Eq. 1**). We used Hexadecane (Sigma Aldrich, USA) as an oil background fluid and red dyed DI water as a droplet fluid for better visibility. Hexadecane was mixed with Span 80 (5% w/v, Sigma Aldrich, USA) to prevent the merging of the droplets and forming larger droplets.[26] First, the microchannel was filled only with Hexadecane by the finger-powered pump. Afterwards, DI water was placed onto the proper solution inlet. By repeatedly conducting the push-and-release sequences, DI water was introduced into the T-junction. Because the dynamic viscosity of Hexadecane is three times larger than that of water at room temperature and the fluidic resistance of the droplet channel is eleven times larger than the main channel, the flow rate of the Hexadecane will be approximately 3.75 times faster than the water flow. At the T-junction, the Hexadecane cut into the path of DI water, resulting in the formation of microdroplets of DI water in Hexadecane (**Fig. 2.12b**). The generated droplets were transported into the observation chamber (to decrease the flow velocity) (**Fig. 2.12c**). A histogram of the generated water-in-oil droplets is shown in **Figure 2.12d**. The average diameter was observed to be 106.9 μm with a standard deviation of 4.3 μm (*i.e.*, CV = 4.02%). The diameter of the droplets can be controlled by changing the channel geometry as key control parameters for droplet formations are the cross sectional area of the channel, and the flow rate ratio of the droplet solution and the solvent solution.[28] The variation of the droplet diameter was larger than other reports due to the larger pressure variations using the push-and-release process.[52] To achieve higher monodispersity, longer duty cycles could be used to reduce the pressure variations. Alternatively, the method of passive microfluidic particle sorting can be integrated after the T-junction to collect droplets with desired diameters.[53]-[55]

For situations in which it is preferable to suspend aqueous samples in oil phase, oil-in-water droplets can be generated in the same prototype system with modified surface properties. PDMS is naturally hydrophobic and suitable for forming water-in-oil droplets. We treated the surface of the microchannels with oxygen plasma and modified it from hydrophobic to hydrophilic.[56] The oil-in-water formation process started with filling the device with DI water (dyed blue for enhanced visibility). Afterwards, Hexadecane was introduced from the droplet solution inlet port. DI water was mixed with Tween 20 (5% w/v, Sigma Aldrich, USA) in advance to prevent the merging of droplets to form larger droplets. **Figure 2.13a** shows the formation of the oil-in-water droplets at the T-junction after the push-and-release procedure on the finger pump. One issue with the PDMS-based prototype devices is that PDMS can degrade over time with organic solvents such as Hexadecane. For example, in device experimentations, slight microchannel deformation was observed after a few minutes of droplet formation. During the formation of water-in-oil droplets (when the system is filled with Hexadecane), such degradation was exacerbated. To prevent this issue, the surface characteristics of the device can be modified or the materials can be changed to more durable materials.[57], [58]

We also experimentally investigated the potential to encapsulate suspended microparticles within the droplets. Because the fabricated prototype included two separate inlets for water phase solutions, one of these inlets can be replaced with a suspension of microparticles (*e.g.*, cells) in order to mix and encapsulate suspended particles in droplets. Experimental device runs revealed effective cell encapsulation using a single human finger by infusing bovine aortic endothelial cells (BAECs) suspended in Dulbecco's modified Eagle medium (DMEM) with 10% fetal bovine serum (FBS). Micrographs of droplet-encapsulated cells are shown in **Figure 2.13b**.

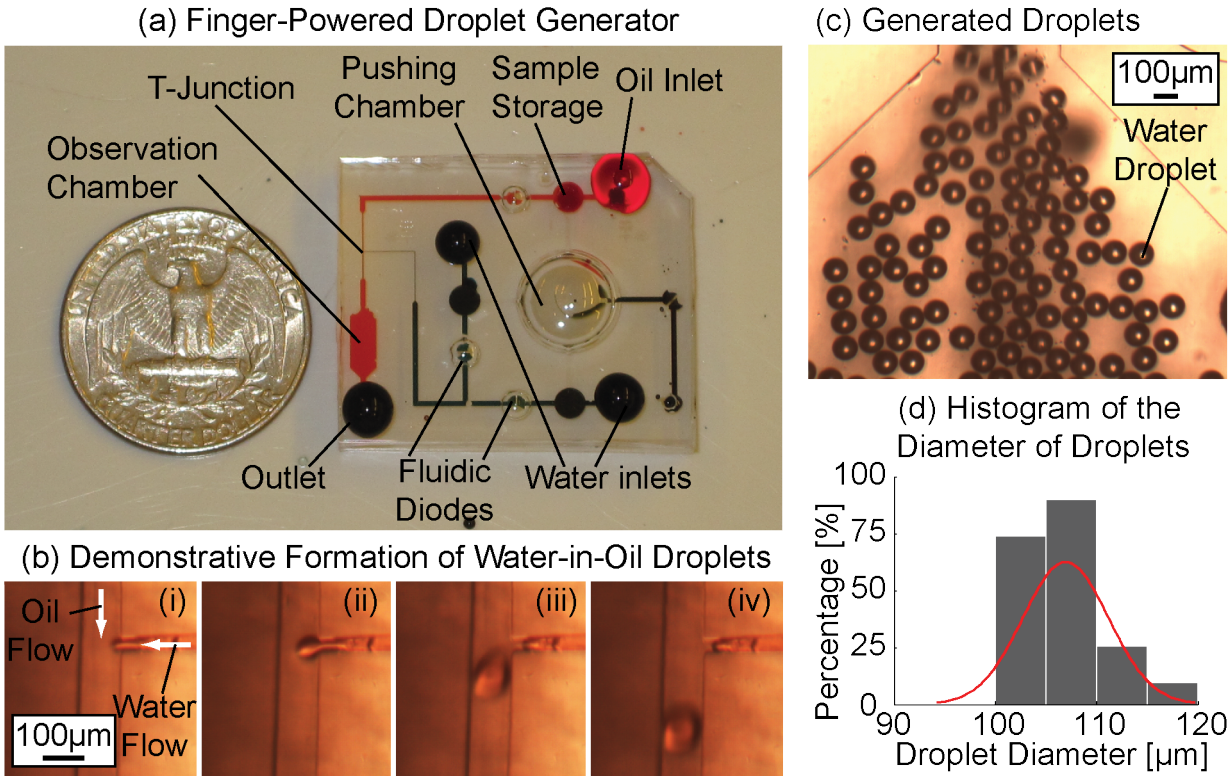

Figure 2.12 *Finger-powered microdroplet generator.* ***(a)*** *Fabrication results for the finger-powered droplet generator with colored oil (red) and water (green) input phases.* ***(b)*** *Sequential micrographs of droplet generation.* ***(c)*** *Generated water-in-oil microdroplets in the observation chamber.* ***(d)*** *Histogram of the diameter of water-in-oil droplets. The mean diameter was 106.9 μm with a standard deviation of 4.3 μm*

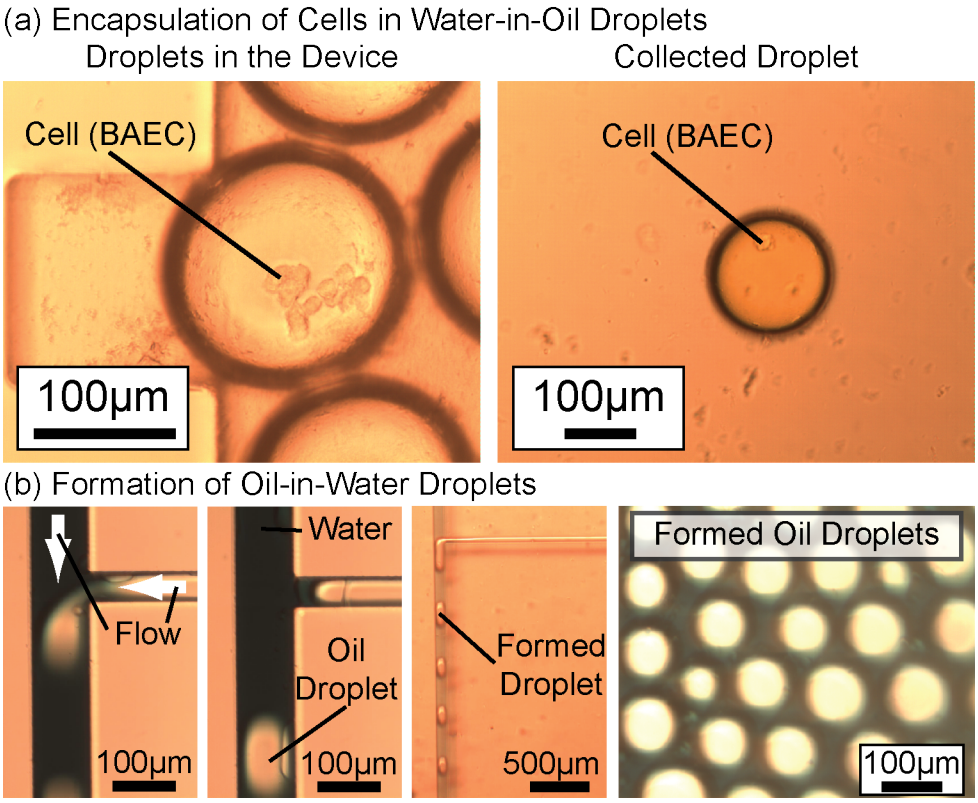

Figure 2.13 *Demonstrations of the formation of other microdroplets from an integrated finger-powered microdroplet generator.* ***(a)*** *Oil-in-water droplets – the surface of the microchannels was modified to hydrophilic with a plasma treatment.* ***(b)*** *Bovine aortic endothelial cells (BAEC) in water-in-oil droplets. BAEC are suspended in Dulbecco's modified Eagle medium (DMEM) with 10% fetal bovine serum (FBS).*

2.3.5 Finger-Powered Bead-in-Droplet Cyctokine Detection System

To demonstrate a possible future application of the finger-powered microdroplet generator for biomedical usages, we employ a bead-in-droplet microfluidic methodology to accomplish biomolecule detection assays. **Figure 2.14a** illustrates the basic concept of the finger-powered bead-in-droplet system. We add additional inlet port to infuse the functionalized microbead suspension, as well as sample cytokine solution, and oil fluids simultaneously. When the pressure chamber (10 mm in diameter) is pushed by a human finger all the solutions are infused into the system. Infused microbeads are mixed with the sample solution at the T-junction that has a 50 μm-wide main channel for the oil fluid and two 25 μm-wide subchannels before forming droplets to maintain equal starting timing for the chemical reactions of the microbeads and the samples.[25] Formed droplets are transferred to the subsequent observation chamber and immobilized at the trapping sites (30 μm square chambers with narrow orifices of 10 μm in width) in the observation chamber.[3] After a droplet with microbeads is trapped, the fluidic resistance through the trapping site is increased, which limits fluid flow. This phenomenon prevents additional droplets from being immobilized once a trapping site is occupied. After

droplets are formed and immobilized (and the sample biomolecules bind to the surface of the functionalized microbeads), we can observe the chemical reaction as an increase in fluorescence on the surface of the functionalized microbeads.

To detect the inflammatory cytokine, interferon-gamma (IFN-γ), we utilize surface modified microbeads with aptamer beacons. Conceptual illustrations of the surface-modified microbeads are shown in **Figure 2.14b**. The aptamer beacon used in this study has been designed previously by Tuleuova *et al*. [59], [60] and consists of two complementary single-stranded DNA sequences of fluorescent aptamer and a quencher. Because quenchers restrict the fluorescent signals emitted from fluorescent aptamers, the microbeads do not indicate fluorescence with its original state.[60], [61] When mixed with a solution of IFN- γ, IFN- γ displaces the quenchers and binds with the fluorescent aptamers, which results in fluorescence, corresponding to the concentration of IFN-γ in the solution. The sequence of the aptamer beacon and the quencher is shown in **Table 2.1**.[59], [60]

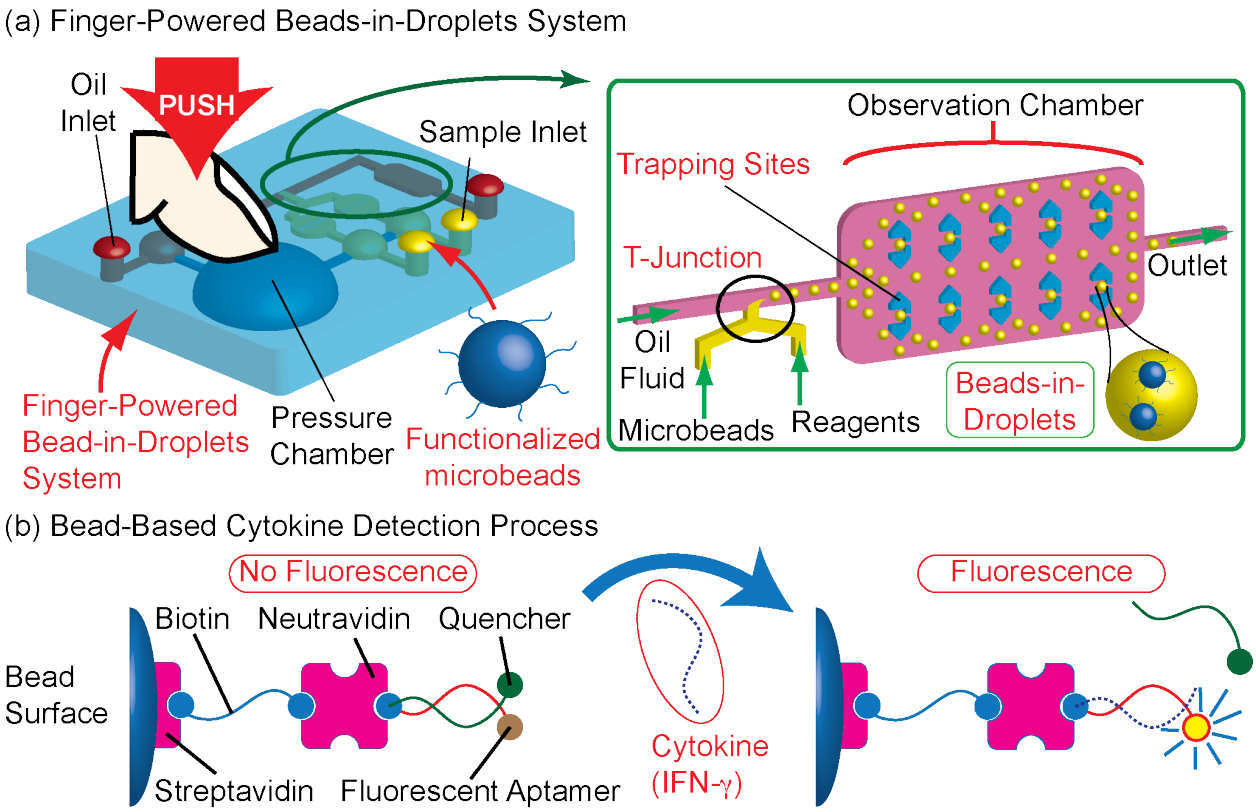

Figure 2.14 *Concept of the 'finger-powered' bead-in-droplet microfluidic system.* ***(a)*** *When pushed by a human finger, the pressure chamber infuses flows into the microchannels (left). Functionalized microbeads are mixed with reagents, encapsulated within microdroplets, and immobilized via trapping architectures (right) for observation. We demonstrate our device by conducting a cytokine detection assay utilizing microbeads functionalized with aptamer beacons. (b) Conceptual illustrations of surface-modified microbeads to detect the cytokine, interferon-gamma (IFN-γ). When IFN-γ binds with the fluorescent aptamer, it replaces the quencher,*

resulting in fluorescence on the surface of the microbeads. The fluorescent intensity corresponds with the concentration of the IFN-γ.

Table 2.1 *Sequences (5'-3' orientation) for the Aptamer Beacon [59], [60]*

Material	Sequence
Fluorescent Aptamer	6-F AM-TGGGGTTGGTTGTGTTGGGTGTTGTGT
Quencher	ACAACCAACCCCA-BHQ-1

We fabricate the prototype device with the same multi-layer soft lithography process as discussed in **Chapter 2.2.3**, except for the thickness of the main channel. We spincoat 15 μm of SU-8/2010 instead of 90 μm of SU-8/2050 to maintain the structure of the trapping sites that is designed for trapping microbeads (ø = 15 μm in diameter, polystyrene). **Figure 2.15** shows the fabricated prototype device (2.8 cm-long, 1.9 cm-wide, and 0.8 cm-thick).

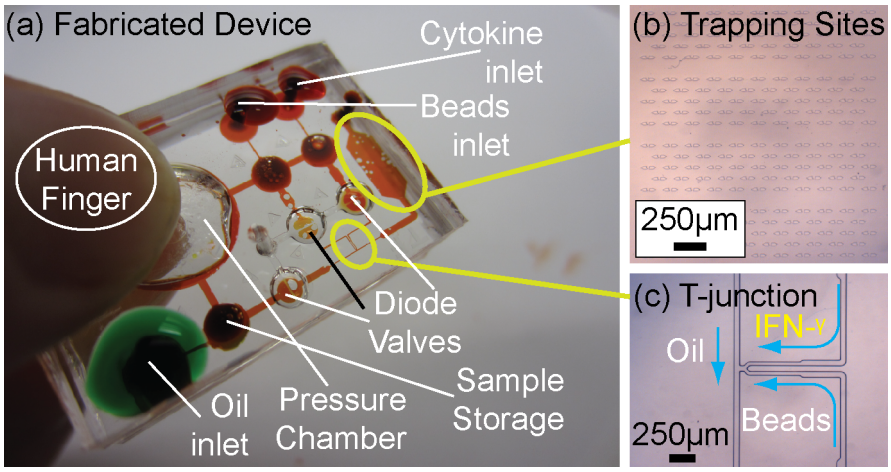

Figure 2.15 *Fabricated device.* ***(a)*** *The device is 2.8 cm-long, 1.9 cm-wide, and 0.8 cm-thick. Oil inlet is shown in green and beads/cytokine inlets are shown in red. It has* ***(b)*** *212 trapping sites and* ***(c)*** *T-junction to form and observe bead-in-droplet.*

The potential to employ the presented device for biomolecular detection has been experimentally demonstrated by detecting the inflammatory cytokine, IFN-γ. First, we infuse the functionalized microbeads suspended with phosphate buffered saline (PBS), 200 μM solution of IFN-γ, and oil into the device and formed microdroplets. We use Hexadecane as an oil phase and added Span80 with a concentration of 5 wt% to Hexadecane to prevent an aggregation of formed droplets. We observe that droplets are formed at the T-junction and some of the droplets contain functionalized microbeads as shown in **Figure 2.16a**. Next, formed droplets containing microbeads are transferred to the observation chamber and immobilized at the trapping sites

(**Fig. 2.16b**). We observe the tendency that the formed droplets without microbeads have relatively less possibility to be trapped at the trapping sites, compared with the droplets with microbeads as droplets without microbeads can be easily deformed by a hydrodynamic pressure and squeeze through the gaps of trapping sites. In addition, very few of the unnecessary droplets such as satellite droplets or aggregated droplets are trapped as the smaller satellite droplets pass through the gaps of the trapping sites.

We acquire fluorescent images of the immobilized microbeads. One of the fluorescent images is shown in **Figure 2.16c**. We can observe that the microbeads in the droplets have higher fluorescent intensity than the droplets without microbeads. These fluorescent images are analyzed using the software, ImageJ. We calculate the total intensity level at the microbeads and the background noise was subtracted from the calculated intensity level. To get a control data, we measure an intensity level of functionalized microbeads mixed with PBS instead of IFN-γ solutions with the same procedure. The results are shown in **Figure 2.16d**. We observe that the intensity level of the functionalized microbeads is higher than the intensity level of the control data. These results suggest that the IFN-γ has successfully displaced the quenchers of the microbead-immobilized aptamer beacons, indicating the presented system has an ability to detect cytokine and could be adapted for point-of-care diagnostics applications.

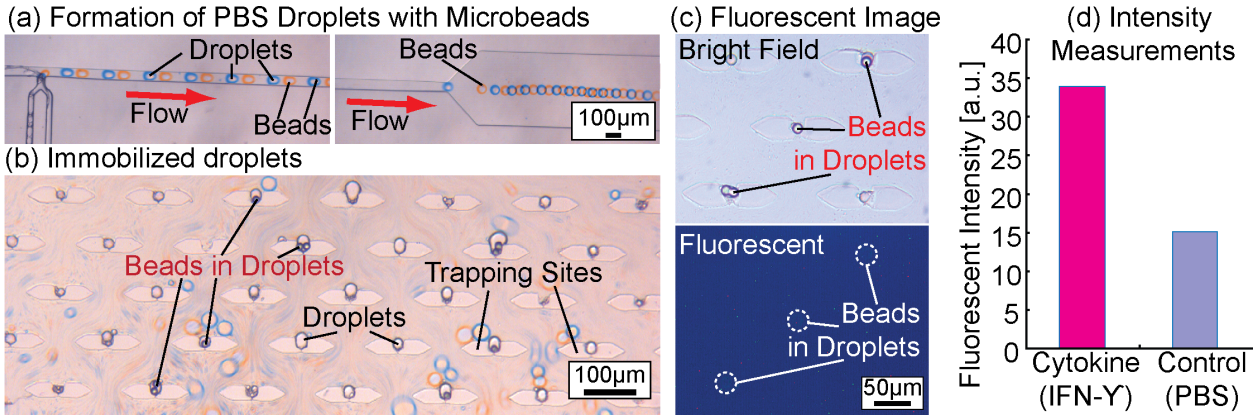

Figure 2.16 *Experimental results for cytokine detection using the 'finger-powered' bead-in-droplet microfluidic system.* ***(a)*** *Droplet formation with microbeads.* ***(b)*** *Immobilizing the droplets at trapping sites and measured its intensity.* ***(c)*** *Bright field image and fluorescent image of immobilized droplets. Microbeads in droplets are indicated as dashed lines in the fluorescent image. Contrast and brightness of the fluorescent image are modified for better visibility.* ***(d)*** *The intensity of the microbeads has increased and successfully detected cytokine in the droplet.*

References of Chapter 2

[1] P. Yager, G. J. Domingo, and J. Gerdes, "Point-of-care diagnostics for global health," *Annu Rev Biomed Eng*, vol. 10, pp. 107–144, 2008.

[2] C. D. Chin, V. Linder, and S. K. Sia, "Lab-on-a-chip devices for global health: Past studies and future opportunities," *Lab on a Chip*, vol. 7, no. 1, pp. 41–57, 2007.

[3] D. Di Carlo, L. Y. Wu, and L. P. Lee, "Dynamic single cell culture array," *Lab on a Chip*, vol. 6, no. 11, pp. 1445–1449, 2006.

[4] D. Di Carlo and L. P. Lee, "Dynamic single-cell analysis for quantitative biology," *Anal Chem*, vol. 78, no. 23, pp. 7918–7925, 2006.

[5] D. Di Carlo, N. Aghdam, and L. P. Lee, "Single-cell enzyme concentrations, kinetics, and inhibition analysis using high-density hydrodynamic cell isolation arrays," *Anal Chem*, vol. 78, no. 14, pp. 4925–4930, 2006.

[6] D. A. Mair, E. Geiger, A. P. Pisano, J. M. J. Frechet, and F. Svec, "Injection molded microfluidic chips featuring integrated interconnects," *Lab on a Chip*, vol. 6, no. 10, pp. 1346–1354, Oct. 2006.

[7] Y.-C. Su, J. Shah, and L. Lin, "Implementation and analysis of polymeric microstructure replication by micro injection molding," *J Micromech Microeng*, vol. 14, no. 3, p. 415, 2003.

[8] F. Sammoura, J. Kang, Y.-M. Heo, T. Jung, and L. Lin, "Polymeric microneedle fabrication using a microinjection molding technique," *Microsystem Technologies*, vol. 13, no. 5, pp. 517–522, 2007.

[9] D. Beebe, G. Mensing, and G. Walker, "Physics and applications of microfluidics in biology," *Annu Rev Biomed Eng*, vol. 4, pp. 261–286, 2002.

[10] K. P. Kamper, J. Dopper, W. Ehrfeld, and S. Oberbeck, "A self-filling low-cost membrane micropump," presented at the Micro Electro Mechanical Systems, 1998. MEMS 98. Proceedings., The Eleventh Annual International Workshop on, 1998, pp. 432–437.

[11] V. Piotter, T. Hanemann, R. Ruprecht, and J. Hausselt, "Injection molding and related techniques for fabrication of microstructures," *Microsystem Technologies*, vol. 3, no. 3, pp. 129–133, May 1997.

[12] N. J. Graf and M. T. Bowser, "Effect of cross sectional geometry on PDMS micro peristaltic pump performance: comparison of SU-8 replica molding vs. micro injection molding," *Analyst*, vol. 138, no. 19, pp. 5791–5800, 2013.

[13] L. J. Kricka, P. Fortina, N. J. Panaro, P. Wilding, G. Alonso-Amigo, and H. Becker, "Fabrication of plastic microchips by hot embossing," *Lab on a Chip*, vol. 2, no. 1, pp. 1–4, 2002.

[14] M. A. Roberts, J. S. Rossier, P. Bercier, and H. Girault, "UV laser machined polymer substrates for the development of microdiagnostic systems," *Anal Chem*, vol. 69, no. 11, pp. 2035–2042, 1997.

[15] G. Walker and D. Beebe, "A passive pumping method for microfluidic devices," *Lab on a Chip*, vol. 2, no. 3, pp. 131–134, 2002.

[16] I. Meyvantsson, J. W. Warrick, S. Hayes, A. Skoien, and D. J. Beebe, "Automated cell culture in high density tubeless microfluidic device arrays," *Lab on a Chip*, vol. 8, no. 5, pp. 717–724, 2008.

[17] P. B. Lillehoj, F. Wei, and C.-M. Ho, "A self-pumping lab-on-a-chip for rapid detection

of botulinum toxin," *Lab on a Chip*, vol. 10, no. 17, pp. 2265–2270, 2010.
[18] A. W. Martinez, S. T. Phillips, and G. M. Whitesides, "Three-dimensional microfluidic devices fabricated in layered paper and tape," *P Natl Acad Sci Usa*, vol. 105, no. 50, pp. 19606–19611, 2008.
[19] A. W. Martinez, S. T. Phillips, E. Carrilho, S. W. Thomas, H. Sindi, and G. M. Whitesides, "Simple telemedicine for developing regions: Camera phones and paper-based microfluidic devices for real-time, off-site diagnosis," *Anal Chem*, vol. 80, no. 10, pp. 3699–3707, 2008.
[20] Y. Su, L. Lin, and A. Pisano, "A water-powered osmotic microactuator," *J Microelectromech S*, vol. 11, no. 6, pp. 736–742, 2002.
[21] Y. Su and L. Lin, "A water-powered micro drug delivery system," *J Microelectromech S*, vol. 13, no. 1, pp. 75–82, 2004.
[22] I. K. Dimov, L. Basabe-Desmonts, J. L. Garcia-Cordero, B. M. Ross, A. J. Ricco, and L. P. Lee, "Stand-alone self-powered integrated microfluidic blood analysis system (SIMBAS)," *Lab on a Chip*, vol. 11, no. 5, pp. 845–850, 2011.
[23] K. J. Cha and D. S. Kim, "A portable pressure pump for microfluidic lab-on-a-chip systems using a porous polydimethylsiloxane (PDMS) sponge," *Biomed Microdevices*, vol. 13, no. 5, pp. 877–883, 2011.
[24] X. Qiu, J. A. Thompson, Z. Chen, C. Liu, D. Chen, S. Ramprasad, M. G. Mauk, S. Ongagna, C. Barber, W. R. Abrams, D. Malamud, P. L. A. M. Corstjens, and H. H. Bau, "Finger-actuated, self-contained immunoassay cassettes," *Biomed Microdevices*, vol. 11, no. 6, pp. 1175–1186, 2009.
[25] J. Tice, H. Song, A. Lyon, and R. Ismagilov, "Formation of droplets and mixing in multiphase microfluidics at low values of the Reynolds and the capillary numbers," *Langmuir*, vol. 19, no. 22, pp. 9127–9133, 2003.
[26] S.-Y. Teh, R. Lin, L.-H. Hung, and A. P. Lee, "Droplet microfluidics," *Lab on a Chip*, vol. 8, no. 2, pp. 198–220, 2008.
[27] A. B. Theberge, F. Courtois, Y. Schaerli, M. Fischlechner, C. Abell, F. Hollfelder, and W. T. S. Huck, "Microdroplets in Microfluidics: An Evolving Platform for Discoveries in Chemistry and Biology," *Angew Chem Int Edit*, vol. 49, no. 34, pp. 5846–5868, 2010.
[28] P. Garstecki, M. Fuerstman, H. Stone, and G. Whitesides, "Formation of droplets and bubbles in a microfluidic T-junction - scaling and mechanism of break-up," *Lab on a Chip*, vol. 6, no. 3, pp. 437–446, 2006.
[29] M. Hashimoto and G. M. Whitesides, "Formation of Bubbles in a Multisection Flow-Focusing Junction," *Small*, vol. 6, no. 9, pp. 1051–1059, 2010.
[30] S. Takeuchi, P. Garstecki, D. Weibel, and G. Whitesides, "An axisymmetric flow-focusing microfluidic device," *Advanced Materials*, vol. 17, no. 8, pp. 1067–+, 2005.
[31] F. Shen, W. Du, J. E. Kreutz, A. Fok, and R. F. Ismagilov, "Digital PCR on a SlipChip," *Lab on a Chip*, vol. 10, no. 20, pp. 2666–2672, 2010.
[32] K. A. Heyries, C. Tropini, M. Vaninsberghe, C. Doolin, O. I. Petriv, A. Singhal, K. Leung, C. B. Hughesman, and C. L. Hansen, "Megapixel digital PCR," *Nat Methods*, vol. 8, no. 8, pp. 649–U64, 2011.
[33] M. Srisa-Art, A. J. deMello, and J. B. Edel, "High-throughput DNA droplet assays using picoliter reactor volumes," *Anal Chem*, vol. 79, no. 17, pp. 6682–6689, 2007.
[34] S.-H. Kim, J. W. Kim, J.-C. Cho, and D. A. Weitz, "Double-emulsion drops with ultra-thin shells for capsule templates," *Lab on a Chip*, vol. 11, no. 18, pp. 3162–3166, 2011.

[35] K. Iwai, R. Sochol, and L. Lin, “Finger-powered, pressure-driven microfluidic pump,” *Micro Electro Mechanical Systems (MEMS), 2011 IEEE 24th International Conference on*, pp. 1131–1134, 2011.
[36] W. Li, T. Chen, Z. Chen, P. Fei, Z. Yu, Y. Pang, and Y. Huang, “Squeeze-chip: a finger-controlled microfluidic flow network device and its application to biochemical assays,” *Lab on a Chip*, vol. 12, no. 9, pp. 1587–1590, 2012.
[37] M. M. Gong, B. D. MacDonald, T. V. Nguyen, and D. Sinton, “Hand-powered microfluidics: A membrane pump with a patient-to-chip syringe interface,” *Biomicrofluidics*, vol. 6, no. 4, p. 044102, 2012.
[38] M. Adams, M. Johnston, A. Scherer, and S. Quake, “Polydimethylsiloxane based microfluidic diode,” *J Micromech Microeng*, vol. 15, no. 8, pp. 1517–1521, 2005.
[39] W. Grover, A. Skelley, C. Liu, E. Lagally, and R. Mathies, “Monolithic membrane valves and diaphragm pumps for practical large-scale integration into glass microfluidic devices,” *Sensor Actuat B-Chem*, vol. 89, no. 3, pp. 315–323, 2003.
[40] B. J. Kirby, *Micro- and Nanoscale Fluid Mechanics*. Cambridge University Press, 2010.
[41] D. Duffy, J. McDonald, O. Schueller, and G. Whitesides, “Rapid prototyping of microfluidic systems in poly(dimethylsiloxane),” *Anal Chem*, vol. 70, no. 23, pp. 4974–4984, 1998.
[42] B. Mosadegh, C.-H. Kuo, Y.-C. Tung, Y.-S. Torisawa, T. Bersano-Begey, H. Tavana, and S. Takayama, “Integrated elastomeric components for autonomous regulation of sequential and oscillatory flow switching in microfluidic devices,” *Nat Phys*, vol. 6, no. 6, pp. 433–437, 2010.
[43] C. A. Crosby, M. A. Wehbe, and B. Mawr, “HAND STRENGTH - NORMATIVE VALUES,” *J Hand Surg-Am*, vol. 19, no. 4, pp. 665–670, 1994.
[44] K. Iwai, W.-H. Tan, H. Ishihara, and S. Takeuchi, “A resettable dynamic microarray device,” *Biomed Microdevices*, vol. 13, no. 6, pp. 1089–1094, 2011.
[45] R. D. Sochol, A. Lu, J. Lei, K. Iwai, L. P. Lee, and L. Lin, “Microfluidic bead-based diodes with targeted circular microchannels for low Reynolds number applications,” *Lab on a Chip*, vol. 14, no. 9, pp. 1585–1594, 2014.
[46] R. D. Sochol, S. Li, L. P. Lee, and L. Lin, “Continuous flow multi-stage microfluidic reactors via hydrodynamic microparticle railing,” *Lab on a Chip*, 2012.
[47] R. D. Sochol, B. P. Casavant, M. E. Dueck, L. P. Lee, and L. Lin, “A dynamic bead-based microarray for parallel DNA detection,” *J Micromech Microeng*, vol. 21, no. 5, p. 054019, 2011.
[48] R. D. Sochol, D. Corbett, S. Hesse, W. E. R. Krieger, K. T. Wolf, M. Kim, K. Iwai, S. Li, L. P. Lee, and L. Lin, “Dual-mode hydrodynamic railing and arraying of microparticles for multi-stage signal detection in continuous flow biochemical microprocessors ,” *Lab on a Chip*, vol. 14, no. 8, pp. 1405–1409, 2014.
[49] R. D. Sochol, A. T. Higa, R. R. R. Janairo, S. Li, and L. Lin, “Unidirectional mechanical cellular stimuli via micropost array gradients,” *Soft Matter*, vol. 7, no. 10, pp. 4606–4609, 2011.
[50] M. W. Toepke and D. J. Beebe, “PDMS absorption of small molecules and consequences in microfluidic applications,” *Lab on a Chip*, vol. 6, no. 12, pp. 1484–1486, 2006.
[51] S. Hu, X. Ren, M. Bachman, C. E. Sims, G. P. Li, and N. L. Allbritton, “Surface-directed, graft polymerization within microfluidic channels,” *Anal Chem*, vol. 76, no. 7,

pp. 1865–1870, 2004.
[52] W.-A. C. Bauer, M. Fischlechner, C. Abell, and W. T. S. Huck, "Hydrophilic PDMS microchannels for high-throughput formation of oil-in-water microdroplets and water-in-oil-in-water double emulsions," *Lab on a Chip*, vol. 10, no. 14, pp. 1814–1819, 2010.
[53] M. Yamada and M. Seki, "Microfluidic particle sorter employing flow splitting and recombining," *Anal Chem*, vol. 78, no. 4, pp. 1357–1362, 2006.
[54] S. Choi and J.-K. Park, "Continuous hydrophoretic separation and sizing of microparticles using slanted obstacles in a microchannel," *Lab on a Chip*, vol. 7, no. 7, pp. 890–897, 2007.
[55] D. R. Gossett, W. M. Weaver, A. J. Mach, S. C. Hur, H. T. K. Tse, W. Lee, H. Amini, and D. Di Carlo, "Label-free cell separation and sorting in microfluidic systems," *Anal Bioanal Chem*, vol. 397, no. 8, pp. 3249–3267, 2010.
[56] S. Bhattacharya, A. Datta, J. M. Berg, and S. Gangopadhyay, "Studies on surface wettability of poly (dimethyl) siloxane (PDMS) and glass under oxygen-plasma treatment and correlation with bond strength," *J Microelectromech S*, vol. 14, no. 3, pp. 590–597, 2005.
[57] L. Tang and N. Y. Lee, "A facile route for irreversible bonding of plastic-PDMS hybrid microdevices at room temperature," *Lab on a Chip*, vol. 10, no. 10, pp. 1274–1280, 2010.
[58] H. Makamba, J. H. Kim, K. Lim, N. Park, and J. H. Hahn, "Surface modification of poly(dimethylsiloxane) microchannels," *Electrophoresis*, vol. 24, no. 21, pp. 3607–3619, Nov. 2003.
[59] N. Tuleuova, C. N. Jones, J. Yan, E. Ramanculov, Y. Yokobayashi, and A. Revzin, "Development of an Aptamer Beacon for Detection of Interferon-Gamma," *Anal Chem*, vol. 82, no. 5, pp. 1851–1857, 2010.
[60] R. Sochol, L. Lo, R. Ruelos, V. Chang, D. Bahri, K. Iwai, J. Lo, M. Dueck, L. Lee, and L. Lin, "Microfluidic Ping Pong for cytokine detection," *Micro Electro Mechanical Systems (MEMS), 2011 IEEE 24th International Conference on*, pp. 936–939, 2011.
[61] B. Moreira, Y. You, M. Behlke, and R. Owczarzy, "Effects of fluorescent dyes, quenchers, and dangling ends on DNA duplex stability," *Biochem Bioph Res Co*, vol. 327, no. 2, pp. 473–484, 2005.

Chapter 3: Continuous-Flow Microdroplets Reaction and Rupture Systems

3.1 Introduction

In various chemical and biological applications, such as nanoparticle synthesis, genomics, cellular studies, and point-of-care diagnostics, rapid and high-throughput processing is essential to handle large numbers of samples and reagents. In recent years, droplet-based microreactors have been proposed [1]-[4] for the aforementioned applications due to a variety of potential benefits; i) rapid reaction time, ii) small amount of samples, iii) low background noise, and iv) good microenvironment control. For example, microreactors technologies have been proposed for the commercial-scale synthesis of nanoparticles with well-controlled size and monodispersity [5], which is critical for various potential applications. In another example, the integration of microbeads and microdroplets as the architecture of "bead-in-droplet" microreactors have been powerful tools using microbeads as substrates in microfluidic assays [6]. Particularly, microbeads have unique properties of high surface area-to-volume ratios, easy handling in microfluidic systems, and functionalization schemes as molecular detection probes in a variety of applications, including high-throughput DNA sequencing [7], [8]. As such, researchers have already developed automated on-chip droplet handling techniques, such as the formation of droplets (*e.g.*, T-junctions and flow focusing techniques) [9], [10], and the fusion of droplets with reagents to initiate chemical reactions inside droplets [11]-[13]. These and other microdroplets-based reports suggest the broad interests and potentials of droplet-based microfluidic systems.

On the other hand, methodologies for the retrieval of the contents inside microdroplets are often laborious and time-consuming, including "off-chip" processes in centrifugication, aspiration and resuspension [5]. For example, nanoparticle synthesis generally requires the retrieval and separation of synthesized nanoparticles in aqueous microdroplets from the typical carrier fluids of various oil solutions. In the example of bead-in-droplet applications, multiple assays such as washing and mixing of beads with different solutions are essential. The complete alterations of solutions inside the microdroplets will require beads in the original microdroplets to be released and transferred into new microdroplets of different solutions. In both of these examples, one critical challenge is the retrieval of contents in the microdroplets (particles or beads) by rapturing the droplets and a continuous-flow reaction system for rapid and high-throughput applications.

In recent years, the methodology of continuous-flow microfluidic systems has been shown as a potential high-throughput process [14]. For example, researchers have developed micropost array railing methodologies to passively guide suspended microparticles (*e.g.*, microbeads, cells and microdroplets) into discrete, adjacent solutions under continuous-flow conditions [5], [15]-[19]. Here, we propose to utilize the continuous micropost array railing system to demonstrate several advanced microfluidic processing capabilities, including the techniques of continuous reaction, wash, and rupture of microdroplets to separate and retrieve their contents (particles or beads) from oil solutions. The proposed microdroplets reaction and rupture scheme is further integrated with other microfluidic components for system-level

demonstrations, including (1) continuous synthesis and centrifugal-free retrieval of nanoparticles, and (2) continuous bead-in-droplet microreactors with varying solutions. The architecture of this continuous-flow microdroplets reaction and rapture systems could expand the potentials of microdroplets for emerging biological/chemical applications when multi-stage processes are required.

3.2 Rupture of Microdroplets

3.2.1 Operation Principle

Figure 3.1 illustrates the basic concept of the microdroplet rupture system. The system consists of arrayed microposts and three microfluidic flow channels, corresponding to continuous loading of water-in-oil droplets with surfactant (*yellow*), oil without surfactant (*blue*), and water flow (*magenta*). As shown in other prior reports, the arrayed microposts enable suspended microparticulates to be guided without disrupting the primary flow directions of the continuously loaded fluids [6], [15], [18]-[20]. At the first junction (*see* **Fig. 3.1**), microdroplets are guided from the oil flow with surfactant to the oil flow without surfactant, which serves to remove the surfactant from the droplets. At the second junction, the shear force of the water flow combined with the surface tension of the droplets result in the collapse of the droplets, thereby releasing the contents of the droplets into the water flow. Thereafter, the water solution containing the contents of the droplets is collected at the outlet while the oil phase flows are directed to the waste ports.

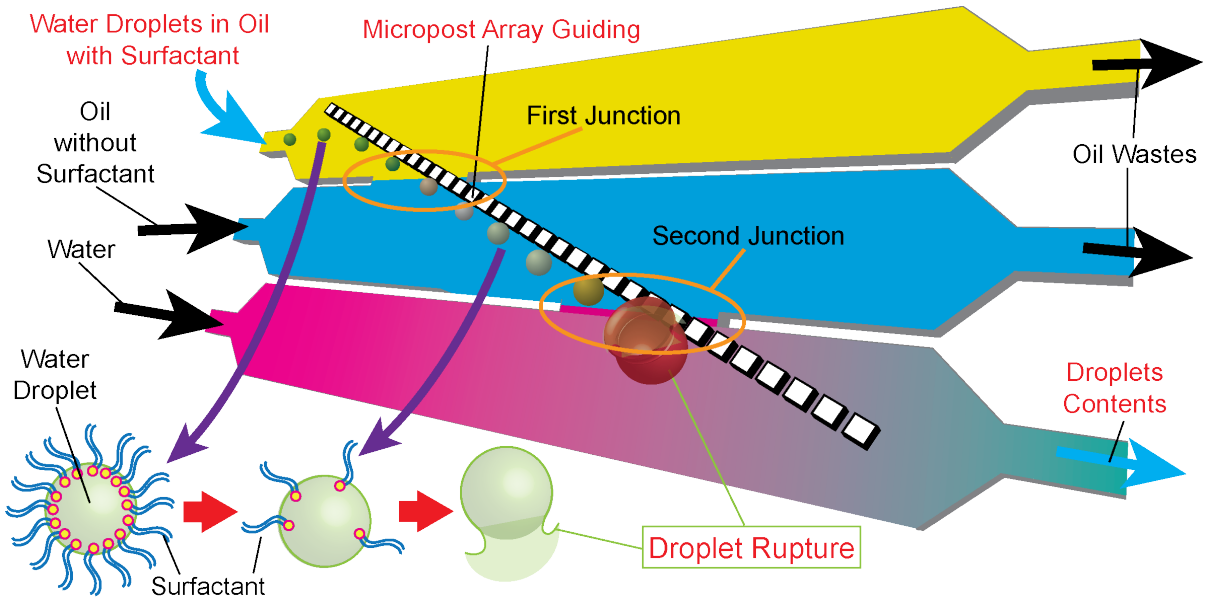

Figure 3.1 *Conceptual illustrations of the continuous flow microdroplets rupture system. Fluids including water-in-oil droplets with surfactant (yellow), oil without surfactant (blue), and water flow (magenta) are continuously inputted in parallel. The arrayed microposts passively guide the droplets into the adjacent flow streams to wash the droplets (and remove the surfactant) and then rupture the droplets. This process enables the contents inside the microdroplets to be retrieved for subsequent analysis and/or use by additional microfluidic components.*

One of the typical surfactants commonly used in experiments is Span 80, which is a non-ionic surfactant with a hydrocarbon chain making it soluble in oil and a polar group giving its affinity to water. The purpose of surfactant is to decrease the interfacial tension between the oil and water phases, thereby facilitating the formation of water droplets (emulsification) as there is only a relatively small increase in the free surface energy associated with emulsion formation. Here, the free surface energy is the energy necessary to form new surface [7], [8], [21] and the interfacial tension is given as:

$$\gamma = \gamma_0 - \pi \tag{3.1}$$

where γ is the interfacial tension energy after the addition of the surfactant, γ_o is the initial surface tension and π is the surface pressure of the absorbed layer of surfactant. When the interfacial tension is reduced to a certain level, formation of stable microdroplets can occur[9], [10], [21]. The thermodynamic stability of the droplets can be explained by the Gibbs adsorption equation,

$$\Gamma = -\frac{c}{RT}\frac{d\gamma}{dc} \tag{3.2}$$

where Γ is the surface excess concentration, c is the concentration in the solvent, R is the ideal gas constant, T is the temperature and γ is the interfacial tension. **Equation 3.2** is the estimation of the absorption of surfactant at the interface based on its concentration and its surface tension as a function of concentration. The concentration of the surfactant above which the interfacial tension is constant is named as critical micelle concentration (c.m.c.) [11]-[13], [21]. The surface tension decreases until the concentration reaches the c.m.c. and then it stays constant above this value. The c.m.c. of Span 80 in various oils such as hexane, pentane, decane, etc. is estimated in the range of 10^{-5} M due to its similar chemistry to other oils used in experiments [5], [22]. In our prototype experiments, the concentration of Span 80 used in hexadecane is 2% by weight which corresponds to a molarity of 36 mM and is much higher than the c.m.c. In other words, droplets formed in the hexadecane with 2% Span 80 are stable and it is not possible to coalesce them easily. Therefore for the purpose of this work, a way to disrupt this stability is required. As shown in **Figure 3.1**, microdroplets are first washed in pure oil (hexadecane without Span 80) to reduce the concentration of surfactants to be below the c.m.c. and to eventually increase the surface tension between oil and water phase such that the emulsion is no longer stable. After flowing droplets in pure hexadecane, it is observed that they started to merge and later release their contents in the water flow.

3.2.2 Design of the Microdroplets Rupture System

Figure 3.2 illustrates the design details of the microdroplets rupture system. In order to make the continuous-flow microdroplets system, microposts (15×15 μm^2 squares; 5 μm separation gap) are arrayed at a 1º angle with respect to the direction of the fluid flow[14], [18], [19]. The microchannels are designed as 200 μm in width and separated with 15 μm-thick walls, and the junctions have 5 mm-long openings (**Fig. 3.2a**), which are designed to accommodate the microposts with 1º angle with the 50 μm gap to the separating walls to allow the passage of microdroplets. The first and second flow microchannels have minimum length of 12.5 mm to guide the microdroplets across the 200 μm-wide channel with 1º angled microposts. In the

prototype design, the first microchannel is 15 mm in length to including the inlet port. The second microchannel for the washing process is 13.5 mm in length, including a portion of 1 mm in length where the microposts are not tilted. This flat portion is designed to demonstrate the flexibility of the system to allow longer processing period. Specifically, if a high concentration surfactant was used, a longer washing time may be required to clean the surfactant. In the third microchannel, microposts are not required because microdroplets are ruptured at the second junction. We design the third microchannel as 10 mm in length including the second junction and placed the microposts halfway to the channel width (100 μm).

It is found that the large opening at the second junction cause unstable boundary between the water and oil flow as water extending its boundary into the oil channel. This phenomenon often causes the water-oil boundary to extend into the oil microchannel and to be stopped by the microposts. Fortunately, the gap between the microposts is very small which stops the further invasion of the water-oil boundary. In order to reduce this effect, the micropost array in the second junction area is modified to have a 30º angle with respect to the direction of the flow (**Fig. 3.2b**). As a result, the opening length of the second junction is dramatically reduced from 5mm to 150 μm, which significantly alleviate the problem of severely extended water boundary to the oil microchannel. Although the higher 30º angle array design may cause clogging and stop the transportation of microdroplets around the microposts as demonstrated with beads (15 μm in diameter) in previous reports [18]-[20], these microdroplets are ruptured at the water-oil boundary without the needs of further transportation as microdroplets and their contents could be naturally transported in the water regions of the water-oil boundary and flushed in the water microchannel directly.

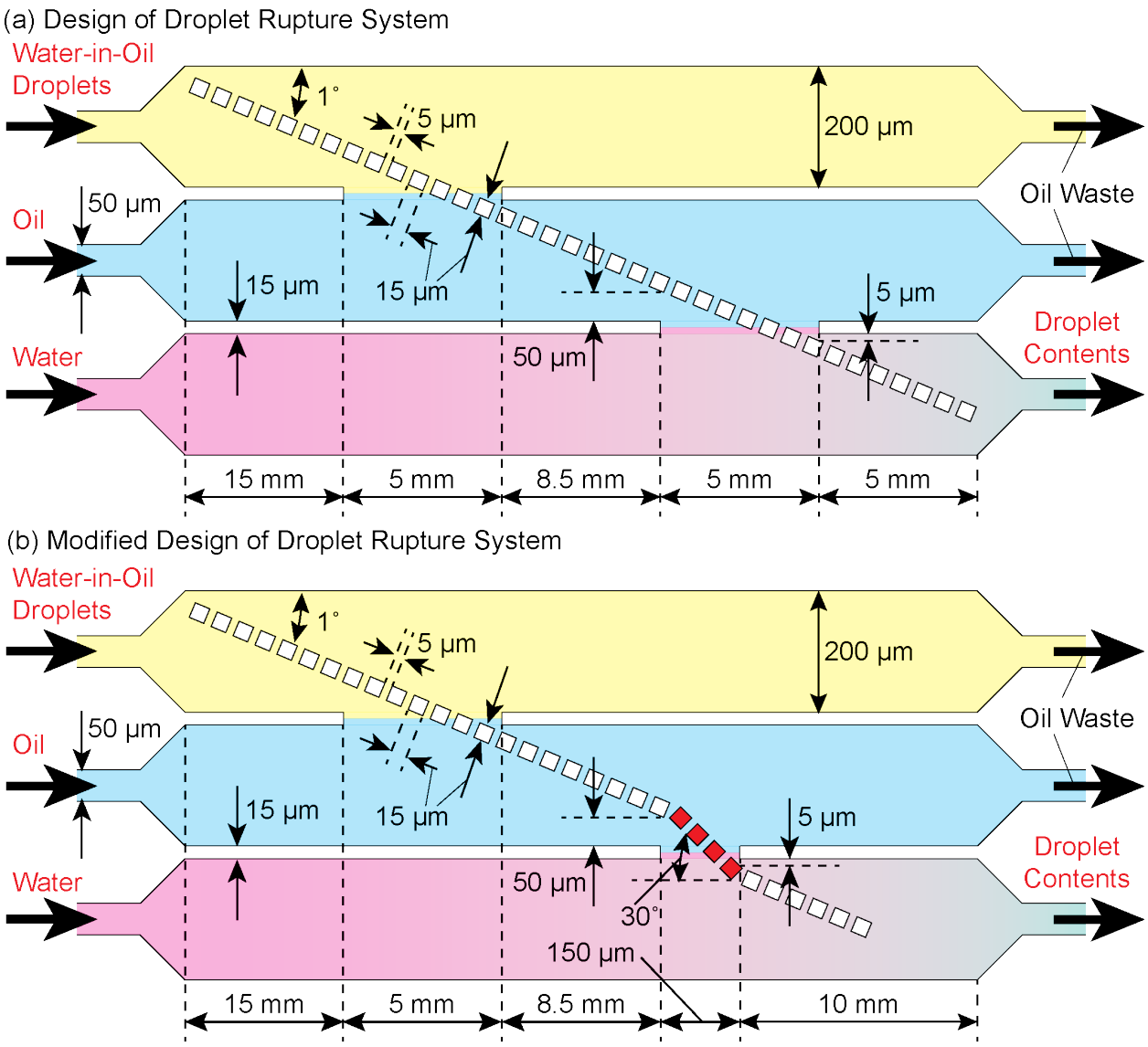

Figure 3.2 *The design details of the microdroplets rupture system. (a) The micropost array is designed to be have the tilted angle of 1° with respect to the flow direction. (b) The modified design has the micropost array with the tilted angle of 30° for the shorter opening at the second junction region to alleviate the problem of the unstable boundary between oil and water.*

3.2.3 Device Fabrication

The microfluidic systems are fabricated *via* the standard single layer soft lithography processes, as shown in **Figure 3.3**. We pre-bake a clean silicon wafer for dehydration at 150 ºC for 15 minute to prevent possible delamination of the structures. A negative photoresist (SU-8/2010, Microchem) of approximate thickness of 17 µm is spin-coated onto the pre-baked silicon wafer. Structures for the microchannels are patterned *via* contact photolithography (Model 200

Mask Aligner, Optical Associates). Developed mold inserts are transferred to PDMS mixture at a ratio of 10:0.9 of base and curing agent (Sylgard 184, Dow Corning). The 10 % less volume of curing agent than the typical value is used to achieve PDMS with softer stiffness to prevent the possible breakage of the structures with high aspect ratio (*i.e.* microposts) during the delamination process from the mold inserts. After curing PDMS at 55 ºC for at least two hours, PDMS is peeled off from the mold inserts and 0.75 mm diameter holes for inlet/outlet ports are punched with a circular-tip cutter (Harris Uni-Core Series, Ted Pella). PDMS part with micropatterned structure is covalently bonded to a glass microscope slide (Fisher Scientific) *via* Oxygen plasma (Reactive Ion Etcher, PETS, Inc.) and thermal treatment at 75 ºC for 1 hour. **Figure 3.4** shows the micrographs of a fabricated device.

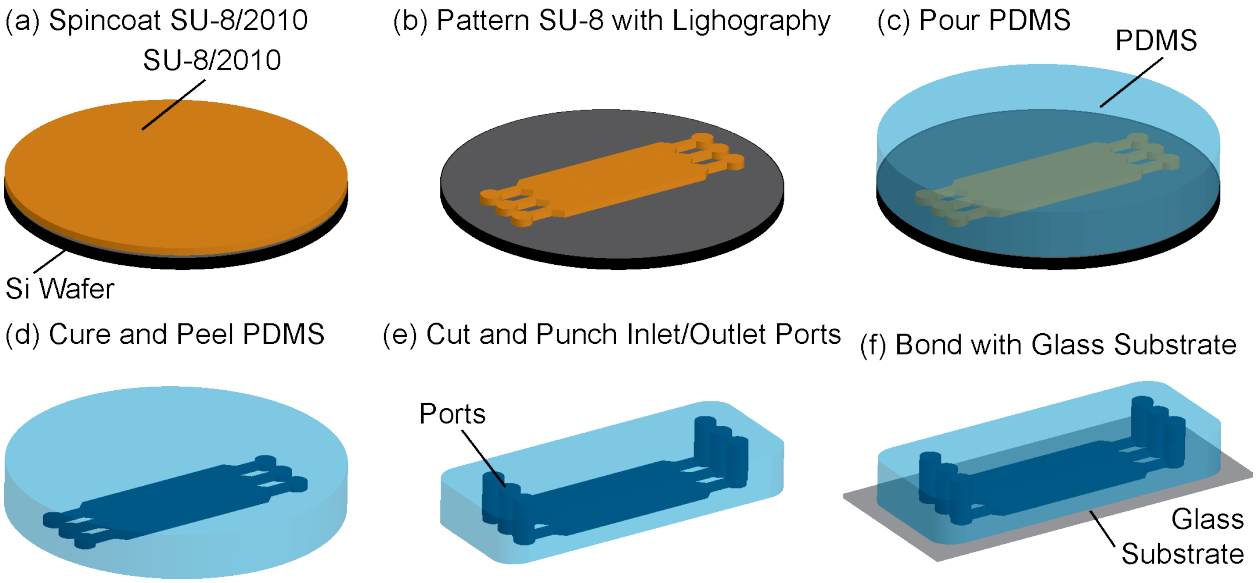

Figure 3.3 *Fabrication process. (a) SU-8/2010 with 17 μm in thickness is spincoated on a silicon wafer. (b) Microchannels are patterned with UV lithography. (c) Pre-mixed PDMS is poured. (d) Cured PDMS layer with microstructures. (e) The PDMS layer is cut and inlet/outlet ports are punched. (f) The PDMS part is covalently bonded to a glass substrate with the assistance of oxygen plasma treatment.*

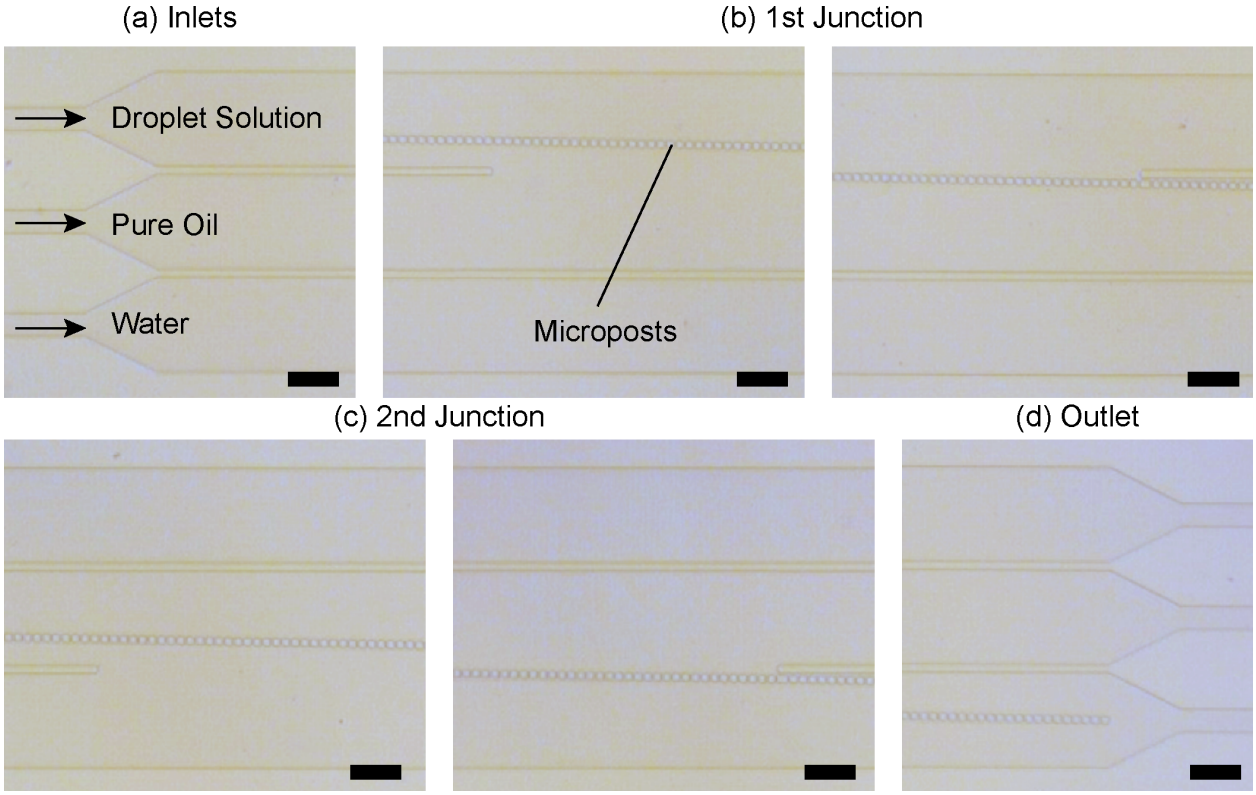

Figure 3.4 *Fabricated device with (a) inlet regions for fluid solutions, (b) first junction, (c) second junction, and (d) outlet regions. The scale bar is 100 μm.*

3.2.4 Materials and Experimental Setup

The water-in-oil microdroplets are formed using the commonly-used T-junction with 50 μm in width for both water and oil microchannels. The outlet microchannel of the device is directly connected to the inlet microchannel of the microdroplets rupture system. Green dyed deionized (DI) water is used for the water phase flow and Hexadecane (99%, Sigma Aldrich) with 2 wt% of Span 80 (Sigma Aldrich) is used for the oil phase flow. Fluid solutions are infused into the fabricated devices with syringe pumps (NE-300, New Era Pump Systems, Inc.). The flow rate is set as 0.2 μl/min for the water microchannel and 0.5 μl/min for the oil microchannels. **Figure 3.5** shows the formation process of the water-in-oil microdroplets. The average diameter of the microdroplets generated in the prototype system is 41.1±1.3 μm.

These microdroplets are immediately transferred to the inlet of the microdroplets rupture system. We infuse pure Hexadecane without surfactant as the washing oil, and red dyed DI water for the collection of the contents of the ruptured droplets. Washing oil and the DI water are infused with a pressure pump (MFCS series with flow-rate platform, Fluigent) to precisely control the pressure between the boundary of oil and water flow at the second junction to prevent extended boundary penetration into the oil microchannel. In the prototype experiments, the

pumping pressure head is set as 1.5 bar for the washing oil and 1.3 bar for the washing water. Qualitatively, it is desirable for the washing oil and washing water to have the same pressure at the second junction to prevent the oil-water interfacing boundary moving into the oil or water microchannel. The pumping pressure head is experimentally adjusted slightly higher at the washing oil input port than the washing water port because the flow resistance is higher in the washing oil due to the existence of the flow obstruction microposts before the second junction. The operation of the microdroplets rupture system is observed under a microscope (Motic AE31, Motic, Inc.) and recorded with a CCD (charge-coupled device) camera (QImaging Corp.) calibrated with QCapturePro (QImaging). Captured images are analyzed with the freely available imaging software, ImageJ (National Institutes of Health (NIH)), to characterize the size of microdroplets.

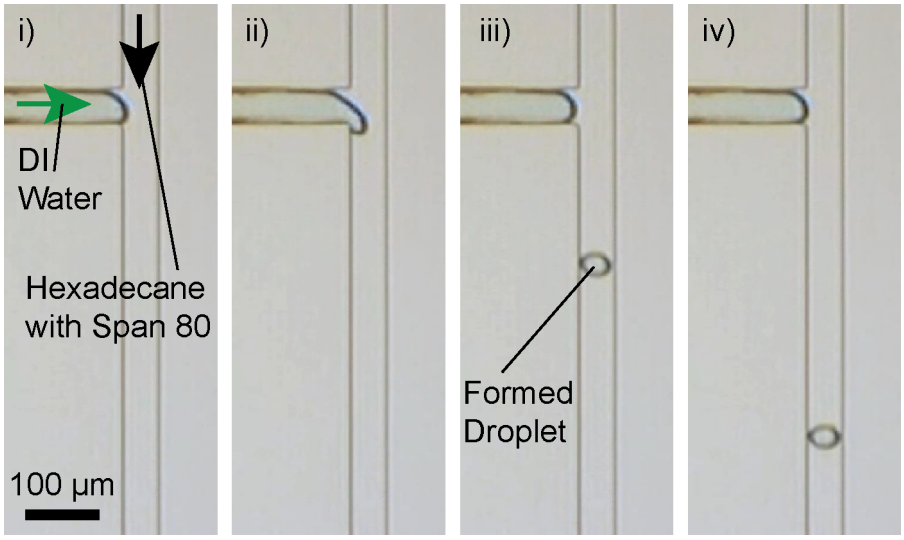

Figure 3.5 *Formation of the water-in-oil microdroplets. Observed average diameter of these microdroplets is 41.1±1.3 µm.*

3.2.5 Experimental Results

Experimentally, green-dyed water-in-oil microdroplets are guided *via* the continuous-flow arrayed microposts from the Hexadecane solution with 2 wt% Span 80 (*first microchannel*) to the pure Hexadecane solution without surfactant (*second microchannel*) through the first junction. It is observed that the boundary of the oil with surfactant-oil moves toward the first microchannel of Hexadecane solution with 2 wt% Span 80 as shown in **Fig. 3.6a**. The sequential images in **Fig. 3.6b** illustrated the sequential photos (33 milliseconds between each image) when the guided microdroplets pass the boundary from the Hexadecane solution with 2 wt% Span 80 to the pure Hexadecane solution in the second microchannel. During the passage via the second microchannel, Span 80 attached on the surface of the microdroplets can by reduced/washed away. At the second junction between the Hexadecane and the water microchannel, the boundary between the Hexadecane and water flow is deformed toward the Hexadecane

microchannel and stopped by the microposts as shown in **Fig. 3.7a**. Furthermore, some droplets are merged together before the second junction area to become a much larger droplet as shown in **Fig. 3.7b(i)** – a phenomenon not observed in the Hexadecane solution with 2 wt% Span 80. This suggests that surfactant on the droplet surface has been reduced/washed away in the pure Hexadecane microchannel to allow the merge of microdroplets. **Figures 3.7b (ii)-(v)** are the sequential photo taken every 66 milliseconds to illustrate the whole rupture process of a microdroplet. When the microdroplet contacted the red-dyed water flow at the second junction, it is ruptured and the contents inside are released into the water microchannel and to be collected at the output port. The color of the water at the second junction region is observed to change from its original red color to a mixture of green and red color (**Fig. 3.7b**). If polystyrene particles ($\varnothing$ = 10 μm) are initially suspended and encapsulated in the green-dyed DI water-in-oil microdroplets, a polystyrene particle is found to be released in the water flow microchannel (**Fig. 3.8**).

Figure 3.9 shows the sequential photos of the rupturing process using the modified system with the micropost array with an angle of 30º at the second junction for better stability of the water-oil boundary. It is observed that the modification doesn't change the key rupturing process and the contents of the droplets (*i.e.* green-dyded DI water) is released into the red DI water flow. These results demonstrate the capability of using the presented continuous flow microdroplets rupture systems to: (*i*) rupture water-in-oil microdroplets, (*ii*) release the inner contents of droplets into water flow, and (*iii*) separate the contents in microdroplets from oil.

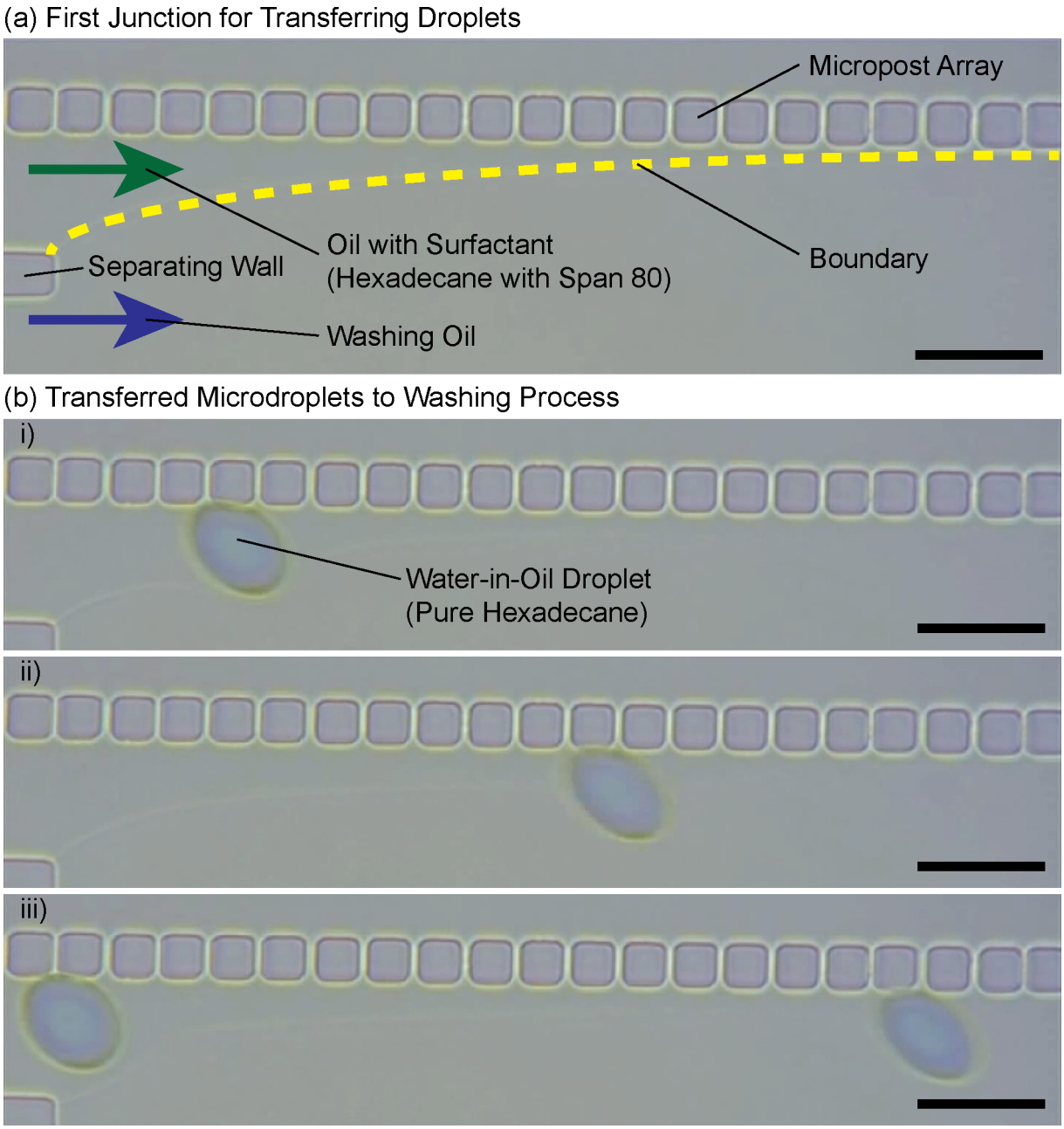

Figure 3.6 *Experimental results of transporting microdroplets at the first junction.* ***(a)*** *Introduced water-in-oil microdroplets are guided by the arrayed microposts from the oil with surfactant (Hexadecane with Span 80) in the first microchannel to pure Hexadecane flow in the second microchannel for the wash step.* ***(b)*** *Sequential optical images showing the passing of a water-in-oil microdroplet over the boundary between the two microchannels. Transferred microdroplets are washed in the second microchannel with pure oil (Hexadecane) flow. These microdroplets are dyed in green color for better visibility. Scale bars = 50 μm.*

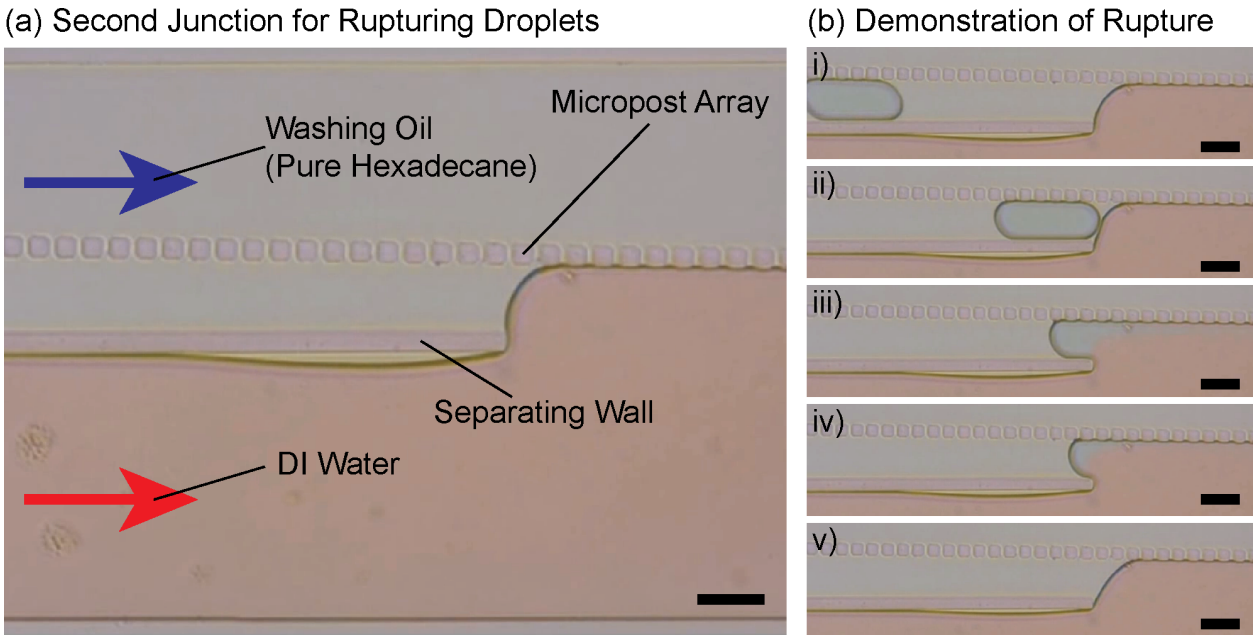

Figure 3.7 *Experimental results showing the rupture of microdroplets at the second junction.* ***(a)*** *Water-oil boundary is extended into the oil microchannel and stopped by the microposts and the surface tension force.* ***(b)*** *Sequential optical photos showing the details of the microdroplets rupturing process.* ***(i)*** *After being washed by the oil solution without surfactant in the middle microchannel, microdroplets could merge and become a large microdroplet.* ***(ii) – (v)*** *A microdroplet is successfully ruptured at the second junction between the Hexadecane without surfactant (second microchannel) and the water (third microchannel). The microdroplets and water are dyed in green and red color, respectively, for better visibility. Clear effects of mixture of color around the microdroplets rupture regions can be identified. Scale bars = 50 µm.*

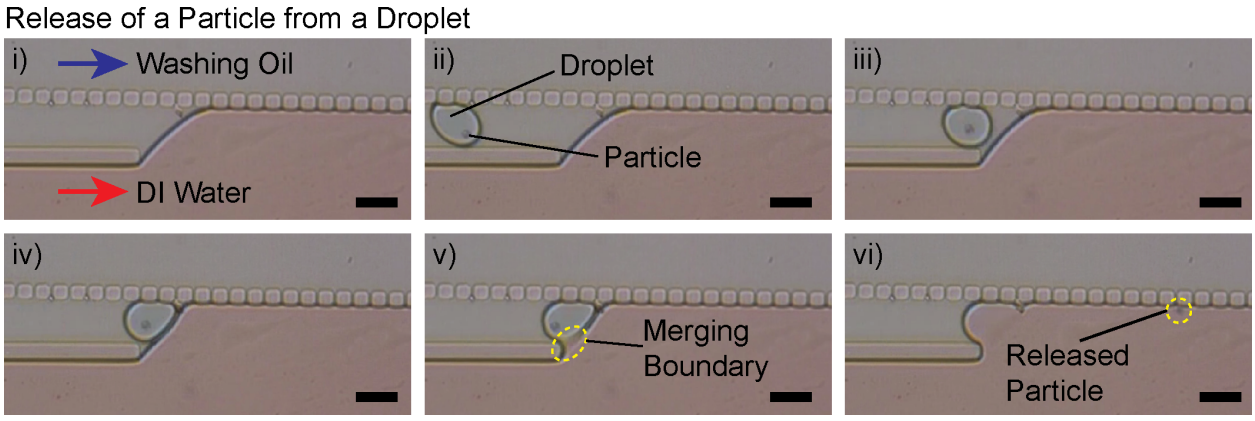

Figure 3.8 *Demonstration example showing the release a cluster of polystyrene particles from a microdroplet. A polystyrene particle (ø = 10 µm) encapsulated in a microdroplet is successfully released into the water microchannel after rupturing at the second junction. Scale bars = 50 µm.*

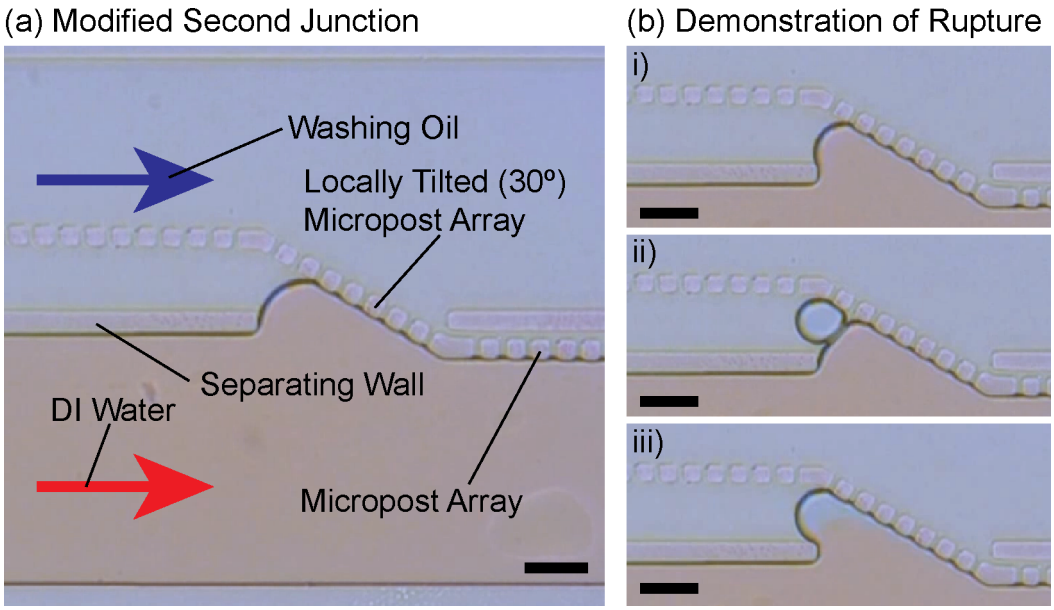

Figure 3.9 *Experimental results showing the rupture of microdroplets using a prototype system with the modified second junction design.* ***(a)*** *Modified second junction by changing the tilted angle of the micropost array from 1° to 30°. This design has much reduced opening width at 150μm of the second junction.* ***(b)*** *Sequential optical images showing the rupture of a microdroplet. Scale bars = 50 μm.*

3.3 Continuous Synthesis and Centrifuge-Free Retrieval of Nanoparticles

3.3.1 Operation Principle

Figure 3.10 illustrates the concept of the continuous-flow microdroplets reaction and rapture system for the synthesis and centrifuge-free retrieval of iron-oxide nanoparticles. The synthesis of iron-oxide nanoparticles is based on the coprecipitation of an aqueous solution of iron salts (*Reagent 1*) when reacted with a base solution (*Reagent 2*). These two reagents (and a third *buffer* solution) are infused into the microfluidic reactor and mixed within the water-in-oil microdroplets *via* a T-junction. Infused reagents forms microdroplets and they are cut by the carrier fluid of oil with surfactant. The buffer solution prevents the reagents from generating nanoparticles prior to droplet formation (which could lead to undesired clogging) and instead localizes the nanoparticle generation inside the microdropets (*yellow*). The S-shaped winding channel induces rapid mixing by chaotic advection to allow for full reactions [4], [23], [24] to synthesize nanoparticles inside these microdroplets. Reagents can be mixed at controlled concentrations by monitoring the input flow rates of each individual fluid, which influences the size of the synthesized nanoparticles.

The continuous-flow, micropost array railing system is then used to passively guide the nanoparticle-containing microdroplets between three distinct flow streams. First, microdroplets are transported from the oil flow with surfactant (*purple*) to the oil flow without surfactant

(*gray*), which serves to remove the surfactant from the droplet surface. At the second junction, the hydro- dynamic forces of the deionized (DI) water flow (*blue*) result in the destabilization of the microdroplets, thereby releasing the iron-oxide nanoparticles into the water flow. Thereafter, the water solution containing the nanoparticles is collected at the outlet, while the remaining oil flow is directed to the waste ports.

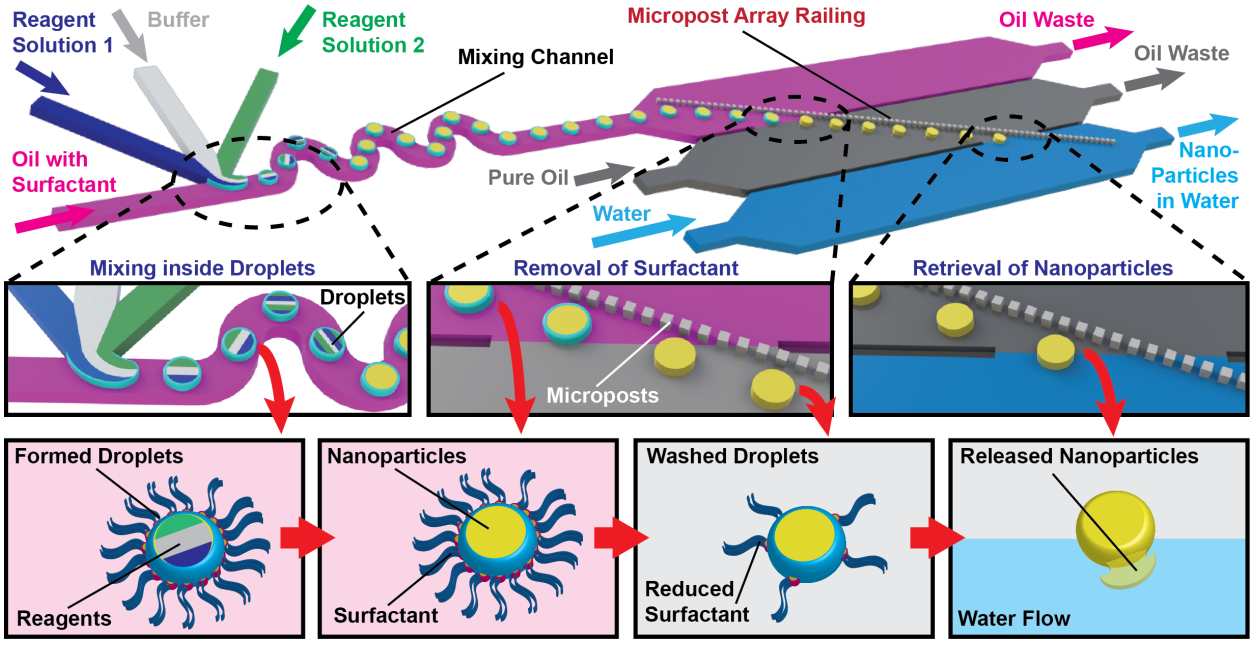

Figure 3.10 *Conceptual illustrations of the microfluidic system for the synthesis and retrieval of nanoparticles. Nanoparticles are synthesized with the mixing of two reagents. A buffer solution of water separates them until they form droplets in order to prevent reaction prior to droplet formation. The arrayed microposts passively guide the droplets into the adjacent flow streams to wash the droplets (and remove the surfactant) and then "rupture" the droplets. The rupture of microdroplets enables nanoparticles inside the droplets to be retrieved for further analysis and characterization.*

3.3.2 Methods

The nanoparticle synthesis method is based on a hydrolyzing of an aqueous mixture containing 6 mM of $FeCl_3$ $6H_2O$, 30 mM of $FeCl_2$ $4H_2O$, and 0.5M HCl (*reagent 1*) using 2 M aqueous ammonia (NH_4OH) (*reagent 2*) [25]. Upon the contact with ammonia, chemical reaction between the iron salt (iron (III) and iron (II)) and the base (NH_4OH) provides precipitation of magnetite, Fe_3O_4 as shown below;

$$2Fe^{3+} + Fe^{2+} + 8NH_4OH = Fe_3O_4 + 8NH_4{}^{+} + 4H_2O \qquad \textbf{(3.3)}$$

Both solutions are prepared with deaerated DI water under argon gas to minimize the oxidation of Fe^{2+} during the preparation.

The nanoparticle synthesis process is performed under an air environment in the microreactors formed *via* a microdroplet (**Fig. 3.11**). The system is made of permeable PDMS and some amount of oxygen can dissolve into the reagents. As $FeCl_2$ can be partially oxidized by the dissolved oxygen in the microchannel before contacting with ammonia, we increase the concentration of $FeCl_2$ by a factor of 10 compared with other large scale synthesis processes [26]. Iron salts (6 mM of $FeCl_3$ $6H_2O$, 30 mM of $FeCl_2$ $4H_2O$ and 0.5M HCl) and base (2 M of aqueous ammonia, NH_4OH) are infused into the microreactors from separate channels with DI water as a buffer from the middle channel. All reagents are infused with syringe pumps (NE-300, New Era Pump Systems, Inc.), and we set the flow rates at 0.5 μl/min for the two reagents and 1.0 μl/min for the DI water, yielding a mixed solution initially containing 1.5 mM of $FeCl_3$ and 7.5 mM of $FeCl_2$, with a stoichiometric excess of base. Infused reagents are briefly mixed to initiate hydrolysis process and form microdroplets in a microchannel containing oil as a carrier fluid. We use Hexadecane as the carrier fluid and add 2 wt% of Span 80 as a surfactant to prevent the merge of microdroplets during the nanoparticle synthesis process. Subsequently, microdroplets are transferred to the winding mixing channel and nanoparticles are synthesized inside the microreactors.

Figure 3.11a shows the design details of the sub-system for the formation of integrated microdroplets. It has a T-junction and three microchannels for reagents (i.e. iron salt, base and buffer solutions). The microchannels are 50 μm in width and the two microchannels on both sides are tilted at 30º leftwards and rightwards to the water microchannel at the middle. The long winding microchannel, which is placed 75 μm away from the junction for mixing and reaction, has a width of 50 μm and length of 3.6 mm. The same fabrication process as shown in **Chapter 3.2.3** is utilized to fabricate the system for the continuous synthesis and centrifuge-free retrieval of nanoparticles. **Figure 3.11b** shows the fabricated results around the reagent inlets and T-junction. We infuse solutions with syringe pumps (NE-300, New Era Pump Systems, Inc.) and set the flow rates at 0.5 μl/min, 1.0 μl/min, 0.5 μl/min, 3.0 μl/min, 3.0 μl/min, and 10.0 μl/min for the iron salt, the buffer, the base solution, oil carrier, washing oil, and DI water, respectively. The flow rate of the washing oil and DI water are approximately the same for the rupture process of microdroplets. Synthesized nanoparticles are characterized with transmission electron microscope (TEM) (JEM-2100, JEOL) and x-ray diffractometry (XRD) (D-5000 X-Ray Diffractometer, Siemens).

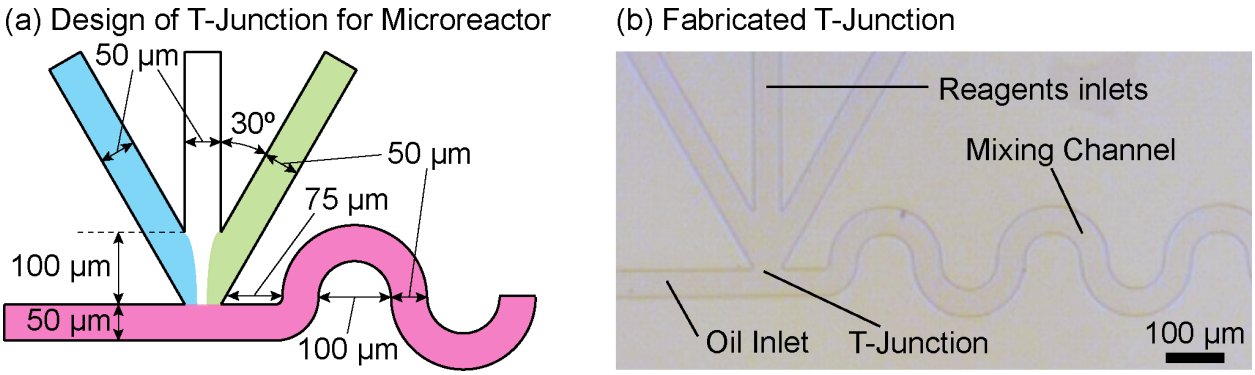

Figure 3.11 *The sub-system for the formation of integrated microdroplets around the sample inlets and T-junction region.* ***(a)*** *Design details of the T-junction with three aqueous solutions.* ***(b)*** *A fabricated prototype. Scale bar = 100 µm*

3.3.3 Results of Iron Oxide Nanoparticle Synthesis and Retrieval

Figure 3.12 shows the infusion of the reagents, buffer, and oil phase to form microdroplets in which the reagents are mixed and reacted to generate nanoparticles. It is observed that infused iron salt solution ($FeCl_2$), buffer and base solution (NH_3OH) formed microdroplets in Hexadecane (with 2 wt% of surfactant Span 80) at the T-junction as shown in **Figure 3.12a**. To prevent the contact of reagents before droplet formation (which can lead to clogging); DI water is provided in the middle channel which successfully separates the two reagents. **Figurer 3.12b** shows the boundaries of the three aqueous solutions at the T-junction with dyed reagents. Generated microdroplets are subsequently mixed in the mixing channel and formed iron-oxide nanoparticles in the microdroplets after these microdroplets are collected in a downstream chamber region (**Fig. 3.12c**). The diameter of microdroplets is characterized as 67.5±2.9 µm after mixing.

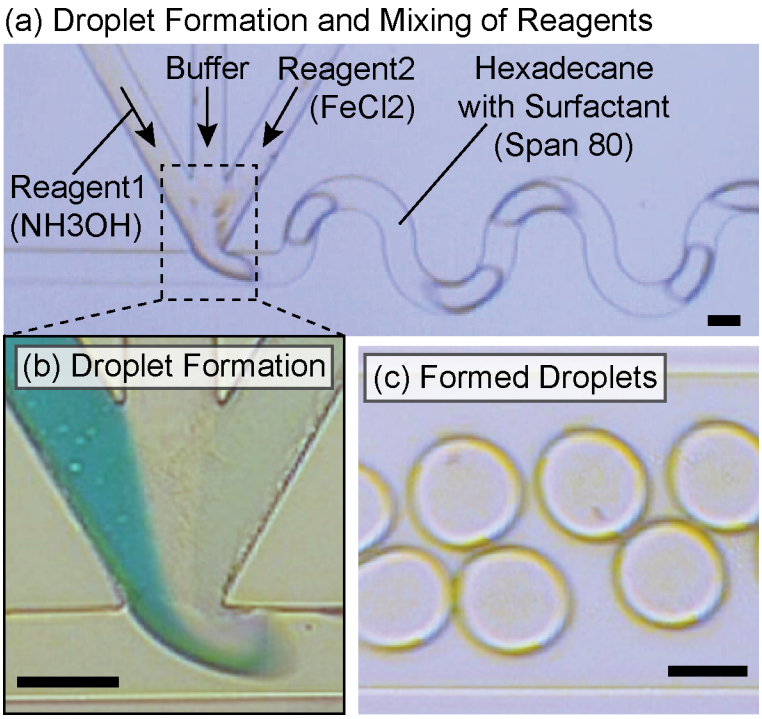

Figure 3.12 *Experimental results of the synthesis of iron oxide nanoparticles.* ***(a)*** *Infused reagents can form microdroplets in the oil solution with surfactant at the T-junction region, and the mixing occur inside the microdroplets to synthesize iron oxide nanoparticles.* ***(b)*** *Clear boundaries of the three input solutions as the two reagents are separated by the middle buffer prior to the droplet formation. The reagents are dyed in blue and green for better visibility.* ***(c)*** *The average diameter of the droplets is 67.5±2.9 μm after the mixing process at a downstream chamber region. Scale bars = 50 μm.*

The typical microdroplets rupture process is recorded in **Figure 3.13**. In **Figure 3.13a,** three continuous flow microchannels are shown with nanoparticle-containing microdroplets in the first microchannel. **Figure 3.13b** shows microdroplets being guided *via* the arrayed microposts and transferred from the first microchannel (Hexadecane solution with Span 80, 2% wt.) to the second microchannel (pure Hexadecane solution) via the first junction. The pure Hexadecane can wash the surface of the microdroplets to reduce the amount of surfactant such that some microdroplets are found to fuse together due to increased surface tension between oil and aqueous phases. At the second junction between the second microchannel and the third microchannel (DI water), microdroplets are transported into the water flow microchannel, resulting in the collapse of the microdroplets and iron oxide nanoparticles are released in the water microchannel. **Figure 3.13c** shows the merging and collapse of the microdroplets into the water, which was dyed in blue for better visibility. The released nanoparticles are collected at the water flow outlet.

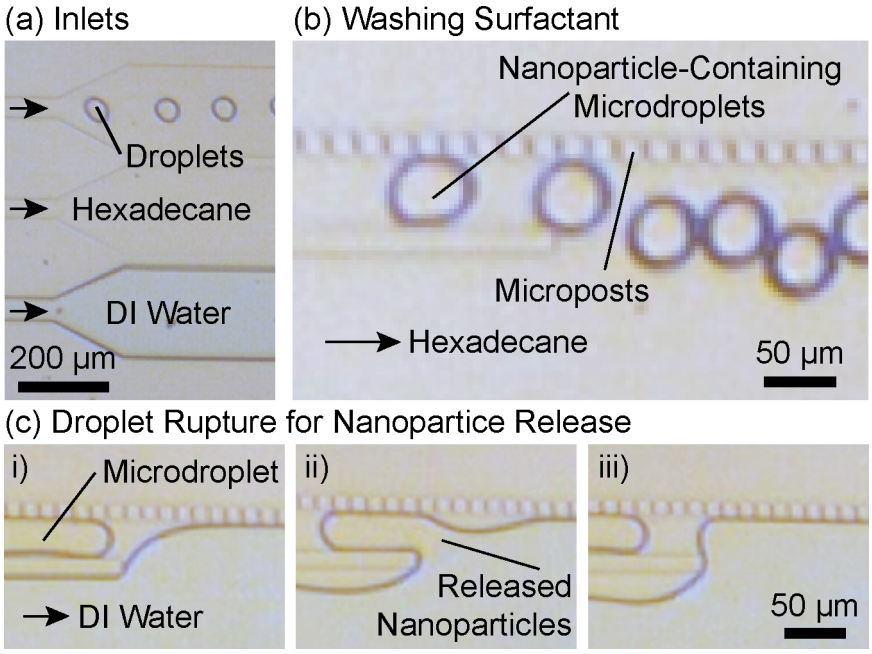

Figure 3.13 *The typical microdroplets rupture process and the retrieval of nanoparticles from the microreactors.* ***(a)*** *Microdroplets with synthesize iron oxide nanoparticles in the oil solution with surfactant. Microdroplets in oil solution with surfactant, oil, and water solutions are infused continuously.* ***(b)*** *Microdroplets are guided by the micropost array and transferred to the second microchannel with pure washing oil flow at the first junction.* ***(c)*** *Microdroplets are ruptured into the third microchannel with water solution and the iron-oxide nanoparticles are released into the water flow.*

The nanoparticles are collected and examined under transmission electron microscopy (TEM) to characterize their material properties (**Fig. 3.14a**). The samples are mounted on the TEM carbon grid and results show clear boundary of each nanoparticle as they are separated from the oil solution. The average diameter of the nanoparticles is characterized as 5.5 nm ± 1.5 nm. The nanoparticles are agglomerated because no ligands are used during the synthesis process to separate them. The XRD analysis in **Fig. 3.14b** shows the 2θ peak at 33º which corresponds to magnetite, Fe_3O_4. Other peaks correspond to goethite, FeOOH, or silicon substrate on which the nanoparticles are mounted. Furthermore, under a magnetic field by using a permanent magnet as shown in **Figure 3.14c**, the nanoparticles aggregate and move towards the magnet, indicating strong magnetic property of the collected nanoparticles. These results suggest that the continuous-flow microdroplets reaction and rapture system can be used for the synthesis and centrifuge-free retrieval of nanoparticles, which could be utilized for diverse nanoparticle-based synthesis processes.

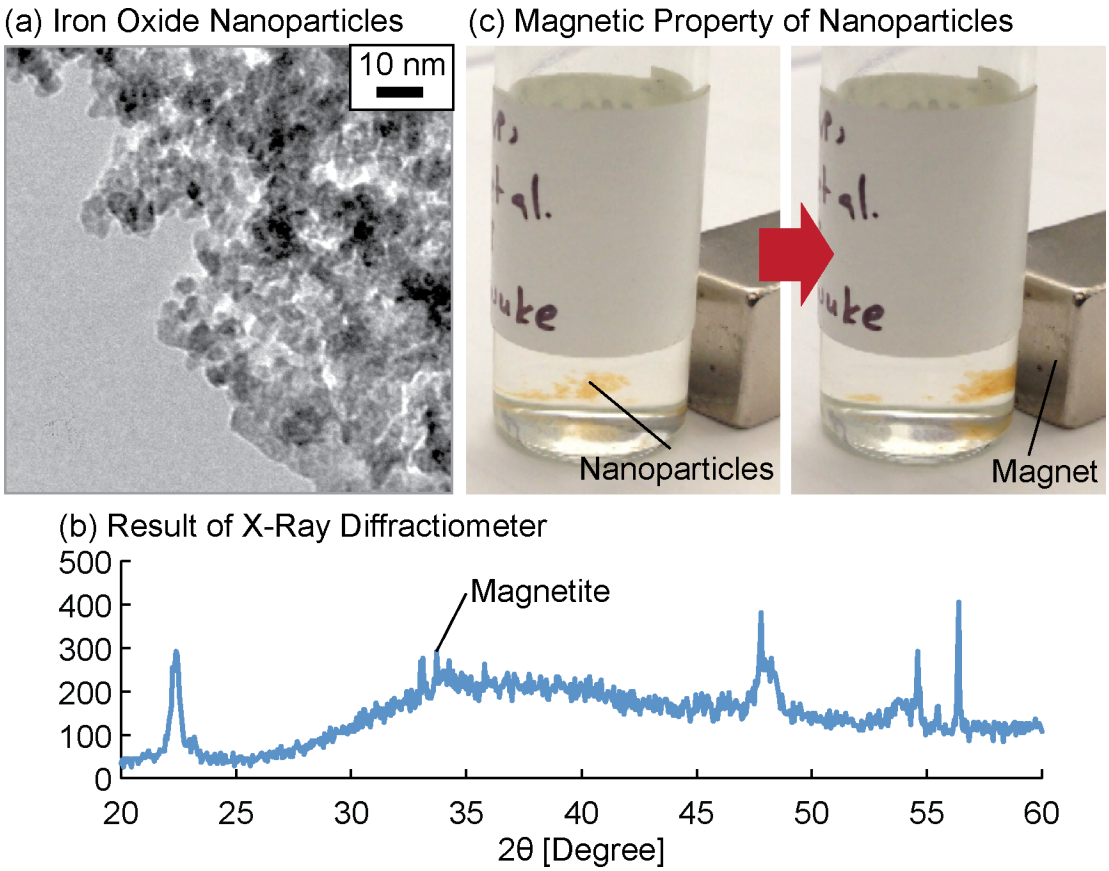

Figure 3.14. *Material characterizations of the synthesized iron-oxide nanoparticles.* ***(a)*** *Nanoparticles under TEM examinations show the size of nanoparticles as 5.5 nm ± 1.5 nm.* ***(b)*** *Under an applied magnetic field by a permanent magnet, nanoparticle move and aggregate toward the magnet.* ***(c)*** *X-ray diffraction (XRD) pattern of synthesized nanoparticles showing a peak signal at 33° which corresponds to the iron oxide magnetite.*

3.4 Continuous Rupture and Solution Alteration for Bead-in-Droplets

3.4.1 Operation Principle

Figure 3.15 illustrates the concept of the bead-in-droplet solution alteration system which consists of three major components: (*i*) the continuous-flow microposts railing system, (*ii*) four microfluidic flow channels in green, grey, yellow and blue colors, respectively, corresponding to continuous loading of water-in-oil droplets containing microbeads suspended in oil with surfactant (*green*), washing oil without surfactant (*grey*), washing water (yellow), and a second solution (*blue*), and (*iii*) a T-junction at the outlet for new droplet formations. Micropost array railing techniques are utilized to guide both droplets [15], [17] and microbeads [18]-[20] into distinct, adjacent fluids of flows (*e.g.*, oil and water). First, loaded bead-containing

microdroplets are passively guided by the arrayed microposts from the initial oil suspension (*green*) into the surfactant-free washing oil (*grey*) at the first junction. In the second microchannel, the washing oil without surfactant removes and reduces the surfactant on the surface of the droplets to allow the droplet to 'rupture'. At the second junction between the washing oil microchannel and washing water (*yellow*) microchannel, bean-in-droplets are broken apart and microbeads are released in to the washing water microchannel. The released microbeads are further guided by microposts to the second solution channels (*blue*) and its outlet port. During the process, microbeads can be washed in the washing water microchannel to remove the initial binding solution on the surface of the beads. Afterwards, a T-junction is used to form new microdroplets containing both the beads and the second solution assay. The bead-in-droplets in the second solution are collected at the outlet for experiments or they can go through other stages of solution alternation processes depending on the overall system/reaction requirements. As such, the specific solutions in the microdroplets can be continuously altered for specific bead-in-droplets microfluidic systems.

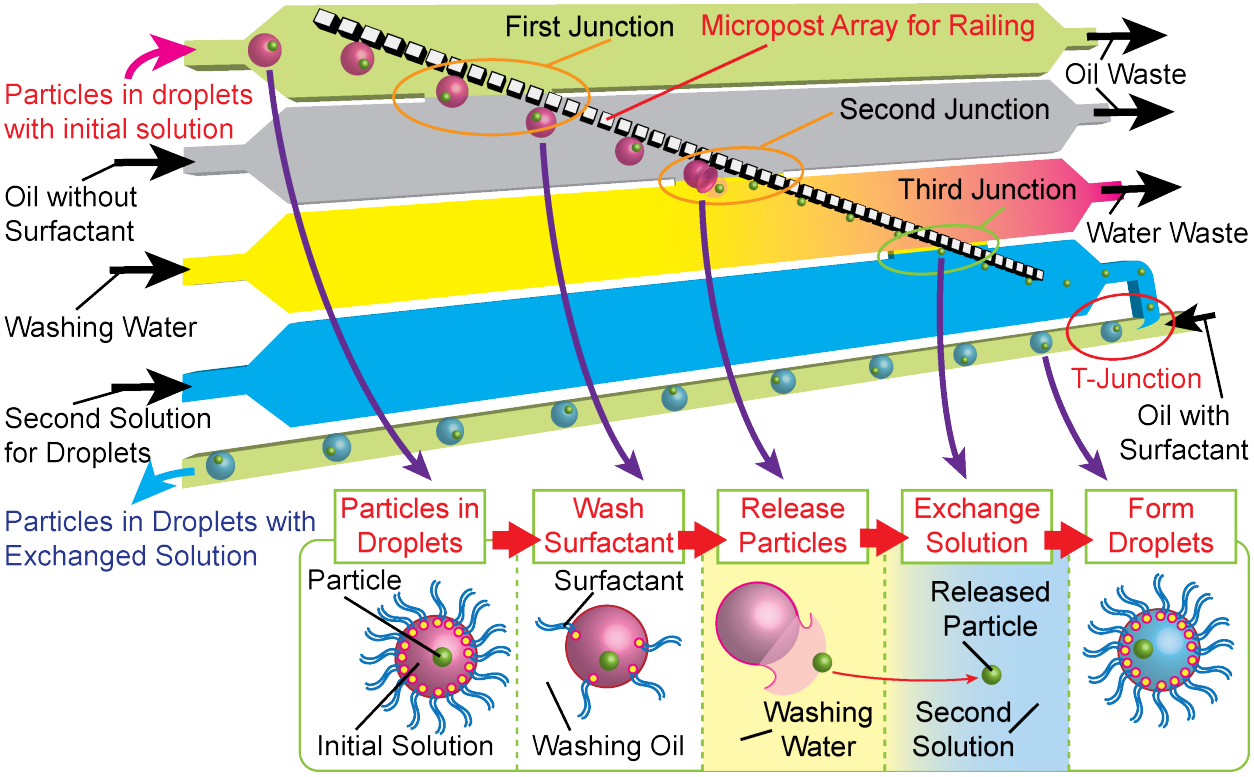

Figure 3.15 *Conceptual illustrations of the continuous-flow bead-in-droplet solution alteration system. Loaded microdroplets containing microbeads and a "first" solution (red) are passively guided into the adjacent flow streams via a micropost array railing technique. Microdroplets are washed by oil without surfactant (grey) to enable the rupture of bead-in-droplets at the interface of oil and water (yellow) microchannels. Microbeads are released into the washing water. Subsequently, released microbeads are transported into the "second" solution (blue). A T-junction is used to form new microdroplets containing microbeads and the second solution.*

3.4.2 Methods

Figure 3.16a shows the design details of a prototype system targeting $\varnothing$ = 15 μm beads based on the design principle described in the previous section (**Chapter 3.2.2**). Specific design parameters include: 15×15 μm^2 square-shape microposts with a 5 μm gap between posts and 1º tilted angle for the microposts array with respect to the flow direction for successful guidance of bead-in-droplets and beads. Similar to the previous design, the main microchannels are 200 μm in width and the inlet and outlet microchannels are 50 μm in width. A 50 μm-wide T-junction design at the final outlet is used to generate new droplets for the microbeads with an approximate distance of 4.5 mm from the rupture component. The prototype system is fabricated with the same procedure shown in the previous section (**Chapter 3.2.3**). **Figure 3.16b** shows optical images of the fabrication prototype system.

Polystyrene beads (Crosslinked Polystyrene Particles, 13.0-17.9 μm in diameter, 2.5 wt%, Spherotech, Inc.) are initially suspended in red-dyed DI water with overall concentration of 0.25 wt% and infused into a T-junction to be encapsulated in the water-in-oil droplets. Washing oil and washing water is infused with a pressure pump (MFCS series with flow-rate platform, Fluigent) to control the pressure head at the microchannel inlet ports set as 1.2 bar for the washing oil and 0.8 bar for the washing water. Syringe pumps (NE-300, New Era Pump Systems, Inc.) are set for infusing solutions with flow rates of 0.1 μl/min, 0.25 μl/min, 0.75 μl/min, and 1.5 μl/min for the bead suspension microchannel, the oil for the first droplet formation microchannel, the second droplet solution microchannel, and the oil for the second droplet formation microchannel, respectively.

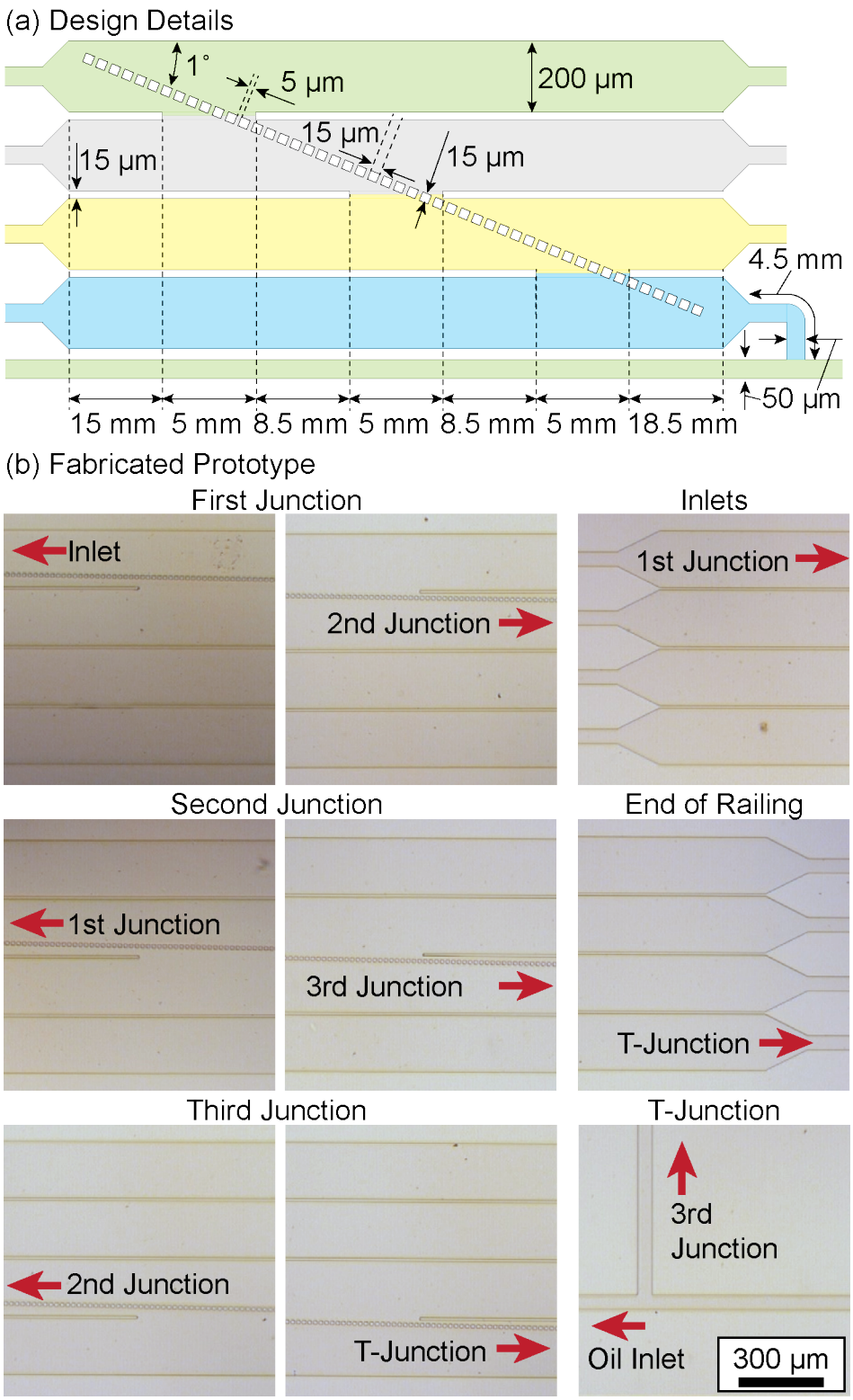

Figure 3.16 *(**a**) Design details of the continuous rupture and solution alteration system for bead-in-droplets with ø = 15 μm microbeads. Square microposts (15×15 μm^2) with 5 μm gaps are arrayed at a 1° tilted angle with respect to the flow direction for successful guidance of microdroplets and microbeads. (**b**) Optical photos of a fabricated prototype system.*

3.4.3 Experimental Demonstrations

First, bead-in-droplets are generated with water as the droplet solution containing ø = 15 µm polystyrene microbeads at a T-junction preceding the inlet with diameter of 61.1±1.4 µm. Red-color dyed deionized (DI) water is used as the first microdroplets solution, and Hexadecane is used as an oil carrier with 2 wt% of Span 80 as surfactant (**Fig. 3.17a**). The bead-in-droplets are transported into the system (**Fig. 3.17b**) from the 50 µm-wide microchannel to the 200 µm-wide microchannel. The larger microchannel causes the reduction in flow rate. As such, the bead-in-droplets are piled together as shown in Fig. 3.17b. It is also observed that most of the microdroplets don't have encapsulated beads due as concentration of beads in the solution is low in the prototype experiments.

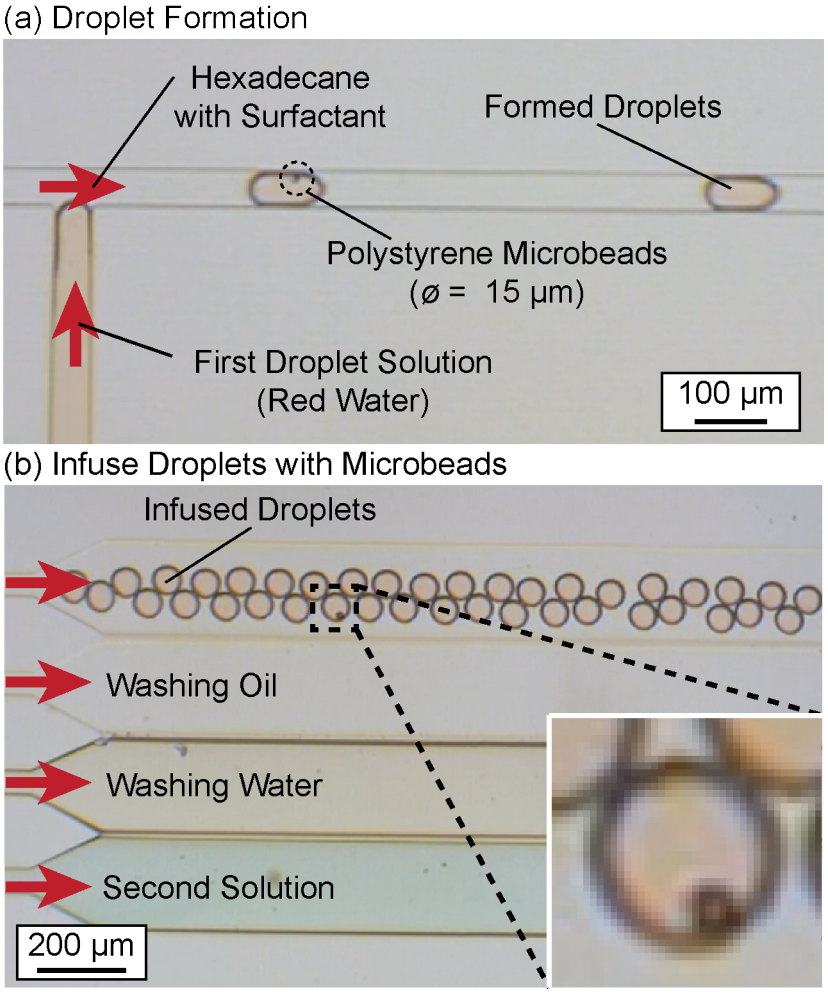

Figure 3.17 *Formation of bead-in-droplet and transportations.* ***(a)*** *Bead-in-droplets containing ø = 15 µm microbeads are formed at the T-junction. Red dyed DI water is used as the first microdroplets solution and Hexadecane with 2 wt% of surfactant Span 80 is used as the oil phase carrier flow.* ***(b)*** *Generated microdroplets and bead-in-droplets (ø = 61.1±1.4 µm) are infused into the system from the 50 µm-wide microchannel to the 200 µm-wide microchannel. The larger microchannel causes the reduction in flow rate and the pile-up of microdroplets.*

These bead-in-droplets and microdroplets are guided by the micropost array to the second flow channel of pure Hexadecane flow to wash away the surfactant (**Fig. 3.18a**). Since the diameter of the microdroplets is larger than the designed gap between the micropost and the dividing wall between the first (Hexadecane with surfactant) and second (pure Hexadecane) microchannels, some of the microdroplets are squeezed above the microposts array as shown in Fig. 3.18a. **Figure 18b** illustrates that after the droplet washing process, the bead-in-droplets can be ruptured at the second junction (oil-water interface) to release microbeads into the water microchannel (yellow dyed DI water). Subsequently, the released microbeads are washed in the water flow and transferred into the second droplet solution flow (blue dyed DI water) in **Fig. 3.18c**. Afterwards, the second T-junction section enables the formation of new microdroplets containing both the microbeads and the second droplet solution (**Fig. 3.18d**).

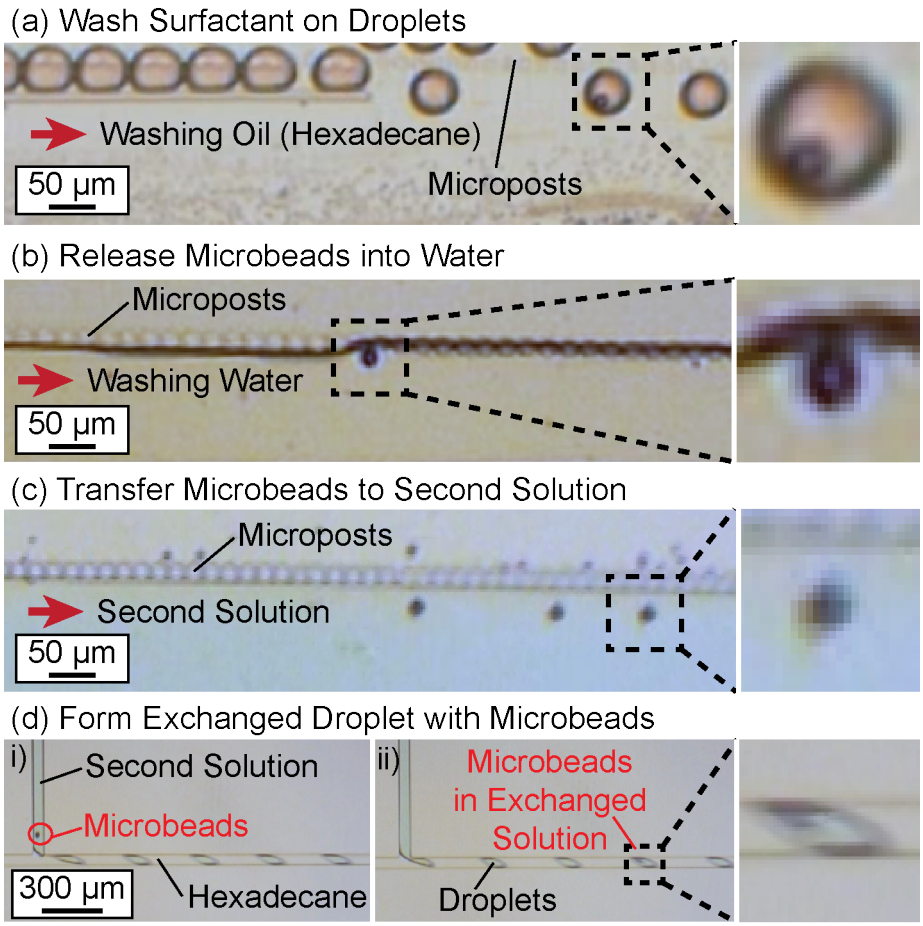

Figure 3.18 *Demonstration of the solution alternatoin process with ø = 15μm microbeads. Infused bead-in-droplets are successfully transferred by the microposts railing system to* ***(a)*** *the pure Hexadecane flow microchannel to wash surfactant;* ***(b)*** *the yellow-dyed water for the rupture of micro droplets and the release of microbeads;* ***(c)*** *blue-dyed water as the second microdroplets solution; and* ***(d)*** *the T-junction section for the formation of bead-in-droplets containing microbeads and the second droplet solution (ø = 38.6±1.0 μm).*

Average diameter of the second microdroplets is measured as 38.6±1.0 μm. The size of the second droplets can be controlled by changing the flow rate of the oil flow at the T-junction. Furthermore, the configuration of these bead-in-droplets is compatible with the existing microdroplets sorting methods [14], [27], [28]. For example, continuous-flow separation of microdroplets can be integrated to the system to increase the collection efficiency of the second bead-in-droplets at the outlet port. These results suggest that the bead-in-droplet solution alteration system could be developed for bead-based microfluidics platforms that require multiple fluidic reactions, for lab-on-a-chip systems, such as genomics, cellular studies, and point-of-care diagnostics.

References of Chapter 3

[1] P. A. Sims, W. J. Greenleaf, H. Duan, and S. Xie, "Fluorogenic DNA sequencing in PDMS microreactors," *Nat Methods*, vol. 8, no. 7, pp. 575–U84, 2011.

[2] T. Nisisako, T. Torii, and T. Higuchi, "Novel microreactors for functional polymer beads," *Chem Eng J*, vol. 101, no. 1, pp. 23–29, 2004.

[3] D. L. Chen, C. J. Gerdts, and R. F. Ismagilov, "Using microfluidics to observe the effect of mixing on nucleation of protein crystals," *J. Am. Chem. Soc.*, vol. 127, no. 27, pp. 9672–9673, 2005.

[4] H. Song, D. Chen, and R. Ismagilov, "Reactions in droplets in microfluidic channels," *Angew Chem Int Edit*, vol. 45, no. 44, 2006.

[5] E. M. Chan, A. P. Alivisatos, and R. A. Mathies, "High-Temperature Microfluidic Synthesis of CdSe Nanocrystals in Nanoliter Droplets," *J. Am. Chem. Soc.*, vol. 127, no. 40, pp. 13854–13861, Oct. 2005.

[6] P. Kumaresan, C. J. Yang, S. A. Cronier, R. G. Blazej, and R. A. Mathies, "High-throughput single copy DNA amplification and cell analysis in engineered nanoliter droplets," *Anal Chem*, vol. 80, no. 10, pp. 3522–3529, 2008.

[7] W. Grover and R. Mathies, "An integrated microfluidic processor for single nucleotide polymorphism-based DNA computing," *Lab on a Chip*, vol. 5, no. 10, pp. 1033–1040, 2005.

[8] S. Dubus, J. Gravel, B. Le Drogoff, P. Nobert, T. Veres, and D. Boudreau, "PCR-free DNA detection using a magnetic bead-supported polymeric transducer and microelectromagnetic traps," *Anal Chem*, vol. 78, no. 13, pp. 4457–4464, 2006.

[9] P. Garstecki, M. Fuerstman, H. Stone, and G. Whitesides, "Formation of droplets and bubbles in a microfluidic T-junction - scaling and mechanism of break-up," *Lab on a Chip*, vol. 6, no. 3, pp. 437–446, 2006.

[10] J. Tice, H. Song, A. Lyon, and R. Ismagilov, "Formation of droplets and mixing in multiphase microfluidics at low values of the Reynolds and the capillary numbers," *Langmuir*, vol. 19, no. 22, pp. 9127–9133, 2003.

[11] W.-H. Tan and S. Takeuchi, "Timing controllable electrofusion device for aqueous droplet-based microreactors," *Lab on a Chip*, vol. 6, no. 6, pp. 757–763, 2006.

[12] Y.-C. Tan, Y. L. Ho, and A. P. Lee, "Droplet coalescence by geometrically mediated flow in microfluidic channels," *Microfluid Nanofluid*, vol. 3, no. 4, pp. 495–499, 2007.

[13] W. Wang, C. Yang, and C. M. Li, "On-demand microfluidic droplet trapping and fusion for on-chip static droplet assays," *Lab on a Chip*, vol. 9, no. 11, pp. 1504–1506, 2009.

[14] M. Chabert and J.-L. Viovy, "Microfluidic high-throughput encapsulation and hydrodynamic self-sorting of single cells," *P Natl Acad Sci Usa*, vol. 105, no. 9, pp. 3191–3196, 2008.

[15] C. Kantak, S. Beyer, L. Yobas, T. Bansal, and D. Trau, "A 'microfluidic pinball' for on-chip generation of Layer-by-Layer polyelectrolyte microcapsules," *Lab on a Chip*, vol. 11, no. 6, pp. 1030–1035, 2011.

[16] S. Matosevic and B. Paegel, "Stepwise synthesis of giant unilamellar vesicles on a microfluidic assembly line," *J. Am. Chem. Soc.*, vol. 133, no. 9, p. 2798, 2011.

[17] P. Abbyad, R. Dangla, A. Alexandrou, and C. N. Baroud, "Rails and anchors: guiding and trapping droplet microreactors in two dimensions," *Lab on a Chip*, vol. 11, no. 5, pp. 813–821, 2011.

[18] R. D. Sochol, S. Li, L. P. Lee, and L. Lin, “Continuous flow multi-stage microfluidic reactors via hydrodynamic microparticle railing,” *Lab on a Chip*, 2012.
[19] R. D. Sochol, D. Corbett, S. Hesse, W. E. R. Krieger, K. T. Wolf, M. Kim, K. Iwai, S. Li, L. P. Lee, and L. Lin, “Dual-mode hydrodynamic railing and arraying of microparticles for multi-stage signal detection in continuous flow biochemical microprocessors ,” *Lab on a Chip*, vol. 14, no. 8, pp. 1405–1409, 2014.
[20] K. Iwai, W.-H. Tan, H. Ishihara, and S. Takeuchi, “A resettable dynamic microarray device,” *Biomed Microdevices*, vol. 13, no. 6, pp. 1089–1094, 2011.
[21] D. J. Shaw, *Introduction to Colloid and Surface Chemistry*. 1992.
[22] L. Peltonen, J. Hirvonen, and J. Yliruusi, “The Behavior of Sorbitan Surfactants at the Water–Oil Interface: Straight-Chained Hydrocarbons from Pentane to Dodecane as an Oil Phase,” *Journal of Colloid And Interface Science*, 2001.
[23] H. Song, J. D. Tice, and R. F. Ismagilov, “A microfluidic system for controlling reaction networks in time,” *Angew Chem Int Edit*, vol. 42, no. 7, pp. 768–772, 2003.
[24] I. Shestopalov, J. D. Tice, and R. F. Ismagilov, “Multi-step synthesis of nanoparticles performed on millisecond time scale in a microfluidic droplet-based system,” *Lab Chip*, vol. 4, no. 4, pp. 316–321, 2004.
[25] L. Frenz, A. El-Harrak, M. Pauly, S. Bégin-Colin, A. D. Griffiths, and J.-C. Baret, “Droplet-Based Microreactors for the Synthesis of Magnetic Iron Oxide Nanoparticles,” *Angew Chem Int Edit*, vol. 47, no. 36, pp. 6817–6820, 2008.
[26] M. Mahmoudi, S. Sant, B. Wang, and S. Laurent, “Superparamagnetic iron oxide nanoparticles (SPIONs): Development, surface modification and applications in chemotherapy,” *Advanced drug delivery …*, 2011.
[27] J. J. Agresti, E. Antipov, A. R. Abate, K. Ahn, A. C. Rowat, J.-C. Baret, M. Marquez, A. M. Klibanov, A. D. Griffiths, and D. A. Weitz, “Ultrahigh-throughput screening in drop-based microfluidics for directed evolution,” *P Natl Acad Sci Usa*, vol. 107, no. 9, pp. 4004–4009, 2010.
[28] J.-C. Baret, O. J. Miller, V. Taly, M. Ryckelynck, A. El-Harrak, L. Frenz, C. Rick, M. L. Samuels, J. B. Hutchison, J. J. Agresti, D. R. Link, D. A. Weitz, and A. D. Griffiths, “Fluorescence-activated droplet sorting (FADS): efficient microfluidic cell sorting based on enzymatic activity,” *Lab on a Chip*, vol. 9, no. 13, pp. 1850–1858, 2009.

Chapter 4: Microdroplets Encapsulated with Magnetic Particles Filled Polymer Shells

4.1 Introduction

The main focuses of carrier-based drug delivery systems include; (*i*) encapsulating active drugs to prevent degradations, (*ii*) targeting the specific locations, and (*iii*) controlling drug release rates while maintaining effective drug concentrations [1]-[3]. In recent years, researchers have been utilizing functionalized micro/nano carriers such as nanoparticles [4], [5], micelles [6], droplets [7], and double emulsions [8], [9] to realize the encapsulations of the drugs and targeted deliveries. The drug delivery rate and effectiveness, however, are difficult to control because the aforementioned methodologies rely on passive drug delivery schemes without active control.

In the state-of-the-art drug delivery applications, magnetic systems are promising due to various potential benefits of the magnetic materials in: (*i*) remote manipulation of the carriers to specific locations *via* the guidance of a magnetic field (*e.g.*, a magnet) [10], [11], and (*ii*) active drug release and control with the assistance of induction heating remotely by altering the porosity of the encapsulating membranes with alternating magnetic fields [12]-[15] (e.g., electromagnetic coil with alternating current). Since the formations of microfluidic double emulsions in flow focusing device have been widely studied [8], [9], [16], [17], the challenge is to integrate magnetic materials with the microdroplets. Previously, the encapsulation of magnetorheological fluid has been achieved in a core-shell microdroplets system [11]. A variety of polymeric structures with embedded magnetic particles have also been demonstrated [10], [18]-[22]. This work investigates the techniques in integrating microdroplets with magnetic polymer shells as the potential carriers for therapeutic drug delivery applications.

Figure 4.1 illustrates the basic concept of the microdroplets encapsulated with magnetic particles filled polymer shells for drug delivery applications. Biocompatible polymer shells containing magnetic nanoparticles are used to encapsulate aqueous phase solutions with active therapeutic drug materials. These magnetic capsules may be injected into blood vessels and guided via the externally applied DC magnetic field to the desirable locations as the "targeting" process [11]. Afterwards, an AC magnetic field may be applied for local heating of the magnetic particles to break or increase the porosity of the polymeric shells for active control of the drug delivery system [15], [23]. The proposed microcapsules have the potential to overcome a number of hurdles associated with current state-of-art technologies: (1) magnetic shells can be guided by DC magnetic field for location control; (2) magnetic particles can be heated by AC magnetic field to break or change the porosity of the shells for active drug release control; and (3) encapsulated microdroplets can prevent the possible degradation and contamination of the drug materials during the transportation processes.

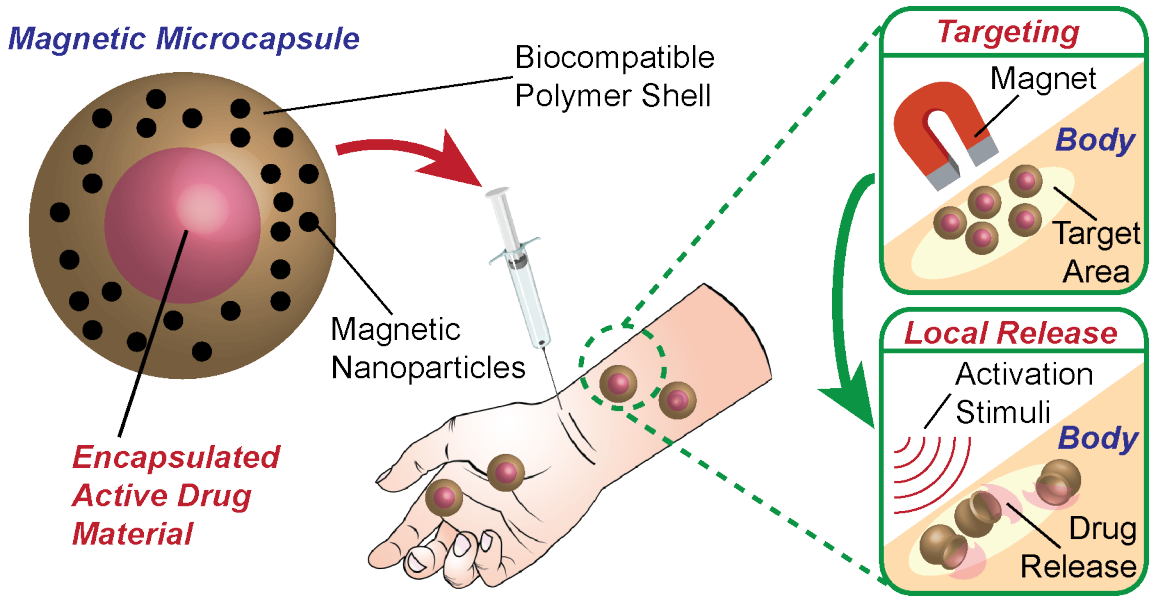

Figure 4.1 *Concept of the microdroplets encapsulated with magnetic particles filled polymer shells for therapeutic applications. Active drug materials are encapsulated in biocompatible polymer shells filled with magnetic particles to provide the magnetic functionality, including (1) to remotely manipulate the location of the carriers via the DC magnetic field, and (2) to release the drug on-demand via the AC magnetic field to heat up the magnetic particles and break or increase the porosity of the polymeric shells.*

4.2 Methods

4.2.1 Formation of Microdroplets with Magnetic Particles Filled Polymer Shells

Figure 4.2 conceptually depicts the synthesis of magnetic particle filled polymer shells with encapsulated microdroplets *via* photopolymerization of emulsion microdroplets formed by the dual-stage flow-focusing junctions [24]. A newly developed magnetic UV curable composite is utilized as the shell material – superparamagnetic iron oxide nanoparticles with fatty acid coatings, dispersed in poly(ethyleneglycol) diacrylate (PEGDA). At the first junction, aqueous solutions are continuously injected into the magnetic PEGDA stream for the formation of water-in-PEGDA microdroplets. At the second junction, the water-in-PEGDA microdroplets are in the magnetic PEGDA stream are injected and compartmentalized into water for the formation of double emulsion. Subsequently, exposure to UV light selectively polymerizes the polymeric shells filled with magnetic particles [25], [26]. Under the proper design and process control, these magnetic microcapsules can be formed continuously as a potential high-throughput process to fabricate these drug delivery carriers. The UV light intensity has to high enough for the polymerization process while low enough without causing any possible damages to the internal drug materials. The property and concentration of the magnetic particles have to be carefully chosen to assure smooth operations for the later drug targeting and delivery operations using both DC and AC magnetic fields.

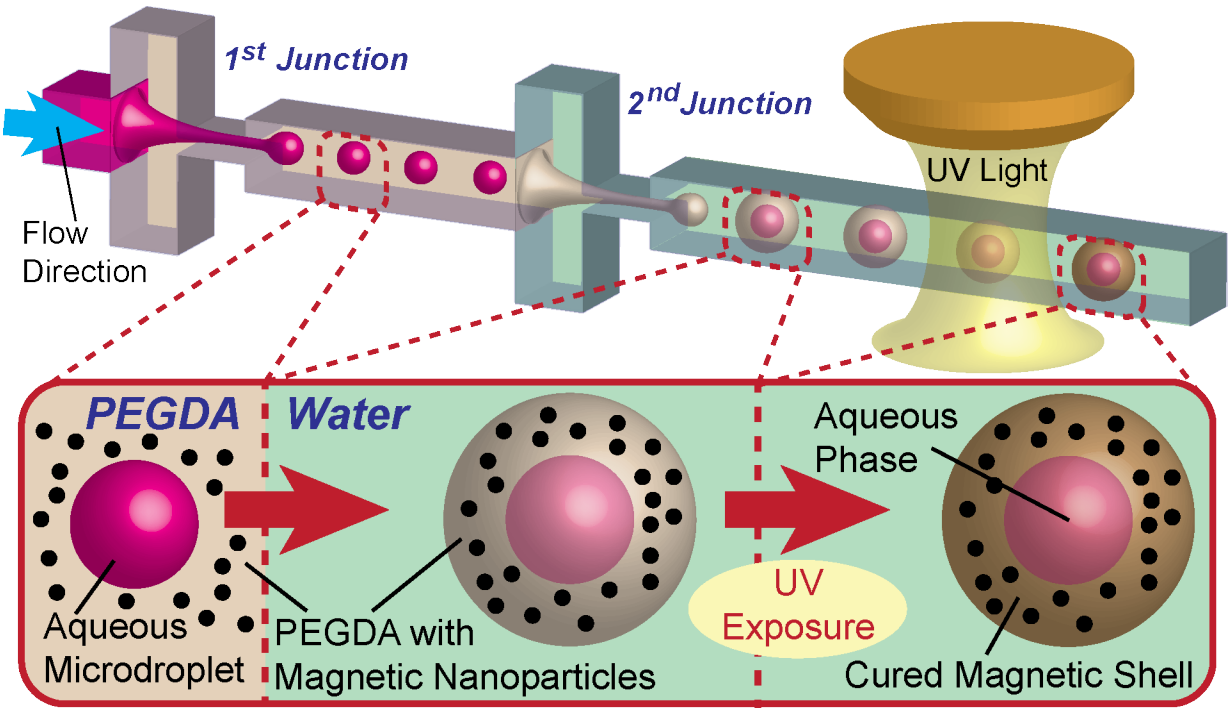

Figure 4.2 *Conceptual diagram showing the formation of magnetic core-shell microcapsules. The multi-stage flow focusing microfluidic system forms double emulsions of inner aqueous phase and outer PEGDA solution with embedded magnetic nanoparticles. The UV exposure process polymerizes PEGDA shells selectively, and results in microcapsules with magnetic nanoparticles filled polymeric shells with aqueous cores as the microcapsules. These magnetic core-shell microcapsules could be used for therapeutic delivery applications with abilities to remotely control the targeting location and release of drugs.*

4.2.2 Device Fabrication

Figure 4.3 shows the prototype design and dimensions of the microfluidic flow-focusing system. The main microchannels are all 200 µm in width and the two junction regions have orifices with 50 µm in width and 200 µm in length. Distance between the two junctions is 800 µm in length. A large UV exposure chamber with 1 mm width and 2mm length is placed after the second flow-focusing junction to reduce the flow rate and increase the duration of the polymerization process. The slower flow rate at the UV exposure chamber is also beneficial for visual observations. The first junction is made hydrophobic for the formation of water-in-PEGDA microdroplets in the magnetic PEGDA fluid [24]. The second junction is made hydrophilic for the formation of PEGDA-in water microdroplets in water [16], [27]. **Figure 4.4** illustrates the fabrication process. The prototype devices are fabricated using standard soft lithography processes [28]. Briefly, SU-8/2050 photoresist (SU-8/2050, Microchem) is patterned on a silicon wafer with a thickness of 100 µm as a master mold to transfer the structures to poly(dimethylsiloxane) (PDMS) (Sylgard 184, Dow Corning). Cured PDMS is then peeled off the mold and the inlet and outlet ports are made by punching holes (ø = 7.5 mm) with

a circular-tip cutter (Harris Uni-Core Series, Ted Pella). The surface of PDMS is treated with oxygen plasma (120W for 10 s) (Reactive Ion Etcher, PETS, Inc.) to modify the surface from hydrophobic to hydrophilic and to promote the bonding process [16], [27], [29], [30]. PDMS is naturally hydrophobic and it turns the state to hydrophilic by applying oxygen plasma. The first junction was selectively covered with Kapton tape (ø = 1.5 mm) to maintain the hydrophobicity state of the PDMS. After attachment to the glass substrate (Fisher Scientific), deionized (DI) water is infused to the second junction from the outlet to keep its hydrophilic state. Plasma-treated PDMS recovers its hydrophobic state after approximately 30 minutes of continuous exposure to air. Thermal treatment at 75°C for 30min is conducted afterward to form covalent bonding between the PDMS and glass substrate. The prototype devices are left in the air under room temperature for at least one hour to recover the hydrophobic state inside the microchannels of the fabricated PDMS devices except for the second junction regions and the chamber/outlet parts where DI water are filled to preserve their hydrophilic states. **Figure 4.5** shows optical micro photos of fabricated microfluidic system for the formation of magnetic core-shell microcapsules: (a) first junction region, and (b) second junction region. The thickness of these microchannels is defined by the SU-8 mold insert with a target of 100 μm.

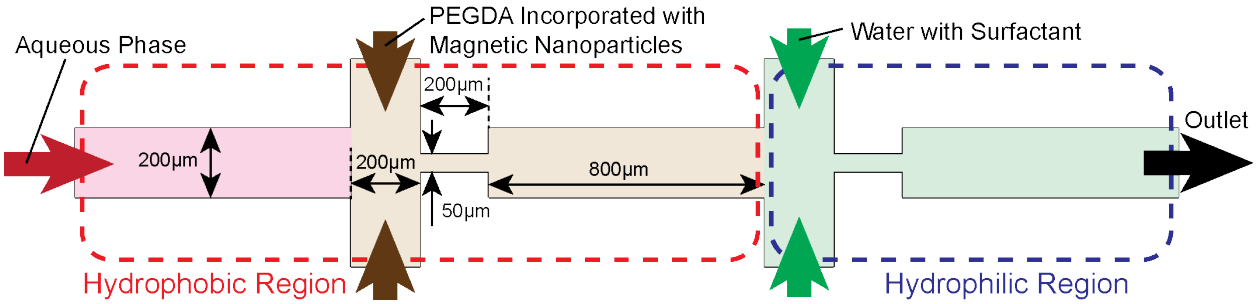

Figure 4.3 *Design details of the microfluidic system for the formation of magnetic core-shell microcapsules. Flow focusing junctions have 200μm-wide main microchannels and 50μm-wide orifices. The first junction is made hydrophobic for the formation of aqueous microdroplets and the second junction is made hydrophilic for the formation of PEGDA-in-water emulsions.*

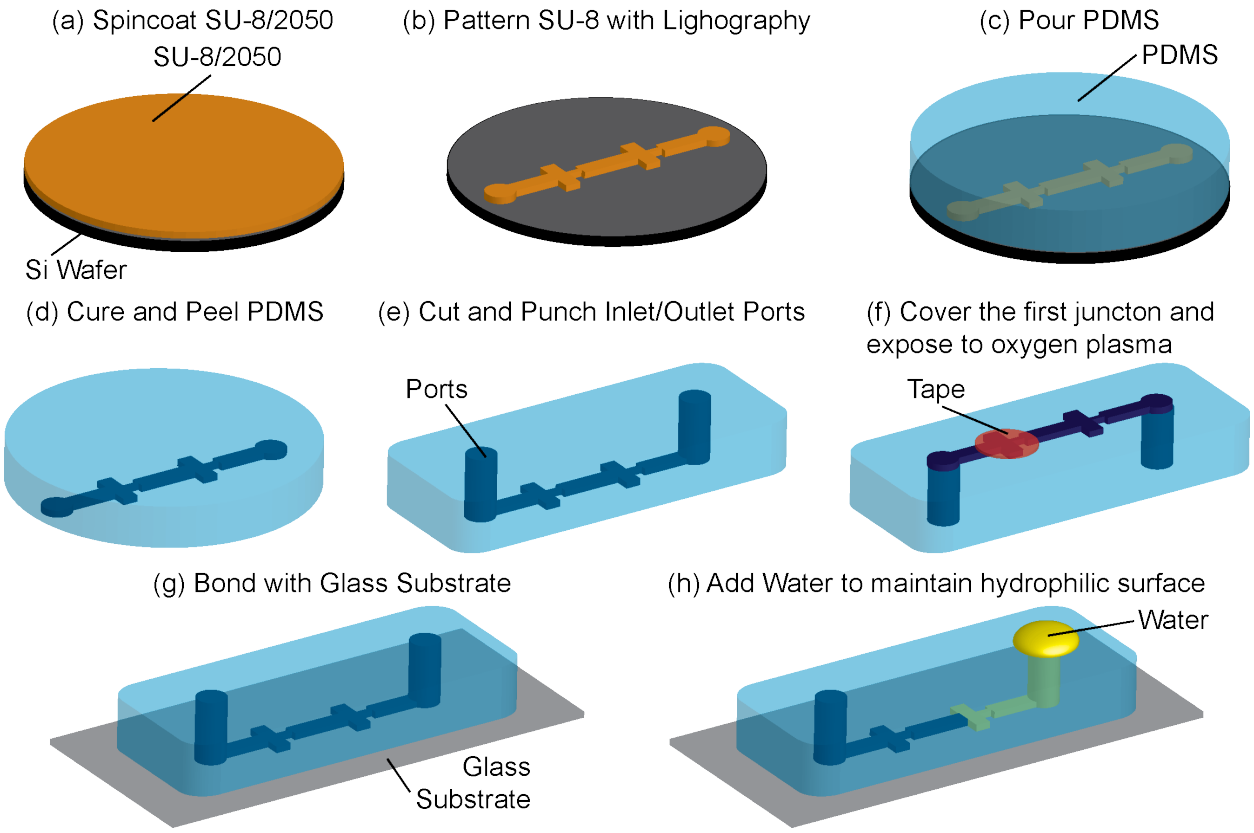

Figure 4.4 *Fabrication process of the microfluidic system for the formation of magnetic core-shell microcapsules.* ***(a)*** *SU-8/2050 with 100 μm in thickness is spincoated on a silicon wafer.* ***(b)*** *Microchannels are patterned with UV photolithography.* ***(c)*** *Pre-mixed PDMS is poured.* ***(d)*** *Microstructures are transferred to the cured PDMS.* ***(e)*** *PDMS is cut and inlet/outlet ports are punched.* ***(f)*** *Surface of PDMS is treated with oxygen plasma while the first junction is covered with a Kapton tape.* ***(g)*** *PDMS is covalently bonded to a glass substrate.* ***(h)*** *DI water is added from the outlet port to maintain the hydrophilic state.*

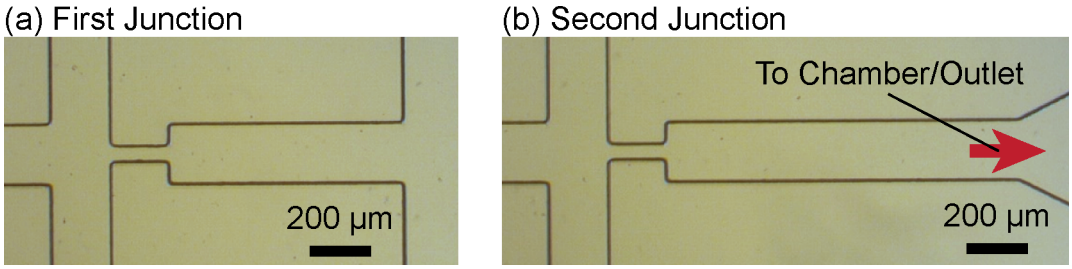

Figure 4.5 *Optical micro photos of fabricated microfluidic system for the formation of magnetic core-shell microcapsules:* ***(a)*** *first junction region, and* ***(b)*** *second junction region.*

4.2.3 Magnetic PEGDA Solution

Iron oxide magnetic nanoparticles (EMG 1200 - dry magnetic nanoparticles, Ferrotec) are added to the PEGDA solution (average Mn = 250, Sigma Aldrich) with surfactant. In order to identify the right surfactant for the prototype microfluidic system for the formation of water-in-PEGDA-in-water double emulsions, three different types of 1 wt% surfactants for PEGDA solution have been considered: Tween 20 (Sigma Aldrich), Span 80 (Sigma Aldrich), and Pluronic F-127 (Sigma Aldrich). The experimental results are presented in the next section. Toluene is added and the mixed solution is sonicated for at least 30 minutes to uniformly disperse the iron oxide nanoparticles. After the dispersion process, we remove the toluene *via* high-speed centrifugation (ARE-310, Thinky). Afterwards, 1 wt% of photoinitiator, 2,2-Dimethoxy-2-Phenylacetophenone (DMPA) (99%, Sigma Aldrich), is added to the magnetic PEGDA solution and the mixture is sonicated for 30 minutes. In the first experiment, the magnetic PEGDA mixture is tested under UV light to determine if the mixture can be the photo cured. The quick experiment is designed to have high UV light intensity to validate the hypothesis that the magnetic mixture can be cured under UV light. In the prototype test, the magnetic PEGDA mixture with 5 wt% of Iron Oxide nanoparticles is poured and sandwiched between two glass slide with an approximate gap of 1mm, and exposed to a UV light (365 nm wavelength, 25 mW/cm^2, UV-KUB1, KLOE) source of approximately 10 cm away for two seconds. The duration of UV exposure in this preliminary experiment is in the same order of the duration of on-chip UV exposure that is used in the following chapters (**Chapter 4.3.2**) with an assumption that the double emulsions path through the exposed area in the microchannel with a few seconds. As expected, it is observed that the suspended magnetic nanoparticles and PEGDA are polymerized together as illustrated in **Fig. 4.6**. After the UV exposure, the two glass slides was attached firmly with the strong adhesion force by the sandwiched magnetic PEGDA mixture, and it confirmed that the polymerization is completed. Because the thickness of the magnetic PEGDA mixture is approximately ten times thicker than the microfluidic device we use in the following experiments, this result indicates that the magnetic PEGDA solution could be photocurable with on-chip UV exposure in the following chapters.

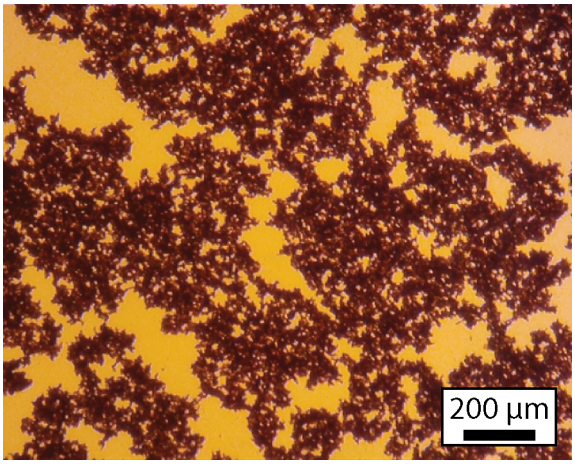

Figure 4.6 *Polymerized magnetic PEGDA solution with 5wt% of Iron Oxide nanoparticles after exposed to the UV light (365 nm wavelength, 25 mW/cm^2) source source of approximately 10 cm*

away for two seconds. Black part is the suspended magnetic nanoparticles (5 wt%) and the matrix is polymerized PEGDA.

4.2.4 Experimental Setup

Different fluids are used in the experiments. First, green-dyed DI water with surfactant is used as the outer fluid is added from the outlet port to maintain the hydrophilic state to the third inlet port right after the fabrication process. The best combinations of surfactants for the prototype system are investigated by conducting a series of experiments on three different types of surfactants in magnetic PEGDA, including Span 80 (Sigma Aldrich), Pluronic F-127 (Sigma Aldrich), and Tween 20 (Sigma Aldrich), as well as in the green-dyed DI water, including Pluronic F-127 (Sigma Aldrich), Pluronic P-85 (BASF), and Pluronic F-68 (BASF) [31]. Second, red-dyed DI water is used as the aqueous core and added to the first inlet port. Third, magnetic PEGDA solution is added to the second inlet port. These fluid solutions are inputed into the fabricated prototype devices by using syringe pumps (NE-300, New Era Pump Systems, Inc.). UV light is directly applied to the prototype system at the UV exposure chamber after the formation of the double emulsions. The light source is a quartz halogen microscope bulb (30 W) and the light is focused through 4',6-diamidino-2-phenylindole (DAPI) filter (350 nm wavelength). The microdroplet formation processes are observed under a microscope (Motic AE31, Motic, Inc.), recorded with a charge-coupled device (CCD) camera (QImaging Corp.) which is caribrated with QCapturePro (QImaging). Captured images are analyzed with the imaging software, ImageJ (National Institutes of Health (NIH)), and MATLAB (The Mathworks) to characterize the size of microdroplets and microcapsules.

4.3 Results and Discussion

4.3.1 Microfluidic Systems for the Formation of Double Emulsions

In the first stage of the experiments, the effects of different types of surfactants are tested by injecting red-dyed DI water solution into the magnetic PEGDA solution (0.5 wt% of iron oxide nanoparticles) at the first junction to form the water-in-PEGDA microdroplets which are then injected into the green-dyed DI water solution at the second junction to form the double emulsions, water-in-PEGDA-in-water microdroplets. The infusion flow rates are 1.5 μl/min, 3.5 μl/min, and 5.5 μl/min for the aqueous core (red-dyed DI water), magnetic PEGDA with 0.5 wt% of iron oxide nanoparticles, and green-dyed DI water, respectively. Various combinations of different types of 1 wt% surfactants have been tested and characterized experimentally to determine the best combinations of surfactants for the formation of double emulsions in the prototype system as listed in **Table 4.1**. In general, the microdroplets may rupture or coalesce with inappropriate surfactant combinations and several of the failed experiments are shown in Figure 4.7. For example, **Fig. 4.7a** is an optical photo showing the rupture of the aqueous core microdroplets around the first junction while **Fig. 4.7b** shows the coalescence of water-in-PEGDA microdroplets around the second junction. It is found that the best combinations of surfactants are 1 wt% of Tween 20 in the magnetic PEGDA solution and 1 wt% of Pluronic F-127 or 1 wt% of P-85 in the green-dyed DI water. Furthermore, several failed experiments have

been observed with poor designs in the microfluidic system or if the surface modification processes are not conducted appropriately. For example, **Fig. 4.7c** is the optical photo showing failure in the formation of the water-in-PEGDA microdroplets without the design of a narrower ejection neck with wetted water flows on the PDMS walls. On the other hand, **Figure 4.7d** shows the formation of green-dyed water-in-PEGDA microdroplets around at the second junction when the surface around the second junction is hydrophobic instead of hydrophilic.

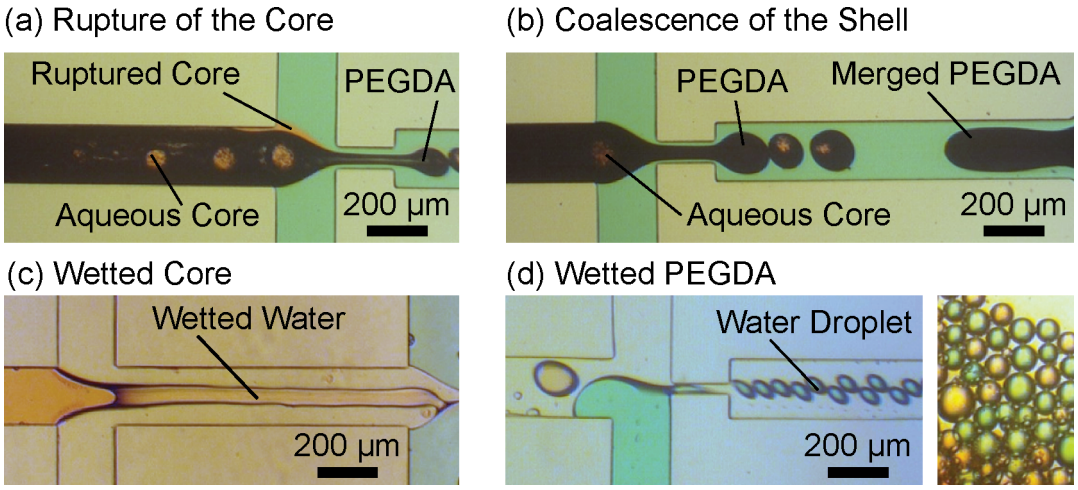

Figure 4.7 *Examples of several failed operations on the formation of double emulsions due to improper combinations of surfactants, inferior designs or surface treatment processes.* ***(a)*** *Some microdroplets with aqueous core (red-dyed water) are ruptured in PEGDA microchannel as observed around the second junction due to improper combinations of surfactants.* ***(b)*** *PEGDA-in-water microdroplets (double emulsions) are merged together around the second junction due to improper combinations of surfactants.* ***(c)*** *Failure in the formation of water-in-PEGDA microdroplets without the design of a narrower ejection neck around the first junction.* ***(d)*** *The undesirable formation of microdroplets of the green-dyed water-in-PEGDA microdroplets around at the second junction when the surface around the second junction is hydrophobic instead of hydrophilic.*

Table 4.1 *Combinations of Surfactants for the Formation of Double Emulsions*

Magnetic PEGDA	Span 80	Span 80	Span 80	F-127	F-127	F-127	Tween 20	Tween 20	Tween 20
Green-Dyed Water	F-127	P-85	F-68	F-127	P-85	F-68	F-127	P-85	F-68
Rupture/ Coalescence	Yes	Yes	Yes	Yes	Yes	Yes	No	No	Yes

When the right combination of surfactants are used in the prototype system with the right design and process parameters, the formation of double emulsions with aqueous core (*red-dyed DI water*) and PEGDA shells (*light brown*) is achieved as shown in **Fig. 4.8**. In this

demonstration, a "standard process" is conducted by using magnetic PEGDA with 0.5 wt% of iron oxide nanoparticles and 1% of Tween 20, and green-dyed water with 1% of P-85 and the infusion flow rates are 1.5 μl/min, 3.5 μl/min, and 5.5 μl/min for the aqueous core (red-dyed DI water), magnetic PEGDA, and green-dyed DI water, respectively,. Specifically, the optical micro photos **Fig. 4.8a** are the (1) formation of water-in-PEGDA microdroplets around the first junction, (2) the formation of water-in-PEGDA-in-water (*green-dyed DI water*) double emulsions around the second junction, and (3) the accumulations of double emulsions around the outlet region. The size distributions of the double emulsions and their aqueous cores are characterized as shown in **Fig. 4.8b**. The outer diameter is measured as 247.0±10.8 μm and the inner diameter is measured 93.6±8.0 μm.

The size of microdroplets can be tuned by changing the flow rates of the fluids [32]. As an example demonstration of size control with different flow rates, PEGDA droplets without the core is formed at the second flow-focusing junction. We infuse the plain PEGDA as the droplet solution and green-dyed water with 1 wt% of P85 as the outer fluid. the size the diameter of the PEGDA droplets increases from 136.6±23.1 to 241.2±30.1 μm by increasing the flow rate of PEGDA from 0.5 μl/min to 2.0 μl/min while keeping the flow rates of outer water at 3.5 μl/min as shown in **Fig. 4.8c**. These results indicate that the size of PEGDA droplets can be tuned with the flow rates. The size distribution of the PEGDA droplets is larger than the results of double emulsions (**Fig. 4.8b**) due to the capacitance from the air bubble in the closed inlet port for the first channel.

Furthermore, in order to increase the magnetic property of the microcapsules, higher concentrations of iron oxide nanoparticles at 5 wt% has been tested by using the prototype microfluidic system. The higher concentration of the magnetic nanoparticles results in opaque magnetic PEGDA shells as seen in **Fig. 4.9a**. Red fluorescent nanoparticles ($\varnothing$ = 500 nm) of 1 wt% are added to the aqueous core solution and the experimental results confirm the successful encapsulations of the aqueous core solutions in these magnetic microcapsules as shown in **Fig. 4.9b**.

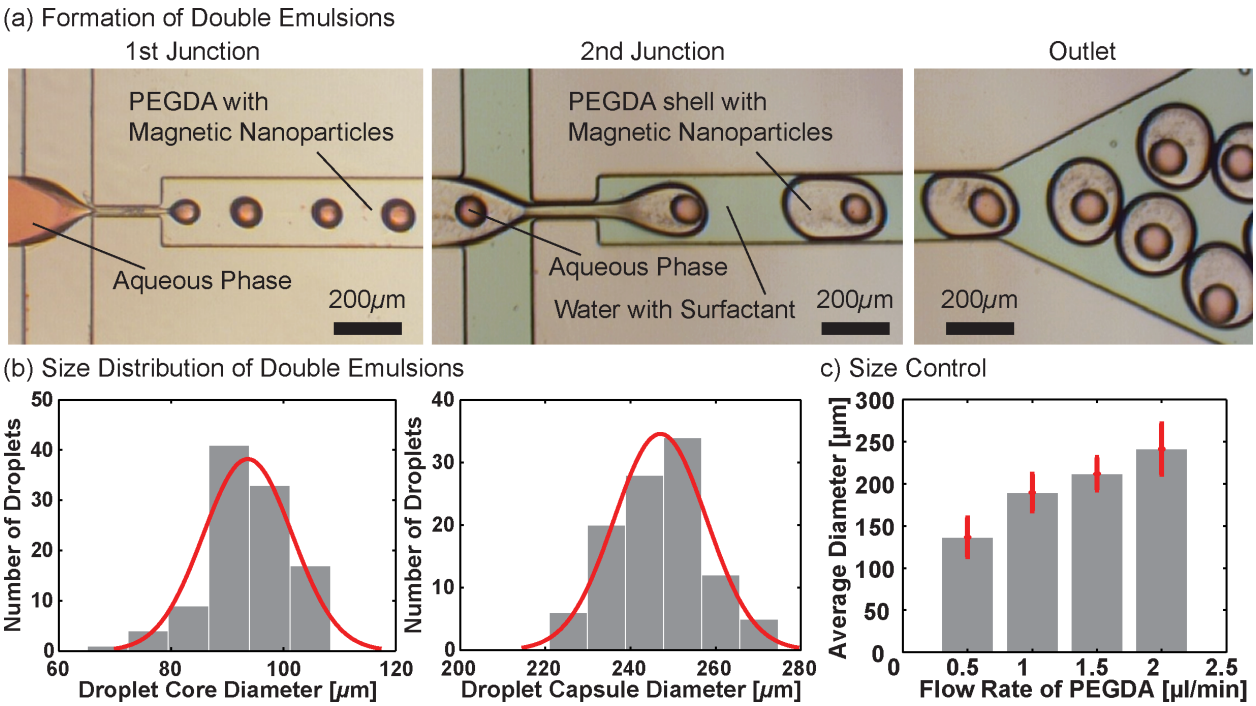

Figure 4.8 ***(a)*** *Sequential optical micro photos showing the formation of double emulsions with aqueous cores and magnetic PEGDA shells at the first junction, second junction and outlet region, respectively. PEGDA shells have 0.5 wt% of iron oxide nanoparticles.* ***(b)*** *The size distributions of the microdroplets with statistical analyses: 247.0±10.8 μm outer diameter and 93.6±8.0 μm aqueous core.* ***(c)*** *The size of the double emulsion microdroplets can be adjusted by using different fluid flow rates. In this example, the outer diameter of the PEGDA droplets increases from 136.6±23.1 to 241.2±30.1 μm when the flow rate of PEGDA is increases from 0.5 to 2.0 μl/min while keeping the flow rates of outer water at 3.5 μl/min.*

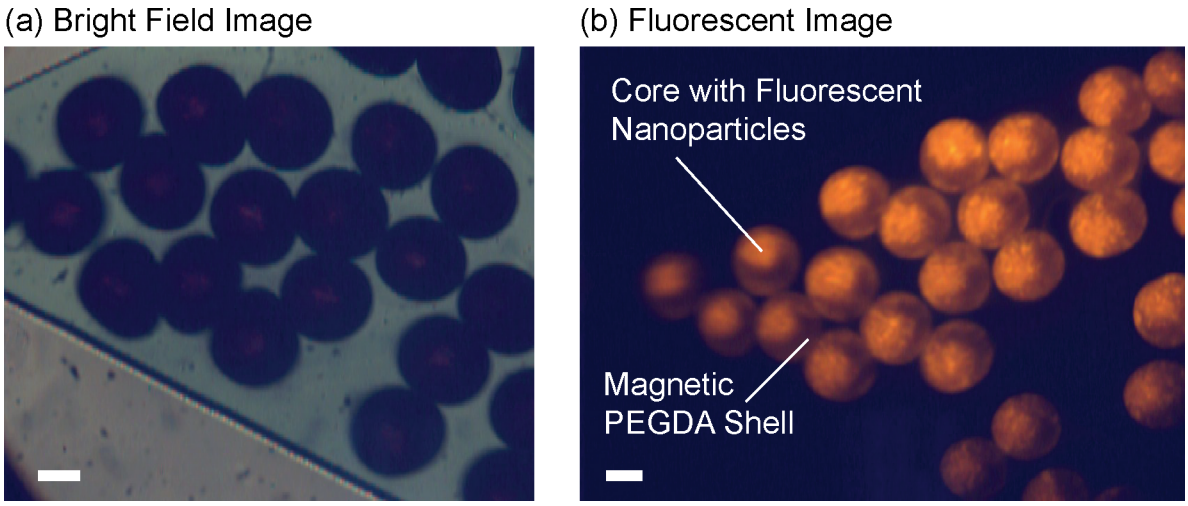

Figure 4.9 *Formation of magnetic microcapsules with increased concentration of Iron Oxide nanoparticles to 5 wt%.* ***(a)*** *The microcapsules become opaque under the bright field image.* ***(b)*** *After adding red fluorescent nanoparticles (ø = 500 nm) in the aqueous core, the fluorescent image photo shows encapsulated aqueous solutions in the magnetic microcapsules. Scale bar is 100 μm.*

4.3.2 Polymerization of Microcapsules

The polymerization process is an important step in the formation of microcapsules. Several characterization processes have been conducted in order to study the optimal processing parameters. First, the quick off-chip experiment is designed to validate the hypothesis that the intensity of directly exposed UV light through the DAPI filter (30 W, 350 nm wavelength) in the optical microscope (Motic AE31, Motic, Inc.) provides sufficient energy to polymerize PEGDA-in-water droplets. We prepare the PEGDA-in-water droplets by sonicating the mixture of the pure DI water and the PEGDA solution (10:1 weight ratio) containing 1 wt% of DMPA and 1 % of F127. We do not add magnetic nanoparticles in the PEGDA solution nor the surfactant to the DI water in this experiment because for ease in observing the polymerization process. Approximate 50 μl of the solution containing PEGDA droplets is placed on a microscope slide, and UV light is exposed from the quartz halogen microscope bulb (30 W) through the DAPI filter and the 10x objective lense (Plan Achromat Inverted Microscope Objective, Motic, Inc.). As expected, it is observed that the PEGDA droplets are polymerized after an exposure for approximately 3 seconds as illustrated in **Fig. 4.10**. The bright field image in **Fig. 4.10i** shows the microdroplet has the typical spherical shape of about 367.3 μm in diameter in the pure DI water. **Figures 4.10ii-iv** are optical photos taken before, during and after the UV exposure under a UV filter. It is observed that during the UV exposure a ring-shape shallow can be observed around the microdroplet. **Figure 4.10v** is the regular optical photo after the UV exposure and it is observed that the size of the polymerized PEGDA droplet is about 345.7 μm in diameter, indicating a 5.87 % reduction in diameter after the polymerization process.

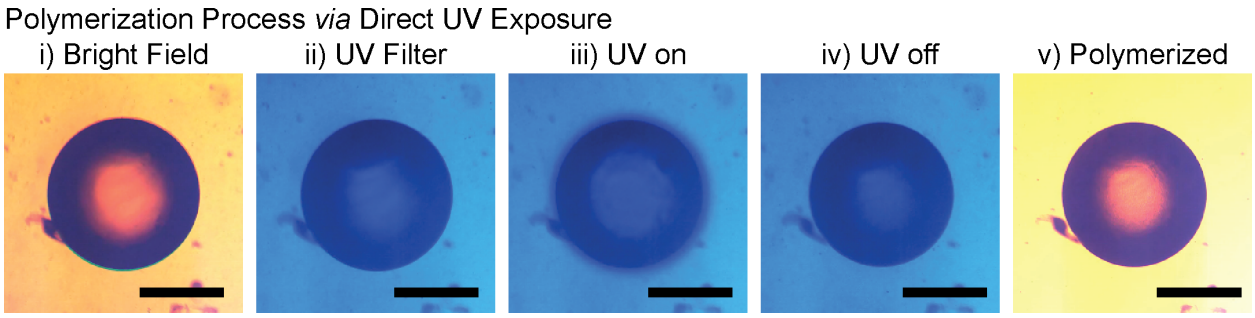

Figure 4.10 *Direct polymerization of PEGDA-in-water emulsions. It is observed that the size of the PEGDA droplet has 5.87 % reduction in diameter after the polymerization process. Scale bar is 200 μm.*

In the second characterization process, we perform the on-chip polymerization while the double emulsions are in the flow. **Figure 4.11** shows the direct polymerization process of the PEGDA-in-water double emulsions without magnetic nanoparticles for better visibility using the mixture of the PEGDA containing 1 wt% of DMPA and 1 % of Tween 20, while the green-dyed DI water contains 1 wt% of Pluronic P-85. The infusion flow rates of fluids are 1.5 μl/min, 3.5 μl/min, and 5.5 μl/min for the aqueous core (red-dyed DI water), PEGDA without magnetic nanoparticles, and green-dyed DI water, respectively. UV light is exposed onto the double emulsions (approximate size of 128.4 μm in outer diameter) in microfluidic channel from the quartz halogen microscope bulb (30 W) through the DAPI filter and the 10x objective lense (Plan Achromat Inverted Microscope Objective, Motic, Inc.) (**Fig. 4.11a**). Aqueous payload (*i.e.*, red-dyed DI water) remains encapsulated inside the microcapsules (approximate size of 118.6 μm in outer diameter) after the polymerization process (**Fig. 4.11b**). We mechanically cut a polymerized microcapsule in half with a needle and the cross sectional view showed the clear boundary of the shell part (**Fig. 4.11c**).

Next, a permanent magnet is used to actuate the magnetic microcapsules fabricated by the same procedure in the previous process with 0.5 wt% of Iron Oxide nanoparticles added. **Figure 4.12a** illustrates experimental results of fabricated and polymerized magnetic microcapsule with a size of about 164 μm in outer diameter. Under a backward flow after the formation and UV exposure of the double emulsions microdroplets. While droplets show easy deformation in the channels with different widths, the cured magnetic capsule showed no deformation at the junction verifying the solidification of shell after UV exposure (**Fig. 4.12b**). The magnetic property of these magnetic capsules were demonstrated by transporting them using ~50 mT external magnetic field from approximate distance of 2cm (**Fig. 4.12c**).

We observe the polymerized magnetic microcapsules under a scanning electron microscope (SEM) (TM-1000 SEM, Hitachi) (**Fig. 4.13a**). **Figure 4.13b** shows the shape of the formed microcapsules is disk shape with clear boundary between the top flat surface and the curved side. One microcapsule is observed to have a leakage from the core (**Fig. 4.13c**). We assume the leakage has been formed during the polymerization process because the size reduction of the PEGDA shell causes a pressure increase in the aqueous core. Increased pressure

would locally break the thin part of the PEGDA shell that is formed due to the squeezed aqueous core. Such issue could be prevented by reducing the size of the core with increased flow rate of the PEGDA solution, or by polymerizing spherical emulsions.

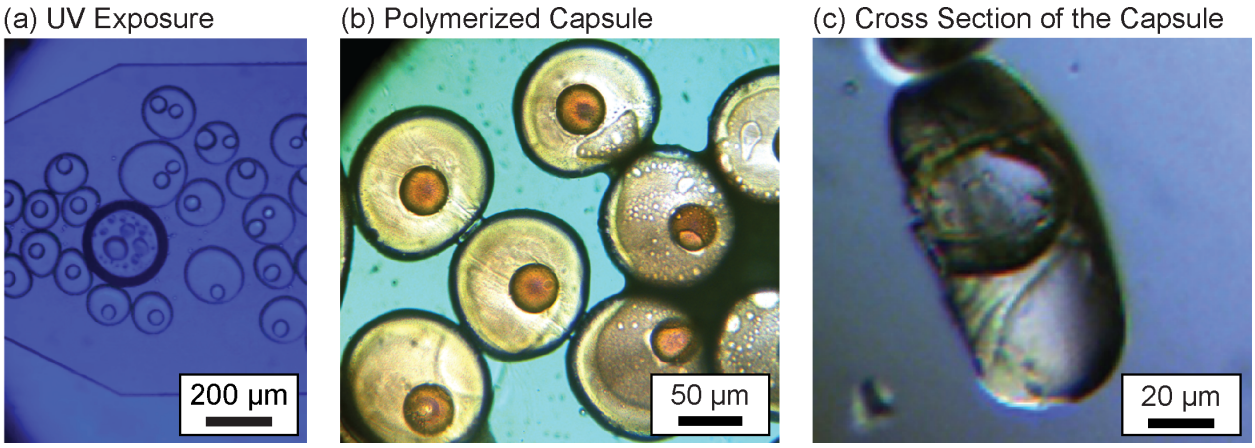

Figure 4.11 *On-chip polymerization of the PEGDA shells of the microcapsules without magnetic nanoparticles.* ***(a)*** *Double emulsions of PEGDA and DI water under UV exposure (approximate outer diameter of 128.4 µm).* ***(b)*** *The aqueous payload remains encapsulated inside the microcapsule after the polymerization process (approximate outer diameter of 118.6 µm).* ***(c)*** *Cross sectional view of the polymerized capsule indicates the clear boundary of the encapsulated core.*

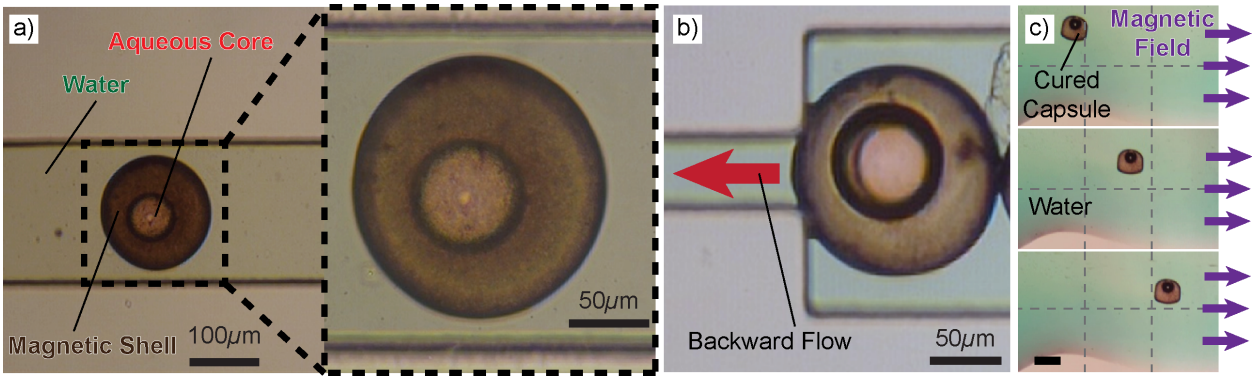

Figure 4.12 *Selective polymerization of the magnetic shells of the microcapsules.* ***(a)*** *Aqueous payload remains encapsulated inside the microcapsule (164 µm in outer diameter).* ***(b)*** *In the presence of a backward flow, the microcapsule is not deformed at the junction verifying that the magnetic PEGDA shell is solidified/cured after UV exposure.* ***(c)*** *Transport of cured magnetic microcapsule with the application of ~50 mT external magnetic field demonstrates the magnetic property of fabricated particles. Scale bar is 200 µm.*

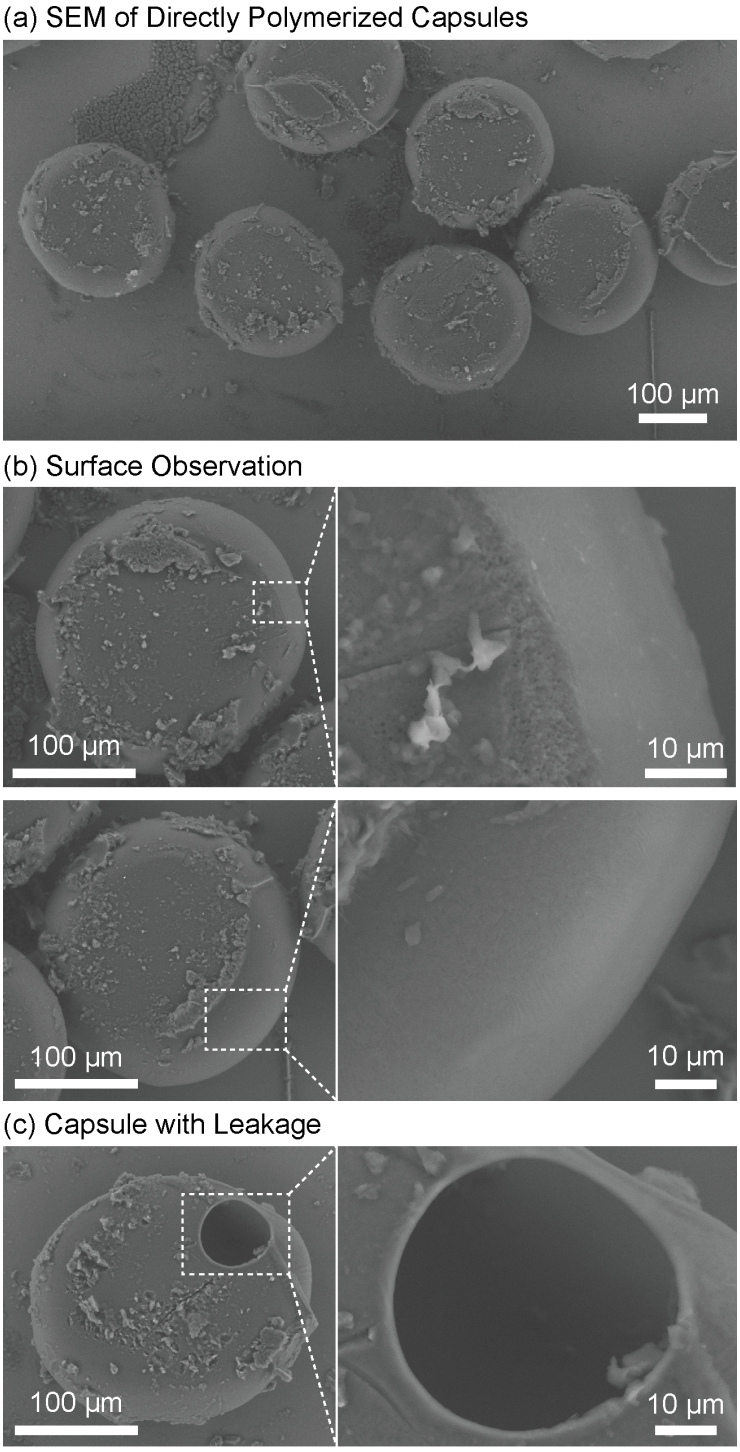

Figure 4.13 *SEM micrograph of directly polymerized magnetic capsules.* ***(a)*** *Polymerized microcapsules were disk-shape.* ***(b)*** *Boundary between the top flat surface and curved side.* ***(c)*** *Ruptured microcapsule during the polymerization process.*

To make spherical microcapsules, we polymerize the double emulsions off-chip. We transfer the uncured double emulsion from the flow-focusing device to a petri dish and expose UV light using a mask aligner (365 nm wavelength, 25 mW/cm^2, UV-KUB1, KLOE) for 10 seconds. **Figure 4.14a** shows the SEM pictures of polymerized microcapsules. Surface of the polymerized microcapsules were spherical without leakage (**Fig. 4.14b**).

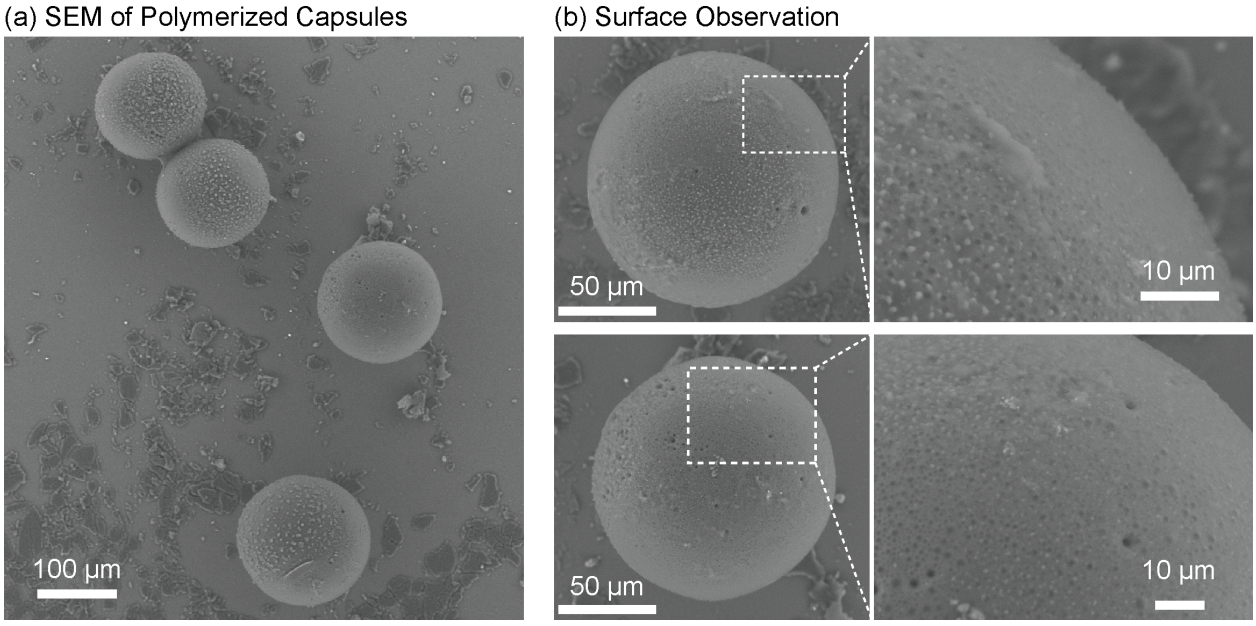

Figure 4.14 ***(a)*** *SEM micrograph of microcapsules polymerized off-chip.* ***(b)*** *Shape of the polymerized microcapsules were spherical compared with the microcapsules polymerized on-chip.*

Furthermore, we perform the off-chip polymerization with magnetic microcapsules with increased concentration of Iron Oxide nanoparticles (5 wt%). **Figure 4.15a** shows the SEM micrographs of the polymerized microcapsules. We observe numbers of holes on the surface of the microcapsules (**Fig. 4.15b**), and one microcapsule has large openings (**Fig. 4.15c**). We assume these holes are formed due to the aggregated Iron Oxide nanoparticles is dissolved into the surrounding water fluid after polymerization. These issues could be solved by reducing the concentration of the magnetic nanoparticles as demonstrated in **Fig. 4.12**, or by utilizing surface-coated Iron Oxide nanoparticles to prevent the aggregation.

Off-chip polymerization process successfully forms spherical microcapsules. On the other hand, it reduces the throughput of the formation process compared with the direct polymerization process. Additionally, we observe more ruptured capsules during the retrieval from the flow-focusing device. Such issues could be solved by exposing UV light at the chamber with locally increased thickness to form spherical microcapsules *via* direct polymerization process.

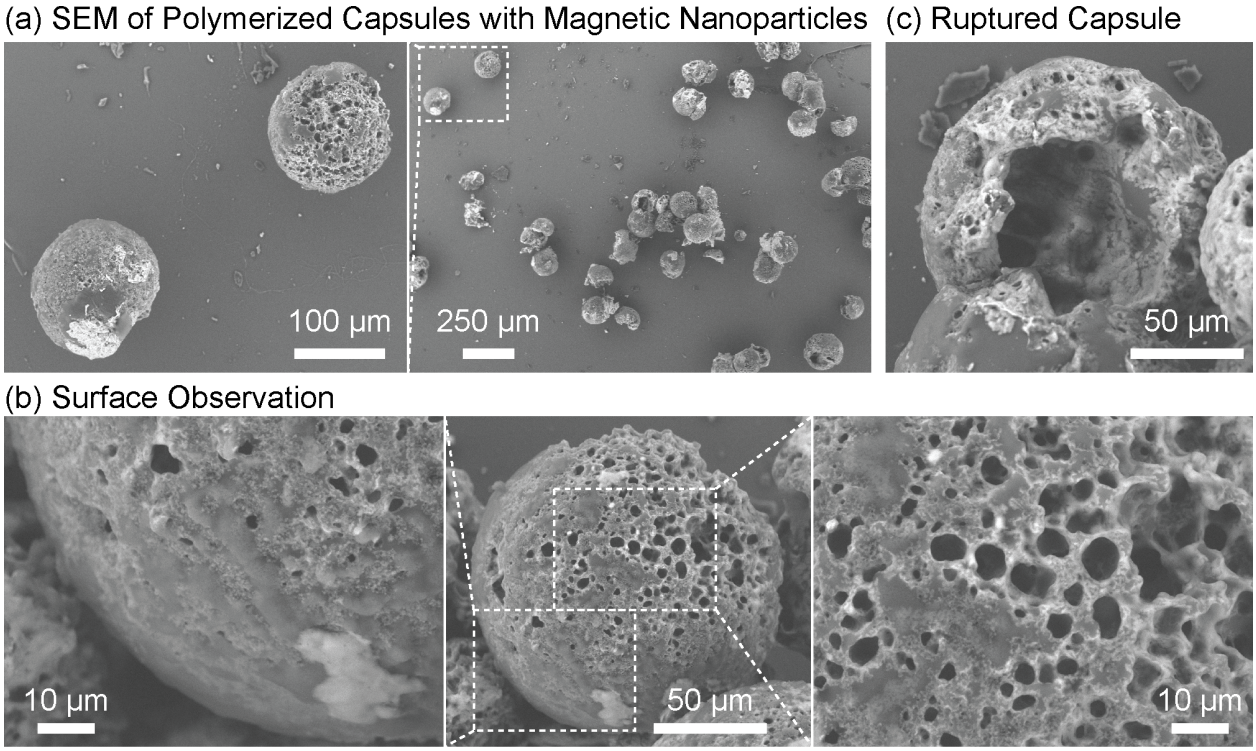

Figure 4.15 ***(a)*** *SEM micrograph of polymerized magnetic capsules with increased concentration of Iron Oxide nanoparticles (5wt%). Aggregated nanoparticles form* ***(b)*** *holes and* ***(c)*** *large openings on the surface of the microcapsules.*

References of Chapter 4

[1] B. P. Timko, K. Whitehead, W. Gao, D. S. Kohane, O. Farokhzad, D. Anderson, and R. Langer, "Advances in drug delivery," *Annu. Rev. Mater. Res.*, vol. 41, pp. 1–20, 2011.

[2] M. L. De Temmerman, J. Rejman, and J. Demeester, "Particulate vaccines: on the quest for optimal delivery and immune response," *Drug discovery today*, 2011.

[3] D. Peer, J. M. Karp, S. Hong, O. C. FaroKHzad, R. Margalit, and R. Langer, "Nanocarriers as an emerging platform for cancer therapy," *Nature Nanotechnology*, vol. 2, no. 12, pp. 751–760, Dec. 2007.

[4] N. K. Verma, K. Crosbie-Staunton, A. Satti, S. Gallagher, K. B. Ryan, T. Doody, C. McAtamney, C. S. Burke, P. Galvin, Y. Volkov, Y. K. Gun'ko, and R. MacLoughlin, "Magnetic Core-Shell Nanoparticles for Drug Delivery by Nebulization," *Journal of Aerosol Medicine and Pulmonary Drug Delivery*, vol. 26, no. 2, pp. A32–A33, Apr. 2013.

[5] M. Mahmoudi, S. Sant, B. Wang, and S. Laurent, "Superparamagnetic iron oxide nanoparticles (SPIONs): Development, surface modification and applications in chemotherapy," *Advanced drug delivery …*, 2011.

[6] A. G. Cuenca, H. Jiang, S. N. Hochwald, M. Delano, W. G. Cance, and S. R. Grobmyer, "Emerging implications of nanotechnology on cancer diagnostics and therapeutics," *Cancer*, vol. 107, no. 3, pp. 459–466, 2006.

[7] K. Hettiarachchi, A. P. Lee, S. Zhang, S. Feingold, and P. A. Dayton, "Controllable Microfluidic Synthesis of Multiphase Drug-Carrying Lipospheres for Site-Targeted Therapy," *Biotechnol Progr*, vol. 25, no. 4, pp. 938–945, 2009.

[8] S.-H. Kim, J. W. Kim, J.-C. Cho, and D. A. Weitz, "Double-emulsion drops with ultra-thin shells for capsule templates," *Lab on a Chip*, vol. 11, no. 18, pp. 3162–3166, 2011.

[9] A. S. Utada, E. Lorenceau, D. R. Link, P. D. Kaplan, H. A. Stone, and D. A. Weitz, "Monodisperse double emulsions generated from a microcapillary device," *Science*, vol. 308, no. 5721, pp. 537–541, 2005.

[10] S. Suh, S. Chapin, T. Hatton, and P. Doyle, "Synthesis of magnetic hydrogel microparticles for bioassays and tweezer manipulation in microwells," *Microfluid Nanofluid*, pp. 1–10, 2012.

[11] J. Rodríguez-López, H. C. Shum, L. Elvira, F. Montero de Espinosa, and D. A. Weitz, "Fabrication and Manipulation of Polymeric Magnetic Particles With Magnetorheological Fluid," *Journal of Magnetism and Magnetic Materials*, 2012.

[12] M. M. Rashad, H. M. El-Sayed, M. Rasly, and M. I. Nasr, "Induction heating studies of magnetite nanospheres synthesized at room temperature for magnetic hyperthermia," *Journal of Magnetism and Magnetic Materials*, vol. 324, no. 23, pp. 4019–4023, 2012.

[13] L. R. Hirsch, R. J. Stafford, J. A. Bankson, S. R. Sershen, B. Rivera, R. E. Price, J. D. Hazle, N. J. Halas, and J. L. West, "Nanoshell-mediated near-infrared thermal therapy of tumors under magnetic resonance guidance," *P Natl Acad Sci Usa*, vol. 100, no. 23, pp. 13549–13554, 2003.

[14] V. Misuk, A. Mai, K. Giannopoulos, F. Alobaid, B. Epple, and H. Loewe, "Micro magnetofluidics: droplet manipulation of double emulsions based on paramagnetic ionic liquids," *Lab on a Chip*, vol. 13, no. 23, pp. 4542–4548, 2013.

[15] T. Hoare, B. P. Timko, J. Santamaria, G. F. Goya, S. Irusta, S. Lau, C. F. Stefanescu, D. Lin, R. Langer, and D. S. Kohane, "Magnetically Triggered Nanocomposite Membranes:

A Versatile Platform for Triggered Drug Release," *Nano Lett*, vol. 11, no. 3, pp. 1395–1400, Mar. 2011.
[16] W.-A. C. Bauer, M. Fischlechner, C. Abell, and W. T. S. Huck, "Hydrophilic PDMS microchannels for high-throughput formation of oil-in-water microdroplets and water-in-oil-in-water double emulsions," *Lab on a Chip*, vol. 10, no. 14, pp. 1814–1819, 2010.
[17] J. Thiele and S. Seiffert, "Double emulsions with controlled morphology by microgel scaffolding," *Lab on a Chip*, vol. 11, no. 18, pp. 3188–3192, 2011.
[18] K. W. Bong, S. C. Chapin, and P. S. Doyle, "Magnetic Barcoded Hydrogel Microparticles for Multiplexed Detection - Langmuir (ACS Publications)," *Langmuir*, 2010.
[19] D. Pregibon, M. Toner, and P. Doyle, "Magnetically and biologically active bead-patterned hydrogels," *Langmuir*, vol. 22, no. 11, pp. 5122–5128, 2006.
[20] D. K. Hwang, D. Dendukuri, and P. S. Doyle, "Microfluidic-based synthesis of non-spherical magnetic hydrogel microparticles," *Lab on a Chip*, vol. 8, no. 10, pp. 1640–1647, 2008.
[21] S. K. Suh, K. Yuet, D. K. Hwang, K. W. Bong, P. S. Doyle, and T. A. Hatton, "Synthesis of Nonspherical Superparamagnetic Particles: In Situ Coprecipitation of Magnetic Nanoparticles in Microgels Prepared by Stop-Flow Lithography," *J. Am. Chem. Soc.*, vol. 134, no. 17, pp. 7337–7343, 2012.
[22] S. K. Suh, K. W. Bong, T. A. Hatton, and P. S. Doyle, "Using Stop-Flow Lithography To Produce Opaque Microparticles: Synthesis and Modeling," *Langmuir*, vol. 27, no. 22, pp. 13813–13819, 2011.
[23] R. M. K. Ramanan, P. Chellamuthu, L. Tang, and K. T. Nguyen, "Development of a Temperature-Sensitive Composite Hydrogel for Drug Delivery Applications," *Biotechnol Progr*, vol. 22, no. 1, pp. 118–125, Feb. 2006.
[24] M. Seo, C. Paquet, Z. Nie, S. Xu, and E. Kumacheva, "Microfluidic consecutive flow-focusing droplet generators," *Soft Matter*, vol. 3, no. 8, pp. 986–992, 2007.
[25] D. Dendukuri, K. Tsoi, T. Hatton, and P. Doyle, "Controlled synthesis of nonspherical microparticles using microfluidics," *Langmuir*, vol. 21, no. 6, pp. 2113–2116, 2005.
[26] D. Dendukuri, D. Pregibon, J. Collins, T. Hatton, and P. Doyle, "Continuous-flow lithography for high-throughput microparticle synthesis," *Nat Mater*, vol. 5, no. 5, pp. 365–369, 2006.
[27] I. Wong and C.-M. Ho, "Surface molecular property modifications for poly (dimethylsiloxane)(PDMS) based microfluidic devices," *Microfluid Nanofluid*, vol. 7, no. 3, pp. 291–306, 2009.
[28] D. Duffy, J. McDonald, O. Schueller, and G. Whitesides, "Rapid prototyping of microfluidic systems in poly(dimethylsiloxane)," *Anal Chem*, vol. 70, no. 23, pp. 4974–4984, 1998.
[29] V. Barbier, M. Tatoulian, H. Li, F. Arefi-Khonsari, A. Ajdari, and P. Tabeling, "Stable modification of PDMS surface properties by plasma polymerization: application to the formation of double emulsions in microfluidic systems," *Langmuir*, vol. 22, no. 12, pp. 5230–5232, 2006.
[30] S. M. Hong, S. H. Kim, J. H. Kim, and H. I. Hwang, "Hydrophilic surface modification of PDMS using atmospheric RF plasma," vol. 34, no. 1, p. 656, 2006.
[31] J.-C. Baret, "Surfactants in droplet-based microfluidics," *Lab on a Chip*, vol. 12, no. 3, pp. 422–433, 2012.

[32] P. Garstecki, M. Fuerstman, H. Stone, and G. Whitesides, “Formation of droplets and bubbles in a microfluidic T-junction - scaling and mechanism of break-up,” *Lab on a Chip*, vol. 6, no. 3, pp. 437–446, 2006.

Chapter 5: Conclusions and Future Directions

5.1 Conclusions

There are numbers of advantages in droplet-based microfluidic systems for potential use in the field of advanced biological and chemical applications. In this dissertation, several novel microfluidic systems have been presented and investigated to promote the potential of droplet-based microfluidic systems.

In **Chapter 2**, we have developed integrated, finger-powered, pressure driven pumps for microfluidic applications, including the formation of microdroplets. The multi-port system with a single pressure chamber has been achieved with the help of sample storage chamber and passive fluidic diodes for the regulations of microfluidic flows. These finger-powered microfluidic systems have been designed and constructed by using either a multilayer soft lithography or injection molding process. Experimental results show that the pressure chamber size can directly influence the maximum pressure, thereby providing an effective means to control working pressure heads. For example, the measured pressure head generated by a human finger from the prototype systems is 4.2 kPa with a PDMS pressure chamber of 10.0 mm in diameter and 7.6 kPa with an injection-molded pressure chamber of 15.0 mm in diameter. The prototype finger-powered microfluidic systems have effectively facilitated microfluidic operations, including basic pumping of fluids from inlet ports to an outlet port, generating microdroplets, and encapsulating endothelial cells in water-in-oil microdroplets. These results suggest that the finger-powered microfluidic systems could be applied to a wide range of systems towards fully integrated lab-on-a-chip applications.

In **Chapter 3**, a variety of continuous-flow microdroplets rupture and content alteration systems have been developed to provide wash, rupture, collection and solution alteration processes for microdroplets in sequences *via* the continuous-flow micropost array railing methodology. The key microdroplets rupture process involves the transportation and guidance of water-in-oil microdroplets into different liquids of microchannels to wash out surfactant with pure Hexadecane and to rupture microdroplets at the interface of the oil-water microchannels. In these experiments, a total of four different microdroplets generations system have been made and the different designs and operation conditions results in different sizes of microdroplets, including 41.1 μm for the basic microdroplets rupture demonstration, 67.5 μm for the nanoparticle synthesis experiments, 61.1 μm in the original solution, and 38.6 μm for the new solution in the bead-in-droplets alternation experiments. By integrating the microdroplets rupture system with microreactors for the synthesis of nanoparticles, iron-oxide nanoparticles have been synthesized inside microdroplets and subsequently released and retrieved within a few seconds without the need of a conventional centrifuge process. This method reduced the post processing time required to remove oil phase from the outputted solution at the end of the synthesis process. In a second demonstration, a rapid solution alteration system for the bead-in-droplet microreactors has been demonstrated *via* the continuous-flow micropost array railing technique. The prototype system has accomplished: (*i*) the retrieval of microbeads in water-in-oil droplets by the 'rupture' of the droplets, (*ii*) transfer of the released microbeads into a second solution, and (*iii*) the formation of new water-in-oil droplets containing the original microbeads

and a different, second aqueous solution. As such, the presented technique could be tailored to a wide range of chemicals, beads and particles for a variety of applications. For example, living cells or functionalized microbeads could be used to conduct cell rupture for high-throughput polymerase chain reaction or bead-based assays for point-of-care diagnostics screenings.

In **Chapter 4**, we have developed microcapsules with nanoparticle-based magnetic shell and aqueous core. We successfully formed double emulsions of water-in-magnetic PEGDA with flow-focusing devices, and selectively polymerized the PEGDA shells containing magnetic nanoparticles. It is observed that these magnetic microcapsules are able to move following the magnetic field using an external permanent magnet. The encapsulated aqueous phase core enables the introduction of water-soluble therapeutic agents into the core of the microcapsules. Additionally, it could be possible to provide heating power remotely with the assistance of an external alternating magnetic field to potential dissolve/alter the porosity of the magnetic shells for controlled drug delivery functions. We believe these functionalized core-shell microcapsules could serve as an effective platform in advanced therapeutic drug delivery applications.

5.2 Future Directions

5.2.1 Finger-Powered Saliva-Based Diagnostics

In the finger-powered microfluidic systems for point-of-care diagnostics discussed in **Chapter 2**, it is often required to prepare body samples in advance of the infusion into the system for point-of-care diagnostic applications. Typical sample preparation steps involve the collection of the sample from human body (*e.g.*, whole blood, saliva, and body liquid) and the separation of the unnecessary materials (e.g., removal of red blood cells from whole blood), which require additional labor and equipment. Therefore, it would be desirable to include parts of the sample preparation processes with the microfluidic systems for point-of-care diagnostic applications [1]-[5]. Since the finger-powered system utilizes negative pressure to fill the fluidic reservoirs when the finger is released from the pressure chamber, this negative pressure could be used to directly collect body samples (*i.e.*, saliva) as illustrated in **Fig. 5.1**. Additionally, microfluidic filter components could be integrated between the inlet of the body samples and the reservoir to separate and adsorb unnecessary particles or molecules [6]. By infusing the oil and reagents after collecting the body sample solution at the reservoir, microdroplets containing the mixture of the samples and reagents, which could be utilized to detect biomolecules of interest at the observation chamber. Since microdroplets-based systems could be utilized as microreactors with less background noise than the conventional bulk processes, the proposed system could provide a powerful approach for quick and accurate detection of the biomolecules such as glucose or cholesterol for diagnostic purposes in the future.

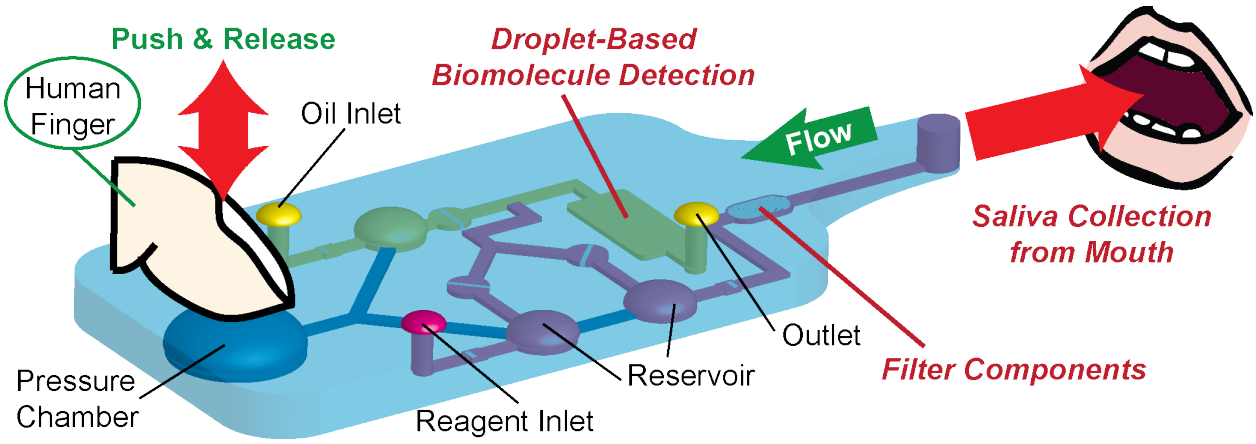

Figure 5.1 *Conceptual illustrations of finger-powered saliva-based diagnostic system. Negative pressure generated in the pressure chamber to collect saliva samples from mouth directly. Integrated filter components separate unnecessary particles and molecules. After infusion of oil and reagents to form droplets of a mixture of the reagents and the samples, droplets could be collected and analyzed at the observation chamber for quick and accurate biomolecule detections.*

5.2.1 Temperature Controlled Synthesis of Nanoparticles

In **Chapter 3.3,** the processes in microdroplets-based synthesis and centrifuge-free retrieval of nanoparticles are all conducted at room temperature. Nanoparticles synthesis, however, often prefers to be processes at an alternative temperature. For instance, CdSe quantum dots are typically synthesized with a temperature change from room temperature to over 200 ºC to initiate the growth of the nanoparticles [7]. Furthermore, the duration of the nanoparticle growth greatly affects the resulting size of the quantum dots, which directly related with the physical characteristics of the quantum dots. Because the microdroplets rupture system is based on the continuous-flow microfluidic system, it is possible to use heated oil stream as one of the microchannels to introduce temperature control in the system as shown in **Fig. 5.2**. Microdroplets are transferred to the hot oil and cold oil sequentially *via* the continuous-flow micropost array railing system. In the heated microchannel, the nanoparticle growth is initiated and in the cooled microchannel, the reaction is quenched. This configuration could enable rapid and fine control of temperature and processing time periods because the heat and mass transfer distance is shorter than in the bulky systems. The reaction time for the nanoparticle growth can be controlled by tuning the flow rate and/or by modifying the dimensions of the system for longer/shorter exposure of the microdroplets. Such rapid temperature adjustment and precise control of the reaction time is nearly impossible in bulk scale processes. As such, the presented system could lead to better monodispersed and high-quality nanoparticles synthesis process.

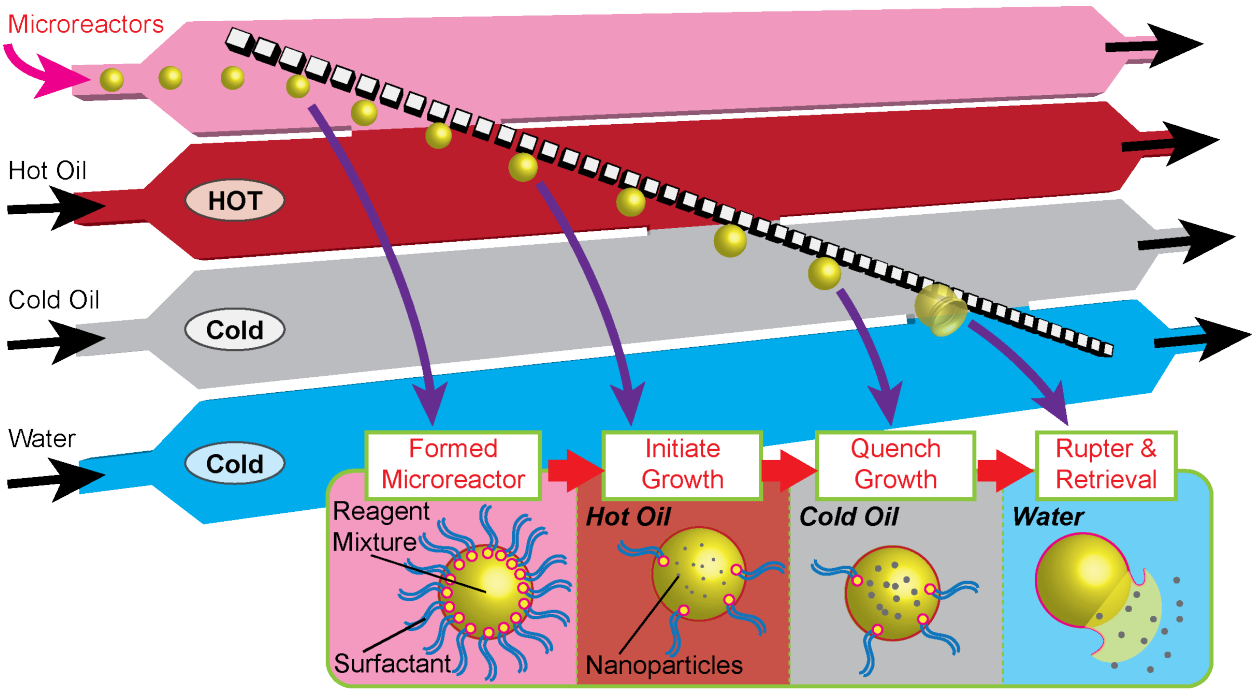

Figure 5.2 *Conceptual illustrations of temperature controlled synthesis of nanoparticles. Microreactors containing reagent mixture is transported through streams of hot oil and cold oil to precisely control the initiation and quenching of nanoparticle growth. Synthesized droplet can be retrieved at the water stream via the droplet rupture process.*

5.2.2 Fusion of Microdroplets for Multi-Step Nanoparticle Synthesis

For the microdroplets-based synthesis and centrifuge-free retrieval of nanoparticles processes as discussed in **Chapter 3.3**, a single step reaction is used to synthesize single crystal iron oxide nanoparticles. Due to the high surface area-to-volume ratio of the nanoparticles, most of the nanoparticles are highly reactive and often requires to be coated with non-reactive materials [8]. Coating of nanoparticles in the microdroplets can be realized in the following approach as illustrated in in **Fig. 5.3a**. Microdroplets with the nanoparticle synthesis process can be merged together with other microdroplets containing coating materials from the bottom microchannel as shown because the surfactant on the microdroplets is washed [9]. The timing and manipulation of these microdroplets in the pure oil microchannel will be carefully designed to assure the merge process. The merged microdroplets will allow the adsorption of coating materials onto the nanoparticles by mixing the nanoparticle solution with reagents containing the coating material [8]. After the coating process, microreactors can be ruptured and the nanoparticles are released at the water stream. By releasing the nanoparticles into the water stream, it also dilutes the excess coating material and the nanoparticles are washed to prevent unnecessary reactions. The presented system would provide high-throughput synthesis and coating of nanoparticles by reducing the labor for mixing and washing of coating materials. **Figure 5.3b** shows the preliminary demonstration of the merging process of water microdroplets in pure oil (Hexadecane). The first microdroplet has nanoparticles inside and the second

microdroplet has coating material inside. They travel in the pure oil microchannel and merge together as shown.

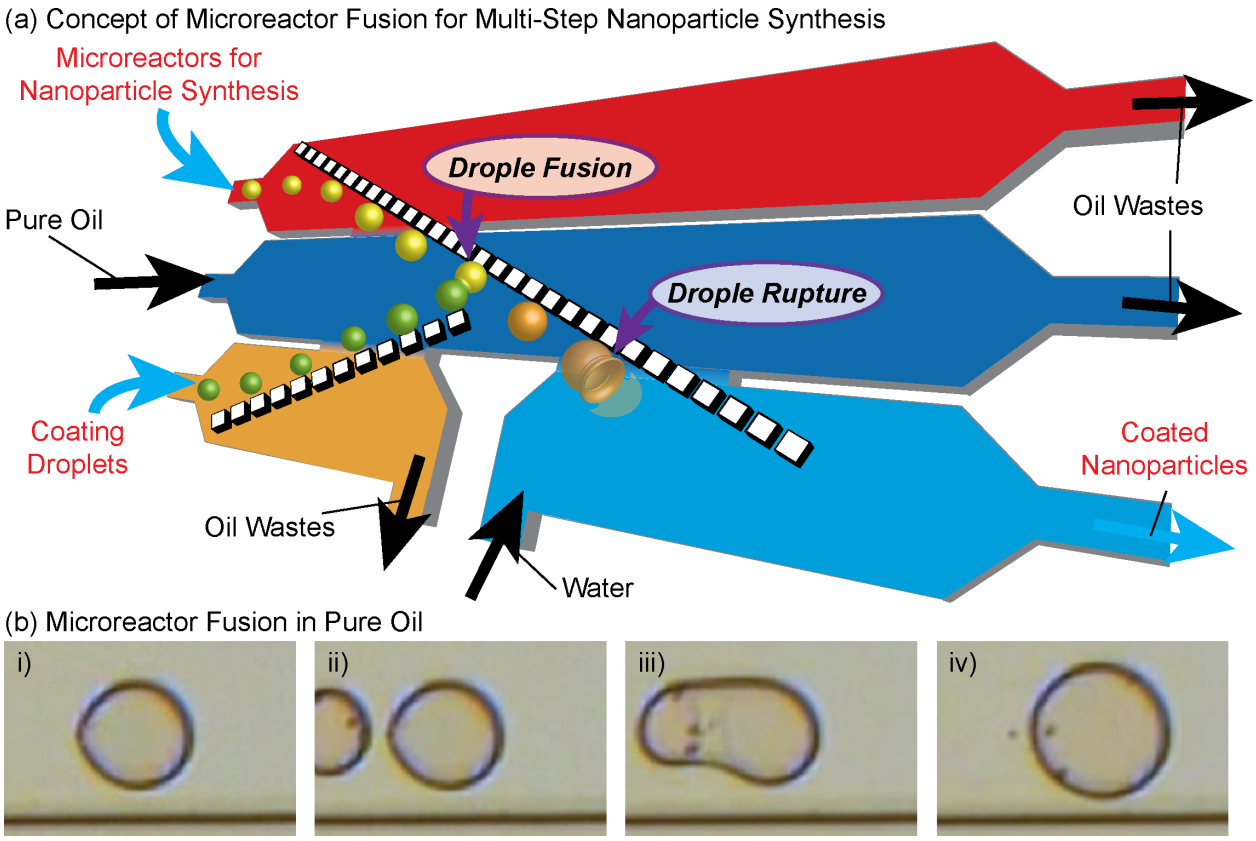

Figure 5.3 ***(a)*** *Conceptual illustration of microrddroplets fusion and merging for the coating of nanoparticles. The additional bottom microchannel of oil with surfactant is added into the original system to allow the second type of coating material-in-oil microdroplets to also feed into the pure oil microchannel. Washed microdroplets with synthesized nanoparticles from the first microchannel and the washed microdroplets from the bottom microchannel are merged at the middle pure oil microchannel for the coating of nanoparticles. After the coating process, microreactors can be ruptured, and the nanoparticles are released and washed in the water stream.* ***(b)*** *Preliminary demonstration of two microdroplets merging in pure oil (Hexadecane). Washed microdroplets merge together and mix their contents.*

5.2.3 Remote and On-Demand Release of Drug Materials from Magnetic Microcapsules

The magnetic characteristics of the magnetic microcapsules discussed in **Chapter 4** can be further studied to remotely transport the microcapsules *via* an external magnetic field. After the microcapsules are injected inside human body, they need to be transported to specific target

sites. These require extended studies on the parameters of the magnitude of the external magnetic field, the concentration of the magnetic nanoparticles in the shells, the size of the microcapsules and other things. In addition to the transportation and targeting capabilities, the feasibility to release the drug material on-demand remotely also requires further investigations [10], [11]. The presented magnetic capsules could be modified by replacing the shell material with different types of polymer such as thermosensitive polymers, to realize the on-demand release of the encapsulated drug materials. Magnetic nanoparticles can be heated remotely *via* induction heating to change the porosity of the shell material [12]. For instance, temperature of iron oxide nanoparticles with approximate size of 5-10 nm in diameter could reach 43 ºC in approximately three minutes by applying AC magnetic field at 500 kHz [13], [14]. Heated thermosensitive polymer changes its characteristics (*e.g.*, faster diffusion rate or transition of hydrophobicity), resulting in the faster release of drugs. As an example of thermosensitive polymer, poly(N-isopropylacrylamide) (PNIPAAm) is a thermosensitive hydrogel that has a lower critical solution temperature (LCST) in the range of 37-39 ºC [15]. Below the LCST temperature, PNIPAAm is in hydrophilic coil state, and above the LCST temperature, a reversible phase transition (*i.e.*, coil-to-globule) occurs and PNIPAAm becomes hydrophobic globule state. In the globule state, porous size of PNIPAAm increases and the diffusion rate through PNIPAAm increases. It could be possible to employ the mixture of PEGDA and PNIPAAM with suspended magnetic nanoparticles as photocurable magnetic polymer with thermosensitivity as the shell material of the capsules. Below the LCST temperature, the coil-state polymer shell retains the encapsulated drug, and it starts releasing the drug materials when it is heated above the LCST *via* induction heating. Such functionality to remotely release drug materials on-demand would enable safe and effective drug delivery.

References of Chapter 5

[1] I. K. Dimov, L. Basabe-Desmonts, J. L. Garcia-Cordero, B. M. Ross, A. J. Ricco, and L. P. Lee, "Stand-alone self-powered integrated microfluidic blood analysis system (SIMBAS)," *Lab on a Chip*, vol. 11, no. 5, pp. 845–850, 2011.

[2] A. V. Govindarajan, S. Ramachandran, G. D. Vigil, P. Yager, and K. F. Boehringer, "A low cost point-of-care viscous sample preparation device for molecular diagnosis in the developing world; an example of microfluidic origami," *Lab on a Chip*, vol. 12, no. 1, pp. 174–181, 2012.

[3] A. J. Mach, J. H. Kim, A. Arshi, S. C. Hur, and D. Di Carlo, "Automated cellular sample preparation using a Centrifuge-on-a-Chip," *Lab on a Chip*, vol. 11, no. 17, pp. 2827–2834, 2011.

[4] V. Srinivasan, V. Pamula, and R. Fair, "An integrated digital microfluidic lab-on-a-chip for clinical diagnostics on human physiological fluids," *Lab on a Chip*, vol. 4, no. 4, pp. 310–315, 2004.

[5] D. Chen, M. Mauk, X. Qiu, C. Liu, J. Kim, S. Ramprasad, S. Ongagna, W. R. Abrams, D. Malamud, P. L. A. M. Corstjens, and H. H. Bau, "An integrated, self-contained microfluidic cassette for isolation, amplification, and detection of nucleic acids," *Biomed Microdevices*, vol. 12, no. 4, pp. 705–719, 2010.

[6] S. Wang, D. Sarenac, M. Chen, S.-H. Huang, F. F. Giguel, D. R. Kuritzkes, and U. Demirci, "Simple filter microchip for rapid separation of plasma and viruses from whole blood," 2012.

[7] E. M. Chan, A. P. Alivisatos, and R. A. Mathies, "High-Temperature Microfluidic Synthesis of CdSe Nanocrystals in Nanoliter Droplets," *J. Am. Chem. Soc.*, vol. 127, no. 40, pp. 13854–13861, Oct. 2005.

[8] Do Kyung Kim, M. Mikhaylova, Y. Zhang, and M. Muhammed, "Protective coating of superparamagnetic iron oxide nanoparticles," *Chemistry of Materials*, vol. 15, no. 8, pp. 1617–1627, 2003.

[9] Y.-C. Tan, Y. L. Ho, and A. P. Lee, "Droplet coalescence by geometrically mediated flow in microfluidic channels," *Microfluid Nanofluid*, vol. 3, no. 4, pp. 495–499, 2007.

[10] N. K. Verma, K. Crosbie-Staunton, A. Satti, S. Gallagher, K. B. Ryan, T. Doody, C. McAtamney, C. S. Burke, P. Galvin, Y. Volkov, Y. K. Gun'ko, and R. MacLoughlin, "Magnetic Core-Shell Nanoparticles for Drug Delivery by Nebulization," *Journal of Aerosol Medicine and Pulmonary Drug Delivery*, vol. 26, no. 2, pp. A32–A33, Apr. 2013.

[11] T. Hoare, J. Santamaria, G. F. Goya, S. Irusta, D. Lin, S. Lau, R. Padera, R. Langer, and D. S. Kohane, "A Magnetically Triggered Composite Membrane for On-Demand Drug Delivery," *Nano Lett*, vol. 9, no. 10, pp. 3651–3657, Oct. 2009.

[12] M. M. Rashad, H. M. El-Sayed, M. Rasly, and M. I. Nasr, "Induction heating studies of magnetite nanospheres synthesized at room temperature for magnetic hyperthermia," *Journal of Magnetism and Magnetic Materials*, vol. 324, no. 23, pp. 4019–4023, 2012.

[13] Q. A. Pankhurst, J. Connolly, S. K. Jones, and J. Dobson, "Applications of magnetic nanoparticles in biomedicine," *J Phys D Appl Phys*, vol. 36, no. 13, pp. R167–R181, Jun. 2003.

[14] S. Wada, K. Tazawa, I. Furuta, and H. Nagae, "Antitumor effect of new local hyperthermia using dextran magnetite complex in hamster tongue carcinoma," *Oral*

Diseases, vol. 9, no. 4, pp. 218–223, Jul. 2003.
[15] R. M. K. Ramanan, P. Chellamuthu, L. Tang, and K. T. Nguyen, "Development of a Temperature-Sensitive Composite Hydrogel for Drug Delivery Applications," *Biotechnol Progr*, vol. 22, no. 1, pp. 118–125, Feb. 2006.